Ángel F. Doval, "A systematic approach to TV holography", Measurement Science and Technology, **11**(1) R1-R36, 2000

http://dx.doi.org/10.1088/0957-0233/11/1/201

A systematic approach to TV-holography

Ángel F. Doval

Departamento de Física Aplicada. E.T.S. de Ingenieros Industriales y de Minas.

Universidad de Vigo. E36200 Vigo (SPAIN)

E-mail: adoval@uvigo.es

Keywords: displacement, shape, vibration, TV holography, electronic speckle-pattern interferometry, non-destructive testing

Abstract

Television holography (TVH) can be defined as "the family of optical measurement techniques based on the electronic recording and processing of holograms". Image-plane TV-holography was introduced in the early seventies with the name "electronic speckle pattern interferometry" (ESPI). Since then, TVH has undergone an impressive development and become one of the most promising optical techniques for non-destructive testing and industrial inspection.

The aim of this article is to propose an original scheme for the systematic treatment of TVH and to review the existing techniques according to it. In this approach we split the measurement process in four highly independent stages —illumination and observation geometry, temporal treatment, secondary correlgram generation and fringe pattern analysis— and establish a common notation to formulate the corresponding techniques. Such strategy allows the free combination of the techniques proposed for each stage as building blocks to obtain every particular variant of the whole TVH measurement process, already reported or not, and also the incorporation of new techniques keeping the compatibility with the existing variants of the previous and following stages.

A systematic approach to TV-holography

1 Introduction

Television holography (TV-Holography or TVH) can be defined as the family of measurement techniques based on the recording of holograms with video cameras and their subsequent processing by electronic means, either analogue or digital.

Classic holography and TV-holography are different in both recording media — photographic in the former and optoelectronic in the later— and processing methods — a sequence of procedures of heterogeneous nature (chemical developing, optical reconstruction and processing and, eventually, optoelectronic recording and post-processing) for the first and pure electronic processing for the second.

TVH appeared at the early seventies resulting of the efforts of several research groups to solve similar problems arisen in the field of classic holography. In the United Kingdom, Butters and Leendertz [1-4] conceived this technique as a natural extension of speckle interferometry, that themselves and other authors had developed to implement holographic measurement techniques using photographic film with less resolution and more sensitivity than the holographic plates. Almost at the same time, in the United States, Macovski *et al* [5] developed an analogous technique in the context of the research on the recording and transmission of holograms by television. Also Schwomma [6] in Austria and Köpf [7] in Germany reached this technique from the field of holographic interferometry.

Of these four pioneer groups, the Austrian and the British matured the new technique up to produce marketable prototypes. But only the British group continued the development of TVH and remained in this field to date. The name that Butters and Leendertz coined “Electronic Speckle Pattern Interferometry” (ESPI), close related to the approach that led to their original technique, became popular very soon and has been

the most usual name for it and also for all the variants that have appeared along the last years.

During the seventies and early eighties, some other research groups —mainly based in European universities— developed their own prototypes, new techniques and the name "TV-holography" was introduced [8, 9]. All these systems had in common that the video signal was processed with analogue techniques and as a result they were expensive, bulky and not enough versatile.

The ultimate impulse for TVH came in the mid eighties with the production of microcomputers and peripherals for the digitalisation and processing of images at affordable prices. The integration of these programmable, versatile and relatively inexpensive digital devices in the processing schemes of the images generated with speckle interferometers was almost immediate [10-12] and encouraged many groups to join the development of TVH. New names as "Computer-Aided Speckle Pattern Interferometry" [11], "Digital TV Speckle Interferometry" [13] and "Digital Speckle Pattern Interferometry" (DSPI) [14] were then proposed to draw a distinction between the digital and analogue implementations.

The numerical handling of speckle interferograms allowed a more comfortable implementation of the original analogue methods, the development of new fringe formation techniques and the automatic analysis of the resulting fringe patterns. The introduction of digital methods in holographic interferometry (HI) and TVH was simultaneous and, since then, both metrological disciplines have evolved in parallel; thus, almost any technique developed for HI is immediately adapted to TVH and vice versa. This parallelism lead some authors to propose new names for the digital implementations of speckle pattern interferometry as "Electro-Optic Holography" (EOH) [15] or "Electronic Holography" [16] and, finally, to reconsider [17] the name "TV-holography", already proposed by Gåsvik [8] for the original analogue techniques.

The continuous increment of the resolution of the video cameras and of the power of the computers have recently allowed the recording of Fresnel and Fourier holograms and their subsequent analysis and reconstruction by numerical methods [18, 19]. With the currently available devices, this is only feasible with small objects located far from the camera and small angles between the object and reference beams; for large objects it is necessary to use diverging lenses to get a virtual image with suitable dimensions and position [20] or to magnify a small portion of the hologram with a converging lens [21]. In spite of being in its earlier development stages, the numerical reconstruction of holograms has been already used to implement methods for the measurement of displacements [22] and derivatives of displacement [23], and applied to the measurement of vibrations [24], surface contouring [25, 26] and the characterisation of wavefronts [27]. This new measurement technique was initially named "Direct Holography" [18] and "Digital Holographic Interferometry" [24], but it has been finally recognised as a variant of TV-holography [21, 25] thus establishing the final connection between classic holography and TVH.

Nowadays, the term "Television Holography" covers a field wider than the original electronic speckle pattern interferometry and its derivations, that can be regarded as image-plane TV-holography techniques, and is a well established technique of Optical Metrology. TVH shares with classic HI many of its best characteristics —as interferometric sensitivity, high precision as well as whole-field and non-contact operation— and inherits from speckle metrology advantages as the possibility of adjusting both direction and magnitude of the sensitivity within a wide range of values, the availability of geometries that provide direct sensitivity to the derivatives of the measurand and that the fringes are always localised on the surface of the object.

But the characteristics that make of TVH one of the optical metrology techniques with a higher potential for industrial application derive from the use of video cameras as recording media:

— Their sensitivity is much higher than that of holographic plates and thus allows to use shorter exposure times than in classic holography. This enables TVH to make measurements in low-stability conditions and with poor vibration isolation, as often happens in field applications.
— The operating cost is insignificant since consumables as holographic plates, photographic film or developing chemicals are not required. This allows its unrestricted use for interactive development processes and its application to massive quality control in production lines.
— The electronic processing of the hologram information is very fast —compared with chemical developing— and is often performed in real-time.
— TVH systems are very easy to use since they can operate in presence of ambient light, there is no need of developing or re-positioning the holograms and their components as well as the signal processing are usually computer controlled. Therefore, they can be even operated by staff not specifically trained in optical metrology.
— The results are usually displayed on a video monitor that allows a comfortable observation even for several operators simultaneously. Being the information in electronic format, either analogue or digital, it can be printed and stored without excessive additional costs.
— The reduced size achieved in modern video cameras allows the development of highly portable systems as needed for field applications, and even to miniaturise the optical sensor using microcameras to inspect remote areas.

Certainly, to get these benefits some of the features of classic holography must be sacrificed:

— The spatial resolution is substantially lower for video cameras than for holographic plates. This means not only that part of the detail is lost, moreover, it reduces the

measurement range as its upper limit is basically set by the maximum fringe density that the recording medium admits.

— In TVH the presence of speckle noise is much more noticeable than in HI, precisely because its size must be kept coarse enough to be resolved.

— The presence of speckle implies a sensitivity to de-correlation induced by the movements of the object, that in HI lead to a de-localisation of the fringes but in TVH can make them disappear.

— The cost of a basic TVH system is comparable to or higher than that of an elementary HI set-up because the first must include a computer equipped with an image digitiser, that is not essential for the second; but the incorporation of automatic fringe analysis and processing techniques to the basic TVH system involves a minimum extra cost.

Fresnel and Fourier TVH techniques are already at their first stages, just few of their potential variants have been investigated and, in our opinion, it is perhaps too early to analyse them from a global point of view. On the other hand, image-plane TV-holography have evolved from the original ESPI techniques during the last three decades and have reached a considerable degree of development.

Many reviews on image-plane TVH have been published and virtually cover all the existing methods and techniques from different points of view. Among them we may highlight those of Butters *et al* [28], Løkberg [29-31], Løkberg and Slettemoen [32], Jones and Wykes [33] and Davies and Buckberry [34].

In this review paper we propose a new systematic treatment for TVH techniques. We split the measurement process in four mutually independent stages, extract the different variants for each of them from the techniques reported by many authors and establish a common notation for all of them. These stages are conceived as building blocks with standard inputs and outputs that allow, on one hand, to combine with almost

total freedom the techniques proposed for each stage to obtain every particular version —already reported or not— of the whole TVH measurement process and, on the other, to incorporate new variants for a given stage keeping the compatibility with the techniques already established for the preceding and following stages so that a whole new set of combinations can be established.

2 A systematic approach to TV-holography

A TVH system (figure 1) comprises two clearly different groups of elements: the optical part, a speckle interferometer with electronic recording (ESPI), where the holograms —speckle interferograms— are generated, and the electronic part, where correlation fringes are eventually generated and analysed.

The ESPI is usually a two-beam interferometer, although it may also be a multiple-beam one. A beam splitter (BS) divides the light of a coherent source —typically a laser— among the two arms of the interferometer, one or both of them interact —either by reflection or transmission— with a diffusing object (OBJ) —or with two different objects to perform comparative measurements— and, finally, they pass through a beam combiner (BC) —that for some designs is the same beam splitter (BS)— to interfere on the sensitive element of a video camera (TVC). The instantaneous value of the measurand X at every point of the object is encoded in the resulting interferogram. The output of the video camera results of the integration of the incident irradiance during the exposure period of a video frame and, consequently, reflects the temporal evolution of the measurand during that time. The ESPI may incorporate additional elements used for the implementation of certain techniques; the most usual are speckle de-correlating devices (SDD), amplitude (AM) and phase (PM) modulators.

The role of the electronic part of the TVH system is to reveal the information related to the measurand that is present in the holograms recorded by the video camera.

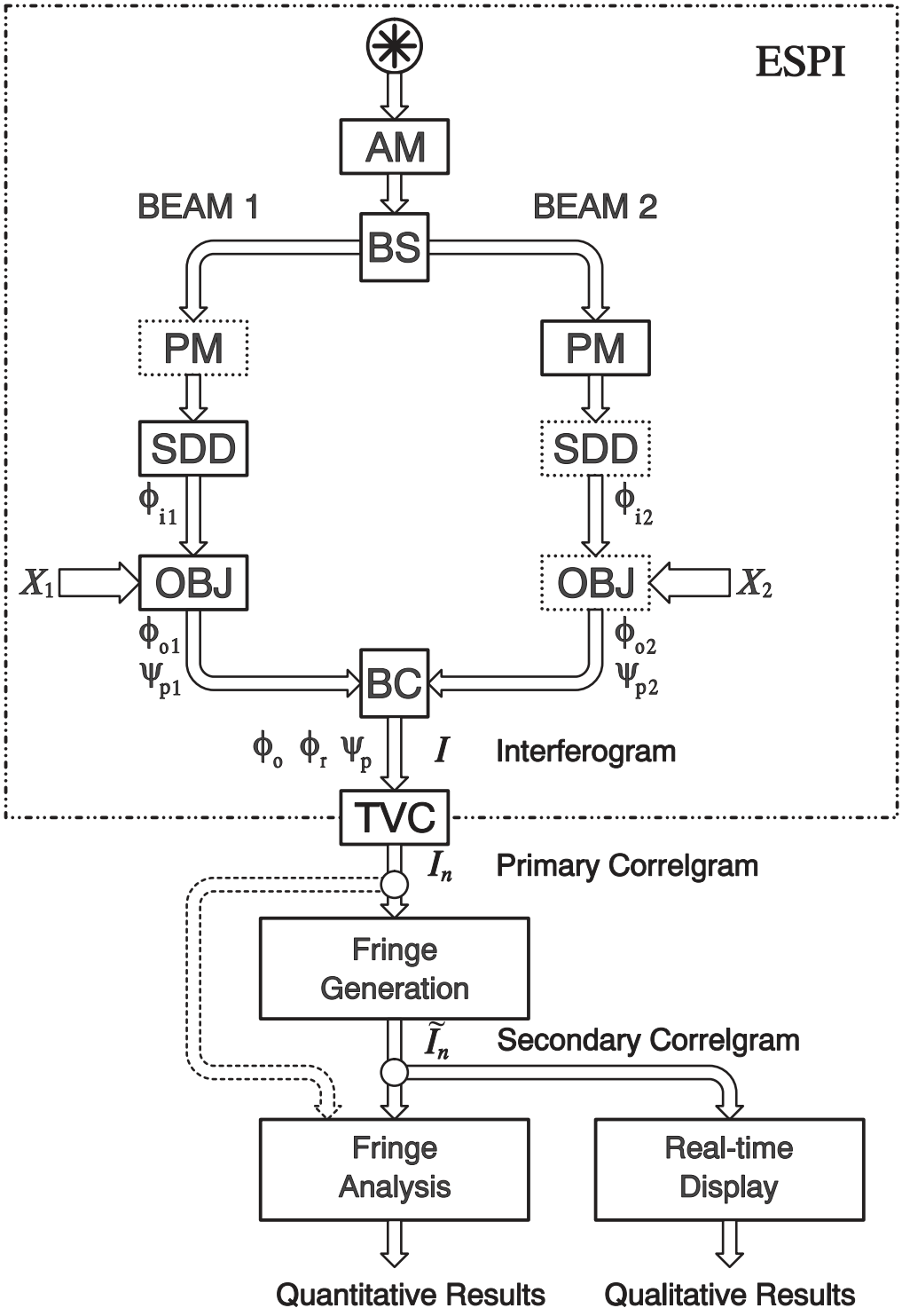

Figure 1 Scheme of a generic TVH system.

Ángel F. Doval

Figure 1

Its most elementary function is the generation of secondary correlation fringes; this corresponds, up to a point, to the reconstruction of a double or multiple-exposure hologram in HI although they are processes of different nature: in HI the secondary fringes are generated by the interference of true reconstructed wave fronts while in TVH they are obtained by electronic processing of the video signal that represents the hologram itself. The secondary fringe pattern is usually displayed in a video monitor, very often in real-time. Its observation provides essentially qualitative information about the value of the measurand.

A further fringe analysis process, also committed to the electronic subsystem and similar to those used with other interferometric techniques although adapted to the characteristic omnipresence of speckle noise, must be applied to either the secondary fringes or directly to the output of the video camera to yield quantitative measurements.

In our systematic approach to TVH we consider four stages in the measurement process, the first two related to the electronic speckle pattern interferometer (ESPI) and the last to the image processing subsystem as shown in figure 2. These stages are highly independent and the techniques corresponding to any of them can be combined with the others' almost without restrictions.

The first stage (§3) is the generation of a *speckle interferogram* with a given illumination and observation geometry. The technique implemented for this stage determines what is the nature of the measurand as well as the magnitude and direction of the sensitivity, i.e., how the measurand $X(\mathbf{x})$ is related to the optical phase-difference associated to the object $\phi_o(\mathbf{x})$ in the interferometer and, ultimately, to the instantaneous value of the intensity of the resulting interferogram.

The second (§4) is connected with the integration of the irradiance of the interferograms at the video camera during the exposure period. Both, the temporal treatment applied to the optical signal —i.e., amplitude and phase modulation— and the dynamic behaviour of the object during the integration period determine how the

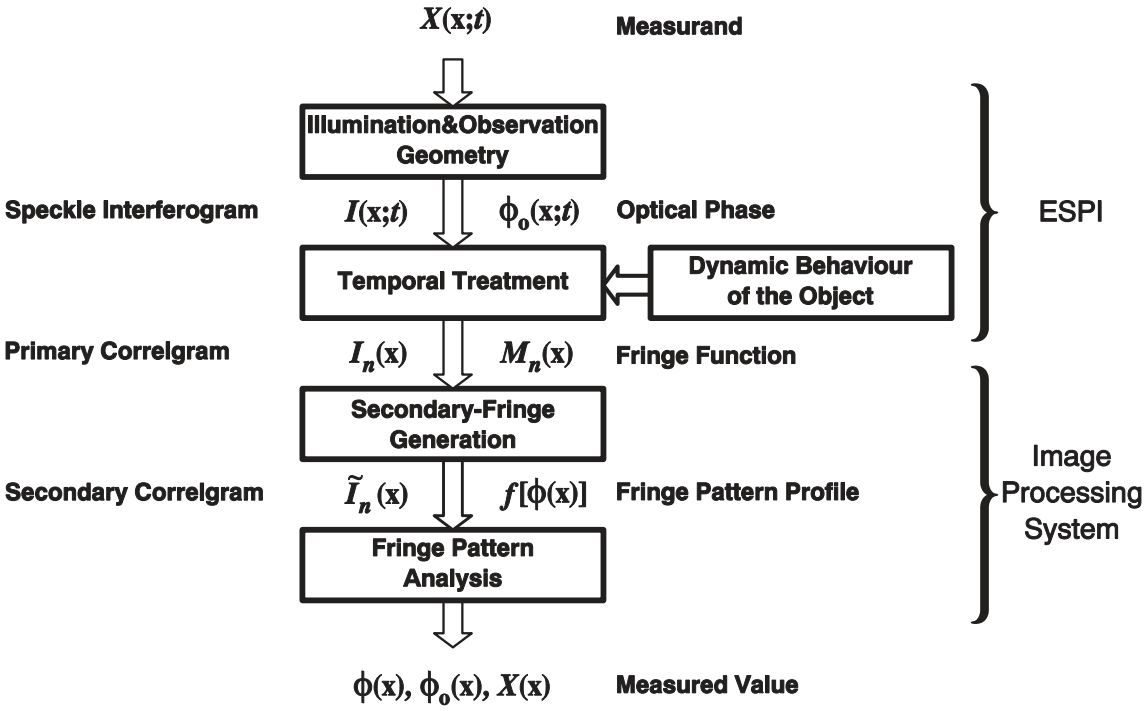

Figure 2 Block diagram of the TVH measurement process.

measurand-related optical phase difference $\phi_o(\mathbf{x})$ is encoded in the electronic images provided by the camera, that we call *primary correlgrams*; this relationship is formalised through the fringe function $M_n(\mathbf{x})$.

In primary correlgrams the information is embedded in the random speckle field. A third stage (§5), the generation of a *secondary correlgram*, must be applied if a fringe pattern with visible changes of the average intensity is required either to be displayed or quantitatively analysed. The phase $\phi(\mathbf{x})$ and the profile of the secondary correlgrams are related to both the fringe function $M_n(\mathbf{x})$ and the technique used to generate them.

The fourth and last of the stages (§6) in the TVH measuring process is fringe analysis to ultimately obtain the value of the measurand $X(\mathbf{x})$, its associated optical phase difference $\phi_o(\mathbf{x})$ or the phase of the fringe pattern $\phi(\mathbf{x})$. Most of current fringe analysis techniques are used in TVH with some particularities arising from the presence of the speckle noise.

3 Illumination and observation geometry

The sensitivity of speckle phase.

Although the optical phase of speckle patterns follows a random distribution in space, its increments due to the displacement of the diffuser, to the modification of the illumination and observation geometry, and to the changes of either the wavelength or the refraction index are deterministic and can be used to make measurements.

Throughout this article we will use a model inherited from holographic interferometry [32, p 465; 33, p 81 ff.] to quantify these increments. As shown in figure 3, the optical phase of a speckle pattern at each point of the observation plane can be written as

$$\psi \;=\; \psi_p + \phi \;=\; \psi_p + \phi_i + \mathbf{k}_i \cdot (\mathbf{r} - \mathbf{r}_i) + \mathbf{k}_o \cdot (\mathbf{r}_o - \mathbf{r}) \qquad (3.1)$$

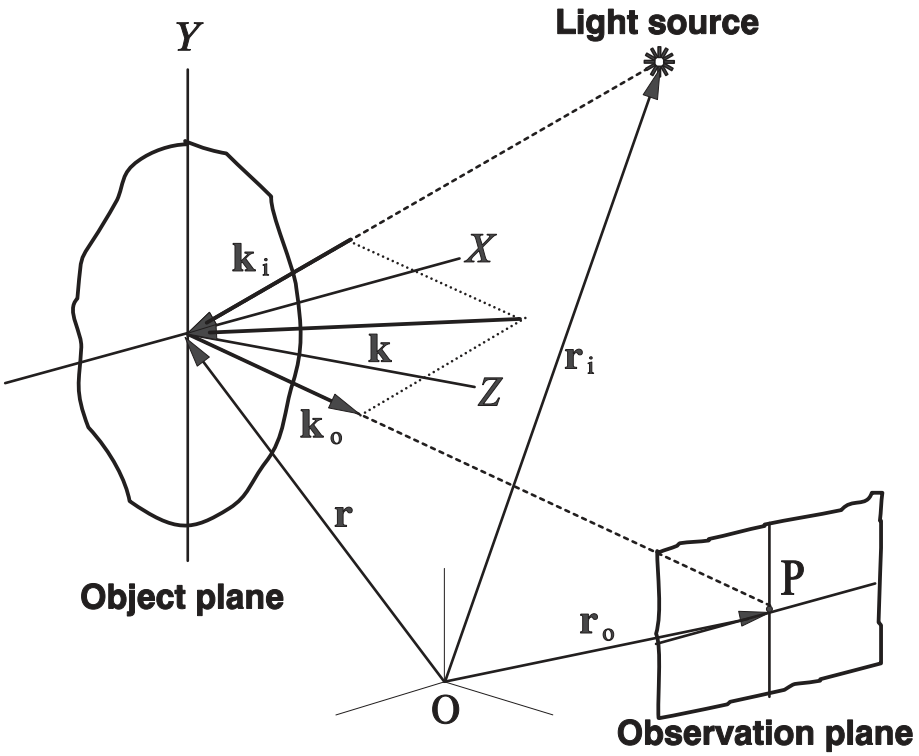

Figure 3 Geometry to analyse the sensitivity of speckle phase.

According to this expression, the phase of speckle ψ results of the sum of a random component ψ_p whose value depends of the particular distribution of roughness across the surface of the diffuser, and a deterministic component ϕ. This last comprises the initial optical phase of the light source ϕ_i as well as the phase delays due to the propagation from the source to the object $\mathbf{k}_i \cdot (\mathbf{r}-\mathbf{r}_i)$ and from this to the observation plane $\mathbf{k}_o \cdot (\mathbf{r}_o-\mathbf{r})$.

Both phase delays are functions of the position vectors of the considered point of the diffuser $\mathbf{r}$, the centre of curvature of the illuminating wave front $\mathbf{r}_i$ —typically representing the position of a point light source— and the observation point $\mathbf{r}_o$. Finally, $\mathbf{k}_i$ and $\mathbf{k}_o$ are the wave vectors of the illumination and observation directions (figure 3)

$$\mathbf{k}_i = \frac{2\pi}{\lambda}\hat{\mathbf{n}}_i \quad ; \quad \mathbf{k}_o = \frac{2\pi}{\lambda}\hat{\mathbf{n}}_o \tag{3.2}$$

being $\hat{\mathbf{n}}_i$ and $\hat{\mathbf{n}}_o$ the corresponding unit vectors.

By use of the *sensitivity vector* (figure 3), defined as

$$\mathbf{k} = \mathbf{k}_i - \mathbf{k}_o = \frac{2\pi}{\lambda}\left(\hat{\mathbf{n}}_i - \hat{\mathbf{n}}_o\right) \tag{3.3}$$

expression (3.1) can be written

$$\psi = \psi_p + \phi' + \mathbf{k} \cdot \mathbf{r} \tag{3.4}$$

with

$$\phi' = \phi_i + \mathbf{k}_o \cdot \mathbf{r}_o - \mathbf{k}_i \cdot \mathbf{r}_i \tag{3.5}$$

Any displacement of the diffuser or change of illumination and observation conditions yields an increment of the phase of speckle, given by

$$\Delta\psi = \Delta\psi_p + \Delta\phi' + \Delta(\mathbf{k} \cdot \mathbf{r}) \tag{3.6}$$

being

$$\Delta\phi' = \Delta\phi_i + \Delta(\mathbf{k}_o \cdot \mathbf{r}_o) - \Delta(\mathbf{k}_i \cdot \mathbf{r}_i) \tag{3.7}$$

and

$$\Delta(\mathbf{k}\cdot\mathbf{r}) = \left[(\mathbf{k}+\Delta\mathbf{k})\cdot(\mathbf{r}+\Delta\mathbf{r})\right] - (\mathbf{k}\cdot\mathbf{r}) = \Delta\mathbf{k}\cdot\mathbf{r} + \mathbf{k}\cdot\Delta\mathbf{r} + \Delta\mathbf{k}\cdot\Delta\mathbf{r} \tag{3.8}$$

where $\mathbf{k}\cdot\Delta\mathbf{r}$ is the phase increment due to the displacement of the object; $\Delta\phi'+\Delta\mathbf{k}\cdot\mathbf{r}$ is due to the changes of illumination and observation geometry, refraction index, wavelength and initial phase of the source; and $\Delta\mathbf{k}\cdot\Delta\mathbf{r}$ is the combined effect of the simultaneous change of both types of parameters.

Whenever changes neither affect the microstructure of the diffuser nor are large enough to produce significant global displacements of the speckle pattern, the random component of its optical phase remain virtually constant —i.e., $\Delta\psi_p \approx 0$— and all the observed increment is due to the deterministic component. Furthermore, in most practical situations it can be assumed that the object is displaced without changing illumination and observation conditions and vice versa, being also $\Delta\mathbf{k}\cdot\Delta\mathbf{r} \approx 0$.

The interference of speckle patterns

To exploit of the sensitivity of speckle phase it is necessary to transform its changes in variations of intensity. This is achieved through the interference of the original speckle pattern with either a smooth reference beam or another speckle pattern. Practically all the classic interferometers —Michelson's, Mach-Zehnder's, Fizeau's, etc— have been or can be adapted to operate with speckle patterns instead of smooth beams.

The interference of two perfectly coherent light fields yields an interference pattern following the well known expression

$$I = I_1 + I_2 + 2(I_1 I_2)^{1/2}\cos(\psi_1 - \psi_2) \tag{3.9}$$

where I_1 and I_2 are the local irradiances and ψ_1 and ψ_2 the optical phases of the interfering beams.

Equation (3.9) can be written in the more convenient form

$$I = \mathcal{I}_0\left[1 + \mathcal{V}\cos\left(\psi_1 - \psi_2\right)\right] \tag{3.10}$$

with the local *average irradiance* $\mathcal{I}_0$ and the *visibility* $\mathcal{V}$ of the interferogram defined as

$$\mathcal{I}_0 = I_1 + I_2 \tag{3.11}$$

$$\mathcal{V} = \frac{2\left(I_1 I_2\right)^{1/2}}{I_1 + I_2} \tag{3.12}$$

Expression (3.10) is also valid for partially coherent light, but the visibility is lower according to the more general definition

$$\mathcal{V} = \frac{2\left(I_1 I_2\right)^{1/2}}{I_1 + I_2}\left|\gamma(\tau)\right| \tag{3.13}$$

being $0 \le |\gamma(\tau)| \le 1$ the modulus of the *complex degree of coherence* [35].

These expressions can be applied in both classic and speckle interferometry; in classic interferometry the spatial distributions of $\mathcal{I}_0$, $\mathcal{V}$, ψ_1 and ψ_2 are essentially smooth and fully deterministic whilst in speckle interferometry they are random and, therefore, noisy.

In this last case, the one we are concerned with, two basic situations are apparent. The first arises when both interfering fields are speckle patterns; then, the statistical properties of the resulting speckle interferogram are similar to those of the original patterns [36, pp 19-29]. The second is the interference of a speckle pattern with a smooth reference beam; the resulting interferogram is also speckled, but with statistical properties departing of the original pattern [36, pp 29-34; 37].

Regardless of the nature of the interfering beams, in TV-holography the information related to the measurand is encoded in the difference between their optical phases $\psi_1 - \psi_2$. To give a uniform treatment for both types of techniques —those using two speckle patterns and those with a smooth reference beam— we shall write this *phase-difference*, using expression (3.4), as

$$\psi_1 - \psi_2 = \left(\psi_{\mathrm{p1}} - \psi_{\mathrm{p2}}\right) + \left(\phi_1' - \phi_2'\right) + \left(\mathbf{k}_1\mathbf{r}_1 - \mathbf{k}_2\mathbf{r}_2\right) = \psi_{\mathrm{p}} - \phi_{\mathrm{r}} + \phi_{\mathrm{o}} \tag{3.14}$$

where $\psi_p = \psi_{p1} - \psi_{p2}$ is the difference of the random components of the phase of the interfering speckle patterns and, therefore, has random spatial distribution and behaves as *phase noise*; $\phi_r = \phi'_2 - \phi'_1$ is the *reference phase-difference* that, in general, is deliberately introduced either changing the initial phases of the beams or modifying illumination and observation conditions —i.e., distance, direction, wavelength, etc—; and finally, $\phi_o = \mathbf{k}_1 \cdot \mathbf{r}_1 - \mathbf{k}_2 \cdot \mathbf{r}_2$ is the *object phase-difference*, related to the instantaneous position of each point of the surface of the diffusing object. This last term is the one that contains the usable information of the *speckle interferogram*, whose expression (3.10) results

$$I = \mathcal{I}_0 \left[1 + \mathcal{V} \cos\left(\psi_p - \phi_r + \phi_o \right) \right] \tag{3.15}$$

In the most general case, all the terms in expression (3.15) are functions of both time t and position $\mathbf{x} = (x,y)$ on the image plane. However, the following simplifying hypothesis can be assumed for most of practical speckle interferometers:

i) the speckle pattern neither experiments significant de-correlation nor transversal displacement during the measuring interval and consequently $\mathcal{I}_0$, $\mathcal{V}$ and ψ_p are independent of t;

ii) the illumination and observation directions for each beam are the same at all the points of the interferogram and therefore $\mathbf{k}_1$, $\mathbf{k}_2$ and ϕ_r do not depend of $\mathbf{x}$.

The first of these hypothesis sets an upper limit for the measurement range as well as stability requirements for the interferometric arrangement.

The second assumes the use of collimated illumination beams and telecentric observation. In practice, this is only feasible with relatively small objects; medium and large sized objects are illuminated with slightly diverging beams —generally obtained with spatial filters or monomode optical fibres— and observed with long focal objectives; condition ii) is then satisfied with a good degree of approximation placing their foci far enough from the object.

Using both hypothesis together with expression (3.15), the instantaneous value of the local intensity of the speckle interferogram corresponding to a given state of the object can be written as

$$I(\mathbf{x};t) = \mathcal{I}_0(\mathbf{x})\{1 + \mathcal{V}(\mathbf{x})\cos[\psi_p(\mathbf{x}) - \phi_r(t) + \phi_o(\mathbf{x};t)]\} \tag{3.16}$$

with

$$\phi_o(\mathbf{x};t) = \mathbf{k}_1(t)\cdot\mathbf{r}_1(\mathbf{x};t) - \mathbf{k}_2(t)\cdot\mathbf{r}_2(\mathbf{x};t) \tag{3.17}$$

In TV-holography, measurements are performed on a temporal intensity change basis that, with these hypothesis, is exclusively determined by the changes of the deterministic component of the optical phase difference $\Delta(\phi_o - \phi_r)$ and, considering that changes of the reference phase-difference $\Delta\phi_r$ are usually known, it lastly reflects the changes of the object phase-difference $\Delta\phi_o$.

Different illumination and observation geometry techniques can be classified in families characterised by the object-related parameter that $\Delta\phi_o$ represents. Attending to expressions (3.16) and (3.17), it is apparent that

i) keeping the sensitivity vectors constant, the object phase-difference changes are only due to the components of the *displacement* vector $\mathbf{u}(\mathbf{x};t) = \Delta\mathbf{r}(\mathbf{x};t)$;

ii) giving a known change to sensitivity vectors while the object is kept undeformed, object phase-difference increment is related to the *shape* of the object $\mathbf{r}(\mathbf{x})$;

iii) when refraction index of the medium surrounding a diffuser of known shape experiments changes, the magnitudes of the sensitivity vectors change accordingly — hypothesis ii) is then violated— and the increments of the object phase-difference reveal the local variations of the *refraction index*.

3.1 Displacement-sensitive interferometers

Displacement is measured in TVH using interferometers with fixed sensitivity vectors; thus, the object phase-difference increment is only related to the local

displacement of the object. The directions of the sensitivity vectors, given by the illumination and observation geometry, determine which component of $\Delta\mathbf{r}$ the interferometer is sensitive to, as well as how large such sensitivity is.

3.1.1 Out-of-plane (axial)

The sensitivity to displacements along the observation direction —out of the object plane of the image forming system and, with "ideal" (telecentric) observation, along the optical axis— is achieved with parallel illumination and observation directions (figure 4) that very often are also perpendicular to the surface of the object.

Only one beam, the *object beam*, illuminates the object while the other, the *reference beam* —that can be either smooth ($\psi_{p2} = 0$) or speckled ($\psi_{p2} \neq 0$)—, does not interact with it. The main difference between using a smooth or a speckled reference beam lies in the statistical properties of the resulting speckle interferograms. Those obtained with smooth reference beams have lower speckle contrast and are intrinsically less noisy; they have also larger average speckle size, what is a valuable feature when low resolution imaging devices as video cameras are used.

For both cases $\hat{\mathbf{n}}_o = -\hat{\mathbf{n}}_i$ and, following (3.3), the sensitivity vector of the object beam results

$$\mathbf{k}_1 = \frac{4\pi}{\lambda}\hat{\mathbf{n}}_i \tag{3.18}$$

while the sensitivity can be assumed zero in the reference beam ($\mathbf{k}_2 = \mathbf{0}$) as long as the state of the object does not affect its optical phase. The increment of the object phase-difference is, consequently, proportional to the axial displacement $w(\mathbf{x};t)$ of the diffuser; after substituting (3.18) in expression (3.17) and using the reference system shown in figure 4, it can be expressed

$$\Delta\phi_o(\mathbf{x};t) = \mathbf{k}_1 \cdot \Delta\mathbf{r}_1(\mathbf{x};t) = \frac{4\pi}{\lambda}\hat{\mathbf{n}}_i \cdot \Delta\mathbf{r}_1(\mathbf{x};t) = \frac{4\pi}{\lambda}\Delta z(\mathbf{x};t) = \frac{4\pi}{\lambda}w(\mathbf{x};t) \tag{3.19}$$

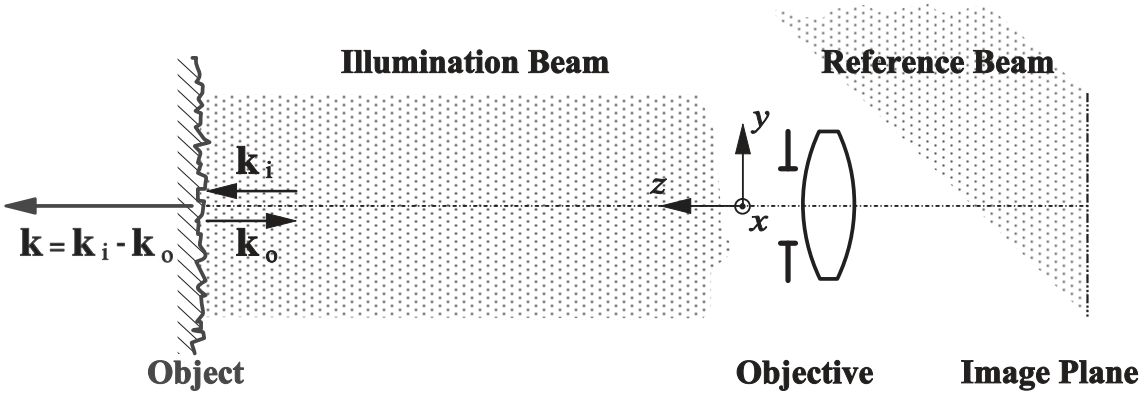

Figure 4 Typical illumination and observation geometry to get sensitivity to out-of-plane displacements.

This geometry is by far the most usual since the first steps of TVH; hence, there is a host of different implementations for it. They can be classified according to the type of reference beam —smooth or speckled—, to the type of classic interferometer they derive from and to the way that the beams are combined.

Out-of-plane sensitive interferometers with smooth reference beams are very popular devices and many configurations have been proposed by different authors.

Most of them derive from the Mach-Zehnder interferometer and use separated optical elements to split and combine again the object and reference beams. Generally, the reference beam is diverged —either real or virtually— from the centre of the output pupil of the objective (*in-line reference beam*) to keep the average grain size of the speckle interferograms as large as possible. This is achieved placing beam splitters —wedges [2], cubes [38], etc— between the objective lens and the image plane, mirrors with a hole the reference beam is passed through [39], tiny mirror balls placed behind the objective [34], concave mirrors carved on the rear surface of the objective lens [40] and optical fibres placed behind the objective [14, 41] or passed through a hole in the centre of the imaging lens [42]. Sometimes, the reference beam is diverged from a point placed out of the output pupil to separate the spectra of interference and additive speckle noise. This can be implemented either using an *off-axis reference beam* [5, 43] or with the aid of special lens apertures as the double slit [44].

Some authors have proposed arrangements based on other classic types of interferometers. For example, replacing one of the mirrors in a Michelson's interferometer by a diffusing object [45] or building quasi-common-path speckle interferometers based on Fizeau's by use of an optical flat [46] or a plano-concave [47] lens placed just in front of the diffuser to obtain a smooth reference beam. Even shearing interferometers with abnormally large shears [48] have been used to get the reference beam from a mirror placed side by side with the object.

Out-of-plane sensitive interferometers with speckle reference beams are not so widespread because they make a less efficient use of the available power —the aperture of the objective must be smaller than in smooth reference beam interferometers to obtain the same speckle average size— and the contrast of speckle noise is higher; on the other hand, they have the merits of ruggedness and simplicity of alignment. Several implementations have been proposed: modified Mach-Zehnder interferometers with the reference beam passed through a piece of ground glass interposed in its path [49], reflected on a diffuser placed at the rim of the objective lens [50], or passed through a diffuser that covers one half of the aperture of the objective [51]; other variants consist in forming an image of the object on a ground-glass screen obliquely illuminated with the reference beam and imaging the resulting speckle interferogram on the video camera [52] or placing a reference diffuser side by side with the object and overlapping their images by means of a sort of shearing interferometer with a stripped beam splitter that also plays the role of a special aperture stop [50]. Finally, the generation of a speckled reference beam through the reconstruction of the hologram of a diffuser [53] has been recently proposed.

Strictly speaking, and with independence of the type of reference beam, the illumination and observation directions must be parallel to get sensitivity only to out-of-plane displacements. Several authors have proposed solutions to satisfy this condition: illuminating and observing the object through a beam splitter, observing the object reflected on a plane mirror with a tiny hole to pass the illumination beam through [39] or illuminating the object with an optical fibre passed through a hole in the centre of the objective lens [42]. Nevertheless, it is very often accomplished with good approximation illuminating and observing from very close places when the object is conveniently far away.

It is worth to remark, finally, that out-of-plane sensitive interferometers can be used to measure displacements with components essentially parallel to the surface of the

object. This is achieved with very oblique illumination and observation [54] that, with the aid of prisms [55], can be made almost parallel to the surface of the object.

3.1.2 In-plane (transversal)

To get sensitivity to the displacements of the diffuser in a direction contained in the object plane —i.e., transversal to the observation direction—, two speckle patterns originated from the same object and obtained with conveniently chosen sensitivity vectors $\mathbf{k}_1$ and $\mathbf{k}_2$ are made interfere point to point —$\mathbf{r}_1(\mathbf{x};t) = \mathbf{r}_2(\mathbf{x};t) = \mathbf{r}(\mathbf{x};t)$— on the image plane of the video camera.

Following expression (3.17), the resulting object phase-difference is,

$$\phi_o(\mathbf{x};t) = (\mathbf{k}_1 - \mathbf{k}_2)\cdot\mathbf{r}(\mathbf{x};t) = \mathbf{K}\cdot\mathbf{r}(\mathbf{x};t) \tag{3.20}$$

The vector $\mathbf{K} = \mathbf{k}_1 - \mathbf{k}_2$ represents the global sensitivity of the interferometer. It is perpendicular to the observation direction whenever $\mathbf{k}_1$ and $\mathbf{k}_2$ have identical components along this last direction. Then, the changes of the object phase-difference can be expressed

$$\Delta\phi_o(\mathbf{x};t) = \mathbf{K}\cdot\Delta\mathbf{r}(\mathbf{x};t) = K_x u(\mathbf{x};t) + K_y v(\mathbf{x};t) \tag{3.21}$$

The geometry most often used in practice, developed by the pioneers of TVH [4], illuminates the object with two beams symmetrically tilted with respect to the observation direction as shown in figure 5. The magnitude of the resulting sensitivity is related to the tilt angle θ

$$K = |\mathbf{K}| = \frac{4\pi}{\lambda}\sin\theta \tag{3.22}$$

and therefore, the sensitivity can be controlled to have values between zero and $4\pi/\lambda$.

Double illumination can be obtained either through a beam splitter [56] or dividing de wavefront of a single illumination beam with a plane mirror placed near the object parallel to the observation direction [38]. Other not so widespread geometries are

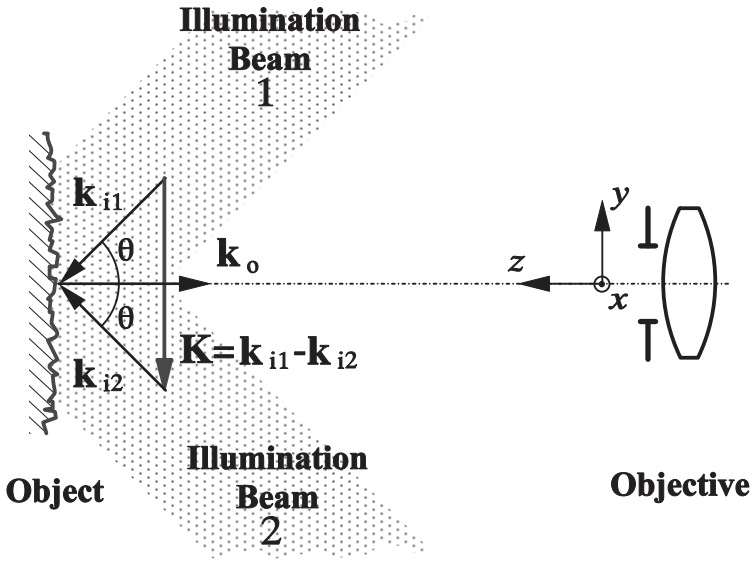

Figure 5 Typical illumination and observation geometry to get sensitivity to in-plane displacements.

the double symmetric observation direction [57], the combination of double illumination and observation to get twofold sensitivity [58, 59], and the double illumination with directions lying on perpendicular planes [28, p 135].

3.1.3 General directions

Speckle interferometers with sensitivity to displacement in general directions, with in-plane and out-of-plane components, are built combining convenient illumination and observation directions, either with object and reference beams or with double illumination. This type of configurations are used to get sensitivity with a particular direction (e.g., perpendicular to the surface of the object [60]), to control the magnitude of sensitivity (e.g., to reduce it [61]) and to obtain different components of the displacement vector, as needed to perform multi-dimensional measurements.

3.1.4 Two and three-dimensional displacements

The changes of the object phase-difference provide only the component of the displacement along the direction of the sensitivity vector. The full calculation of the displacement vector requires three measurements of object phase-differences made with independent sensitivity vectors $\mathbf{k}_1$, $\mathbf{k}_2$ and $\mathbf{k}_3$; the displacement vector is then obtained as the solution of the following system of linear equations [62]

$$\left.\begin{aligned}\Delta\phi_{o1} &= \mathbf{k}_1 \cdot \mathbf{u}\\ \Delta\phi_{o2} &= \mathbf{k}_2 \cdot \mathbf{u}\\ \Delta\phi_{o3} &= \mathbf{k}_3 \cdot \mathbf{u}\end{aligned}\right\} \Leftrightarrow \begin{pmatrix}\Delta\phi_{o1}\\ \Delta\phi_{o2}\\ \Delta\phi_{o3}\end{pmatrix} = \begin{pmatrix}k_{1x} & k_{1y} & k_{1z}\\ k_{2x} & k_{2y} & k_{2z}\\ k_{3x} & k_{3y} & k_{3z}\end{pmatrix}\begin{pmatrix}u\\ v\\ w\end{pmatrix} \Leftrightarrow \Delta\Phi_o = \mathbf{K}\cdot\mathbf{u} \tag{3.23}$$

$$\mathbf{u} = \mathbf{K}^{-1}\cdot\Delta\Phi_o \tag{3.24}$$

In-plane displacements are two-dimensional and, therefore, only two components are needed for their complete description. Their measurement is usually performed with

in-plane sensitive interferometers (§3.1.2) either sequentially, rotating the object [63] or the interferometer [64], or simultaneously, with crossed polarisation [65].

Three dimensional measurement techniques use three or more sensitivity vectors. This is achieved combining two in-plane an one out-of-plane sensitive interferometers [66], using a smooth reference beam interferometer with three [62, 67] or four [68] independent illumination directions in sequence or even with simultaneous multiple observation directions [69] and, finally, with a double illumination interferometer [70] keeping constant one of the illuminating directions and changing sequentially the other.

3.1.5 Difference of displacements

In the interference of two speckle patterns produced by two macroscopically identical objects illuminated and observed with the same geometry —i.e., $\mathbf{k}_1=\mathbf{k}_2=\mathbf{k}$— the object phase-difference is, according to expression (3.17)

$$\phi_o(\mathbf{x};t)=\mathbf{k}\cdot\left[\mathbf{r}_1(\mathbf{x};t)-\mathbf{r}_2(\mathbf{x};t)\right] \tag{3.25}$$

and its changes measure the difference of the displacements experimented by the objects

$$\Delta\phi_o(\mathbf{x};t)=\mathbf{k}\cdot\left[\Delta\mathbf{r}_1(\mathbf{x};t)-\Delta\mathbf{r}_2(\mathbf{x};t)\right]=\mathbf{k}\cdot\left[\mathbf{u}_1(\mathbf{x};t)-\mathbf{u}_2(\mathbf{x};t)\right] \tag{3.26}$$

The superposition of these speckle patterns is achieved by means of modified Twyman-Green interferometers with the objects instead of mirrors [71, 72] or with shear interferometers where the images of the objects, placed side by side, are superimposed by an abnormally large lateral shear [73]. The main use of these configurations is to compare the behaviour of production items with a standard prototype.

3.2 Spatial derivative of displacement sensitive (shearing) interferometers

Sensitivity to the spatial derivatives of displacement is obtained with image shearing interferometers, that can be regarded as a special class of difference of displacement sensitive interferometers where only one object is used.

Two images of the object, both obtained with the same illumination and observation directions —i.e. with the same sensitivity vector $\mathbf{k}_1 = \mathbf{k}_2 = \mathbf{k}$—, are superposed slightly out of record. As shown in figure 6, at each point of the sensor one has the interference of light coming from two different points of the object whose separation $\delta\mathbf{x}_o = (\delta x_o, \delta y_o)$ is the object shearing and its conjugate $\delta\mathbf{x} = (\delta x, \delta y) = M\ \delta\mathbf{x}_o$ is the image shearing.

Therefore

$$\mathbf{r}_2(\mathbf{x};t) = \mathbf{r}(\mathbf{x};t) \tag{3.27}$$

$$\mathbf{r}_1(\mathbf{x};t) = \mathbf{r}_2(\mathbf{x}+\delta\mathbf{x};t) = \mathbf{r}(\mathbf{x}+\delta\mathbf{x};t) \tag{3.28}$$

according to expression (3.17), the object phase-difference is

$$\phi_o(\mathbf{x};t) = [\mathbf{k}\cdot\mathbf{r}](\mathbf{x}+\delta\mathbf{x};t) - [\mathbf{k}\cdot\mathbf{r}](\mathbf{x};t) \tag{3.29}$$

and for small values of the shearing it becomes approximately proportional to the spatial derivatives of $\mathbf{k}\cdot\mathbf{r}$

$$\delta\mathbf{x}\to 0 \quad\Rightarrow\quad \phi_o(\mathbf{x};t) \approx \delta x\frac{\partial}{\partial x}[\mathbf{k}\cdot\mathbf{r}](\mathbf{x};t) + \delta y\frac{\partial}{\partial y}[\mathbf{k}\cdot\mathbf{r}](\mathbf{x};t) = (\delta\mathbf{x}\nabla)[\mathbf{k}\cdot\mathbf{r}](\mathbf{x};t) \tag{3.30}$$

Assuming that $\mathbf{k}$ is constant, (3.29) evidences that the changes of the object phase-difference measure the difference of displacement between the points of the object that have been imaged together

$$\Delta\phi_o(\mathbf{x};t) = \mathbf{k}\cdot[\Delta\mathbf{r}(\mathbf{x}+\delta\mathbf{x};t) - \Delta\mathbf{r}(\mathbf{x};t)] = \mathbf{k}\cdot[\mathbf{u}(\mathbf{x}+\delta\mathbf{x};t) - \mathbf{u}(\mathbf{x};t)] \tag{3.31}$$

that, with the approximation (3.30), is proportional to the spatial derivatives of displacement

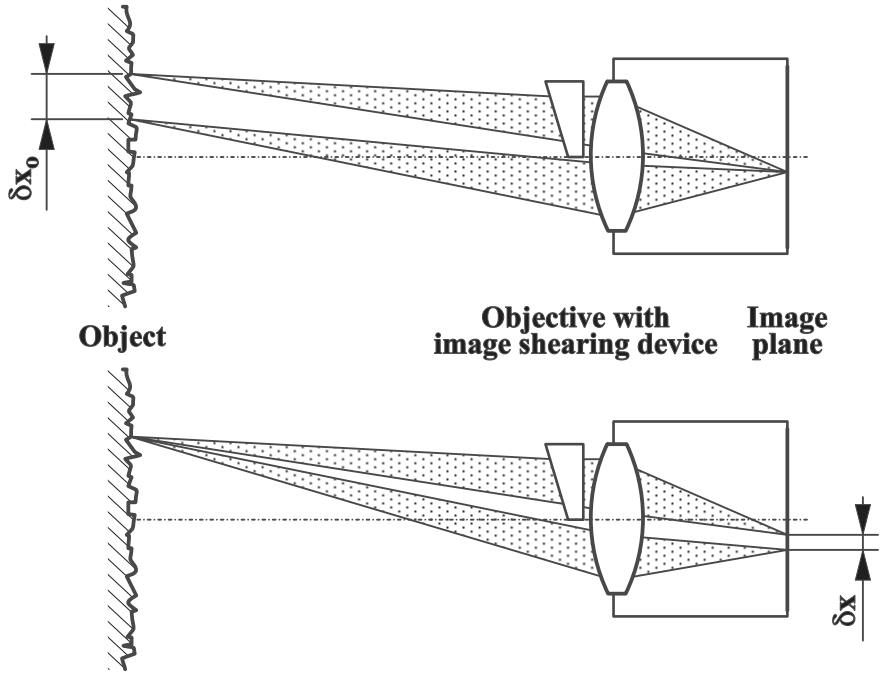

Figure 6 Geometry of an image shearing speckle interferometer. Two points of the object are imaged together at each point of the sensor and, reciprocally, each object point has two images.

$$\Delta\phi_o(\mathbf{x};t) \approx (\delta\mathbf{x}\nabla)[\mathbf{k}\cdot\mathbf{u}](\mathbf{x};t) = \delta x \frac{\partial}{\partial x}[\mathbf{k}\cdot\mathbf{u}](\mathbf{x};t) + \delta y \frac{\partial}{\partial y}[\mathbf{k}\cdot\mathbf{u}](\mathbf{x};t) \qquad (3.32)$$

As in displacement sensitive interferometers, the direction of the sensitivity vector **k** establishes which components of the displacement are present in $\Delta\phi_o$. Out-of-plane is the most usual, but in-plane [74, 75] and three-dimensional sensitivity [45] can be also achieved.

The direction of the shearing vector $\delta\mathbf{x}$ sets the direction of the spatial derivative. The overall sensitivity is proportional to the magnitude of the shearing as well as to that of the sensitivity vector.

The direction and magnitude of $\delta\mathbf{x}$ may be either the same or different at every point of the interferogram. According to this, several types of shearing are defined.

Lateral shearing is the most widely used variant. One of the images is transversally displaced and all its points experiment the same shearing regardless of their positions. Typically $\delta\mathbf{x} = (\delta x, 0)$ or $\delta\mathbf{x} = (0, \delta y)$ are taken to get derivatives along the coordinate axes. There have been described many techniques to obtain this kind of shearing [76]; among the most popular are: modified Michelson's interferometers with the object as light source and one of the mirrors tilted to introduce the shearing [33, p 156; 77]; wedge prisms [78], Fresnel's biprisms [79] or difraction gratings [80, 81] placed in front of the objective; split lenses [82, 83] or special difractive optical elements [84] used as objectives; and Wollaston prisms combined with circularly polarised light [85, 86].

Other types of shearing are radial [87], rotational, inversion and folding [88]. They can be implemented either with specific or general shearing devices [89].

Shearing and displacement-sensitive interferometers can be combined in a single instrument [48, 90] to get simultaneous sensitivity to the displacement and to its derivatives in the same interferogram.

One of the main benefits of shearing interferometry is that both beams follow almost the same path. This allows to use light sources with lower coherence than other TVH techniques; it is even possible to illuminate several areas on the object with different light sources [91] and get good interferograms.

3.3 Shape-sensitive interferometers

Unlike displacement-sensitive interferometers, in shape-sensitive ones the position of the points of the object **r** is constant and the sensitivity vector is changed by a known amount $\Delta\mathbf{k}$ to get an object phase-difference increment that follows an expression of the type:

$$\Delta\phi_o = \Delta\mathbf{k} \cdot \mathbf{r} \tag{3.33}$$

where the sensitivity to object shape is given by $\Delta\mathbf{k}$.

All the points with a given value of $\Delta\phi_o$ are placed on the intersection of the object with a set of surfaces —the *contouring surfaces*— that are perpendicular to the vector $\Delta\mathbf{k}$ and separated by a distance $2\pi/|\Delta\mathbf{k}|$ —the *contouring interval*.

Contouring surfaces may have any shape and orientation, although the interpretation of the resulting fringes is easier when they are planes perpendicular to the observation direction.

Contouring techniques can be classified in three groups according to the shape of the illuminating wavefront [92, pp 180-191]:

a) *Absolute contouring.* Using collimated illumination the sensitivity vector is the same at every point, contouring surfaces are planes, and object phase-difference increments reveal the shape of the object. This is the most usual variant and will be assumed henceforth unless other is specified.

b) *Relative contouring*. Illuminating wavefronts are shaped with optical elements to be spherical or cylindrical [93]. Contouring surfaces became more general and $\Delta\phi_o$ measures the difference between these and the shape of the object.

c) *Comparative contouring*. The illuminating beam is generated, either directly [94] or holographically [95], from a standard nominally identical to the object under test to contour their differences.

The change $\Delta\mathbf{k}$ induced in the sensitivity vector must be small to avoid speckle de-correlation [96]. Care must also be taken to avoid unwanted changes of the reference phase-difference ϕ_r. These two restrictions impose a limit to the range of sensitivities that can be achieved with TVH contouring techniques.

As the sensitivity vector is (3.3)

$$\mathbf{k} = \mathbf{k}_i - \mathbf{k}_o = \frac{2\pi}{\lambda}(\hat{\mathbf{n}}_i - \hat{\mathbf{n}}_o) = \frac{2\pi n}{\lambda_0}(\hat{\mathbf{n}}_i - \hat{\mathbf{n}}_o) \tag{3.34}$$

its increments $\Delta\mathbf{k}$ can be induced by changing the wavelength in vacuum λ_o of the light source, the index of refraction n or the directions of illumination $\hat{\mathbf{n}}_i$ and observation $\hat{\mathbf{n}}_o$. Each of these three options gives rise to a different family of contouring techniques.

3.3.1 Two-wavelength contouring

This technique derives from a former method developed for holographic interferometry and was one of the first contouring techniques used with TVH. It is often implemented with out-of-plane sensitive interferometers (§3.1.1) where the wavelength of the light source is changed from λ_a to λ_b while the object remains undeformed. The sensitivity vector experiments thus an increment [33, pp 204-233; 92]:

$$\Delta\mathbf{k} = \frac{2\pi}{\Lambda}(\hat{\mathbf{n}}_i - \hat{\mathbf{n}}_o) \tag{3.35}$$

where

$$\Lambda = \frac{\lambda_a \lambda_b}{\lambda_a - \lambda_b} \tag{3.36}$$

is the *equivalent contouring wavelength*.

Contouring surfaces are perpendicular to the sensitivity vector —$\Delta\mathbf{k}$ is parallel to $\mathbf{k}$— and the contouring interval is proportional to Λ. The sensitivity of contouring increases with the change of wavelength up to a limit imposed by speckle de-correlation [96].

Wavelength changes can be attained switching among emission lines of Argon ion [92], dye or pulsed ruby lasers [25] and also by means of current [97] or temperature [98] modulation of laser diodes.

3.3.2 Double refraction index contouring

This technique also derives from holographic interferometry, and consists in changing the refraction index surrounding the object between exposures, generally by inmersion in a liquid [99, p 86]. Assuming that the refraction index is uniform, the sensitivity of contouring is

$$\Delta\mathbf{k} = \frac{2\pi}{\lambda_o}\Delta n\left(\hat{\mathbf{n}}_i - \hat{\mathbf{n}}_o\right) \tag{3.37}$$

In practice submerging the object to be contouring is very seldom possible and, therefore, this technique is rarely used.

3.3.3 Contouring by change of geometry

In this family of techniques, the increment of the sensitivity vector is induced by a change of the illumination $\hat{\mathbf{n}}_i$ or the observation direction $\hat{\mathbf{n}}_o$. Two groups of techniques can be considered according to the number of illumination beams used.

3.3.3.1 Single illumination

Implemented with modified Mach-Zehnder interferometers with sensitivity in general directions (§3.1.3) where $\Delta\mathbf{k}$ is induced slightly tilting the illumination direction [100-102]

$$\Delta\mathbf{k} = \frac{2\pi}{\lambda}\Delta\left(\hat{\mathbf{n}}_{\mathrm{i}} - \hat{\mathbf{n}}_{\mathrm{o}}\right) = \frac{2\pi}{\lambda}\Delta\hat{\mathbf{n}}_{\mathrm{i}} \tag{3.38}$$

If the tilt angle $\delta\beta$ is small, $\Delta\hat{\mathbf{n}}_{\mathrm{i}} \perp \hat{\mathbf{n}}_{\mathrm{i}} \Rightarrow \Delta\mathbf{k} \perp \mathbf{k}_{\mathrm{i}}$ and, consequently, contouring surfaces are parallel to the illumination direction and the contouring interval is

$$\frac{2\pi}{|\Delta\mathbf{k}|} \approx \frac{\lambda}{\delta\beta} \tag{3.39}$$

3.3.3.2 Double illumination

Although it is possible to design contouring techniques with general geometries [103, 104], it is usual to employ interferometers with double illumination symmetrical with respect to the observation direction as those dedicated to the measurement of in-plane displacements (§3.1.2). The global sensitivity vector of the interferometer **K** is modified by a relative tilt between the object and the illumination directions

$$\Delta\mathbf{K} = \Delta\left(\mathbf{k}_1 - \mathbf{k}_2\right) = \frac{2\pi}{\lambda}\Delta\left(\hat{\mathbf{n}}_{\mathrm{i}1} - \hat{\mathbf{n}}_{\mathrm{i}2}\right) \tag{3.40}$$

The orientation of the contouring surfaces and the value of the contouring interval are determined by how the tilt is performed:

a) *Tilting the object*

If the object is rotated a small angle $\delta\beta$ [105] the magnitude of **K** does not change and therefore $\Delta\mathbf{K} \perp \mathbf{K}$ and the contouring surfaces are perpendicular to the observation direction. The contouring interval depends of the illumination θ and tilt $\delta\beta$ angles and of the tilt axis [106]; for a tilt axis in the object plane and perpendicular to the sensitivity vector **K** its value is

$$\frac{2\pi}{|\Delta\mathbf{K}|} \approx \frac{\lambda}{2\delta\beta\sin\theta} \tag{3.41}$$

b) *Tilting the illumination*

The observation direction is kept constant while one or both illuminating beams are slightly tilted by $\delta\beta$ around an axis perpendicular to the plane that contains the illumination and observation directions. Three variants have been proposed [103, 107]:

— *Only one illumination beam is tilted*. As for single illumination (§3.3.3.1) the contouring surfaces are perpendicular to this beam and the contouring interval follows expression (3.39).

— *Both beams are tilted by the same angle in the same direction*. This is equivalent to tilting the object (§3.3.3.2 a). The contouring surfaces are perpendicular to the observation direction and the contouring interval is given by expression (3.41).

— *Both beams are tilted by the same angle in opposite directions*. The contouring surfaces are parallel to the observation direction and the contouring interval follows once again expression (3.41).

The tilting of the illumination directions, common to all these techniques, can be implemented with tilting mirrors, translating lenses [107, 108], switching two sets of fixed illumination beams [109] or with tilting diffraction gratings [110]. Large objects have to be illuminated with diverging beams; in that case the tilt can be performed translating their foci [101], but the effect of the curved wavefront must be corrected [111] for absolute contouring.

3.3.4 Contouring by limited coherence

This last group of techniques is also called *single fringe contouring* [112]. Low coherence sources and balanced interferometers are used to get non-zero visibility in the speckle interferogram —$\mathcal{V}(\mathbf{x})\neq 0$— just in the points of the object where the optical path

difference is almost zero. This single fringe of contrasted speckle is used to scan the contour of the object as the length of one of the arms of the interferometer is changed.

3.4 Refraction index sensitive interferometers

The measurement range of TV-holography has been recently extended to the measurement of spatial distributions of refraction index —*phase objects*— as those due to pressure or temperature fields in liquids and gases.

The techniques proposed up to date use interferometers with parallel illumination and observation directions, generally with an uniform reference beam, and the phase object is placed in front of a diffusing background. The object phase-difference is related, aside of the shape of the diffuser **r**(**x**), to the *optical thickness* of the phase object along the observation direction (z axis) by

$$\phi_o(\mathbf{x};t) = \mathbf{k}\cdot\mathbf{r}(\mathbf{x}) + q\frac{2\pi}{\lambda_0}\int_{\text{Object}}[n_o(x,y,z;t)-n]dz \tag{3.42}$$

being q the number of times the illumination beam passes through the object, λ_o the wavelength in vacuum of the light source, n the refraction index of the medium surrounding the set-up and $n_o(x,y,z;t)$ that of the phase object at a given position and time.

With a static background, the increment of ϕ_o measure the changes of the optical thickness. The spatial distribution of refraction index $n_o(x,y,z;t)$ can be obtained measuring the optical thickness along different directions and applying tomographic reconstruction techniques [113-116].

Two variants can be considered from the basic geometry [117]: reflection and transmission.

3.4.1 Reflection geometry

The diffuser is illuminated from the same side that the object is observed (figure 7-a) so that illumination and observation have opposite directions and light passes twice through the phase object. The object phase difference is then given by

$$\phi_{\mathrm{o}}(\mathbf{x};t)=\frac{4\pi}{\lambda_0}\left\{\hat{\mathbf{n}}_{\mathrm{i}}\cdot\mathbf{r}(\mathbf{x})+\int_{\mathrm{Object}}[n_{\mathrm{o}}(x,y,z;t)-n]dz\right\} \tag{3.43}$$

3.4.2 Transmission geometry

The diffuser is illuminated and observed in the same direction [113] and light passes just once through the object. The sensitivity vector is

$$\mathbf{k}_{\mathrm{i}}=\mathbf{k}_{\mathrm{o}}\Rightarrow\mathbf{k}=\mathbf{k}_{\mathrm{i}}-\mathbf{k}_{\mathrm{o}}=0 \tag{3.44}$$

and the object phase-difference becomes

$$\phi_{\mathrm{o}}(\mathbf{x};t)=\frac{2\pi}{\lambda_0}\int_{\mathrm{Object}}[n_{\mathrm{o}}(x,y,z;t)-n]dz \tag{3.45}$$

This implies that, although one half sensitive to optical thickness, this variant is much less sensitive to the instabilities of the diffuser than the previous.

The object may be placed either in front of or behind the diffuser (figure 7-b and c). The last of these configurations avoids the de-correlation of speckle by the changes of direction that light may experiment as it passes through the phase object [118].

4 Temporal treatment

The description of the temporal treatment of speckle interferograms in TVH is greatly simplified using the concept of *fringe function*, introduced by Stetson [119] for holographic interferometry and later developed by other authors.

According to expression (3.16), the instantaneous irradiance at each point $\mathbf{x} = (x,y)$ of the sensor of the camera is

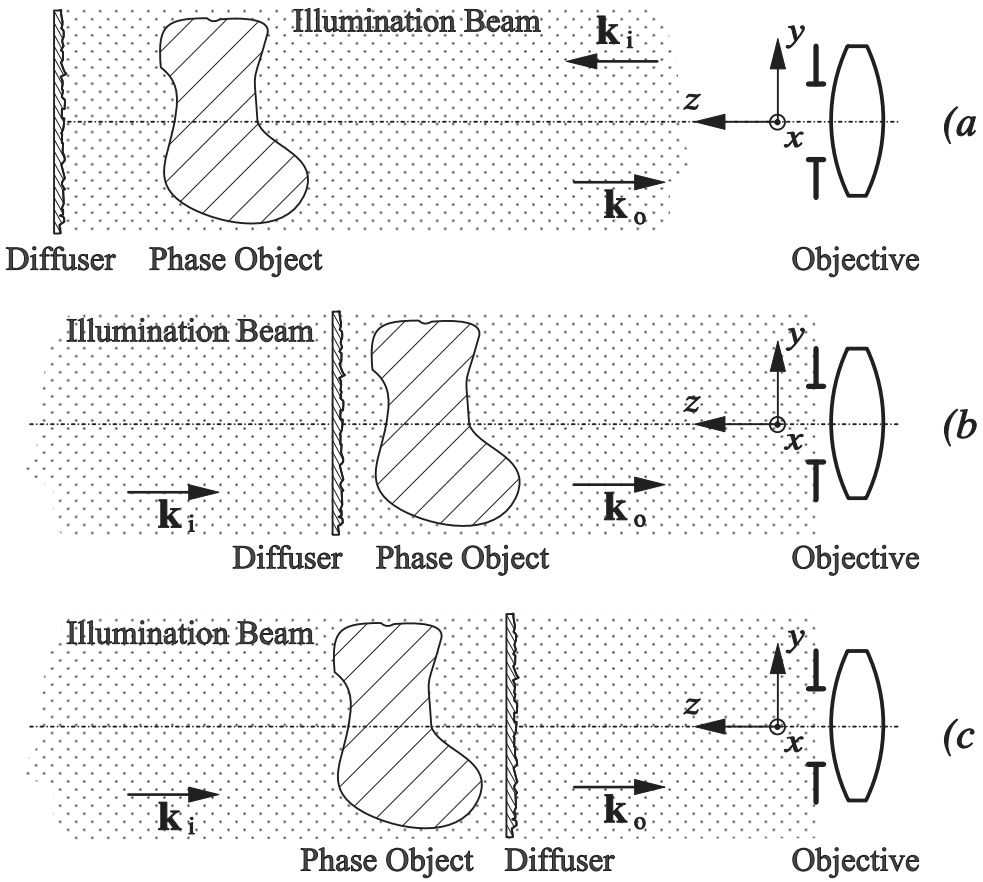

Figure 7 Illumination and observation geometries for the measurement of phase objects: a) reflection, b) transmission with the object in front of the diffuser, c) transmission with the diffuser in front of the object.

$$I(\mathbf{x};t) = \mathcal{I}_0(\mathbf{x})\left\{1 + \mathcal{V}(\mathbf{x})\cos\left[\psi_{\mathrm{p}}(\mathbf{x}) - \phi_{\mathrm{r}}(t) + \phi_{\mathrm{o}}(\mathbf{x};t)\right]\right\} \tag{4.1}$$

Video cameras integrate this irradiance in both space —over a pixel— and time —during a period equal or shorter than their frame period T_F—. As a result, the measured irradiance in the n-th video frame can be expressed [32, p 464]

$$I_n(\mathbf{x}) = I_n(x,y) = g\int_{-\infty}^{\infty}\int\left[\int_{-\infty}^{\infty} I(x',y';t')s_n(t')m_n(t_n - t')dt'\right]h_n(x-x',y-y')dx'dy' \tag{4.2}$$

This expression corresponds to an optoelectronically generated additive correlation pattern that from now on we will call a *primary correlgram*. Its parameters are:

$g = g(\lambda)$ the *spectral sensitivity* of the camera for the wavelength λ.

$t_n = t_n(x,y)$ the *reading instant*, corresponding to the end of the integration period of the pixel placed at position $\mathbf{x} = (x,y)$. Its expression depends on the integration mode of the camera [120].

$m_n(\Delta t)$ the *normalized exposure weighting function* of the camera [32, 120] that establishes the relative contribution of the instantaneous irradiance, within as well as out of the integration period, to the measured irradiance taking into account effects as persistence, electronic shuttering, ghost images, etc. Løkberg [32] includes in this function the effect of intensity modulation of the light source, but we find more convenient to consider this separately —$s_n(t)$— because its time dependence may not be referred to the reading instant as $m_n(\Delta t)$ is.

$s_n(t)$ the *intensity modulation* or *"shutter" function* of the light source. The definition of this function characterises each type of temporal treatment.

$h_n(\Delta x,\Delta y)$ the *spatial impulse response* of the camera, that describes its resolving power. It can be generalized to comprise factors as the temporal transfer

function of the amplifiers and filters of the camera [37] or the spatial resolution of the image storage systems.

Combining expressions (4.1) and (4.2) results

$$I_n(x,y) = g\int_{-\infty}^{\infty}\int \mathcal{I}_0(x',y')\times \\ \times\left\{1+\mathcal{V}(x',y')\int_{-\infty}^{\infty}\cos\left[\psi_{\mathrm{p}}(x',y')-\phi_{\mathrm{r}}(t')+\phi_{\mathrm{o}}(x',y';t')\right]s_n(t')m_n(t_n-t')dt'\right\}\times \\ \times h_n(x-x',y-y')dx'dy' \tag{4.3}$$

where

$$\cos\left[\psi_{\mathrm{p}}(x',y')-\phi_{\mathrm{r}}(t')+\phi_{\mathrm{o}}(x',y';t')\right] = \mathrm{Re}\left(\exp\left\{\mathrm{i}\left[\psi_p(x',y')-\phi_r(t')+\phi_o(x',y';t')\right]\right\}\right) \tag{4.4}$$

The *fringe function* is defined [119] as

$$M_n(\mathbf{x}) = M_n(x,y) = \int_{-\infty}^{\infty}\exp\left\{\mathrm{i}\left[\phi_o(x',y';t')-\phi_r(t')\right]\right\}s_n(t')m_n(t_n-t')dt' \tag{4.5}$$

if speckle does not experiment de-correlation during the exposure period ψ_{p1} and ψ_{p2} are constants and (4.3) can be written as

$$I_n(x,y) = g\int_{-\infty}^{\infty}\int \mathcal{I}_0(x',y')\left[1+\mathcal{V}(x',y')\mathrm{Re}\left\{\exp\left[\mathrm{i}\psi_{\mathrm{p}}(x',y')\right]M_n(x',y')\right\}\right]h_n(x-x',y-y')dx'dy' \tag{4.6}$$

The fringe function $M_n(\mathbf{x})$ gives an explicit description of the secondary fringes that can be extracted from the primary correlgram by fringe generation techniques. Here is the importance of its role: it quantifies the output of the TVH system. The expression of $M_n(\mathbf{x})$ as a function of ϕ_{o} and ϕ_{r} is characteristic of each temporal treatment technique.

When the average size of speckle is greater than or equal to a pixel and secondary fringes are wide —i.e., $\mathcal{I}_0$, ψ_{p}, $\mathcal{V}$ and ϕ_{o} are locally uniform at every pixel— expression (4.6) becomes simpler

$$I_n(\mathbf{x}) = g\mathcal{I}_0(\mathbf{x})\left[1 + \mathcal{V}(\mathbf{x})\,\mathrm{Re}\left\{\exp\left[\mathrm{i}\psi_\mathrm{p}(\mathbf{x})\right]M_n(\mathbf{x})\right\}\right] \tag{4.7}$$

Moreover, if the integration of irradiance in the camera is uniform during the whole integration period and persistence or ghost images are not present

$$m_n(\Delta t) = \begin{cases} \dfrac{1}{T_{\mathrm{e},n}} & 0 \le \Delta t \le T_\mathrm{F} \\ 0 & \text{otherwise} \end{cases} \tag{4.8}$$

where $T_{\mathrm{e},n}$ is the *effective exposure time*, that can be calculated from the intensity modulation function

$$T_{\mathrm{e},n} = \int_{t_n - T_\mathrm{F}}^{t_n} s_n(t')dt' \tag{4.9}$$

in this case, the fringe function is

$$M_n(\mathbf{x}) = \frac{1}{T_{\mathrm{e},n}} \int_{t_n - T_\mathrm{F}}^{t_n} \exp\left\{\mathrm{i}\left[\phi_\mathrm{o}(\mathbf{x};t') - \phi_\mathrm{r}(t')\right]\right\} s_n(t')dt' \tag{4.10}$$

Expressions (4.7) and (4.10), although corresponding to the most favourable conditions, are a good approximation for many real situations. We will use them to describe the main temporal treatment techniques used in TV-holography.

4.1 Time-average

The object is illuminated during a given *exposure interval* $[t_{1,n}, t_{2,n}]$ with a duration $T_{\mathrm{e},n} = t_{2,n} - t_{1,n}$ shorter than or equal to the frame period T_F.

Continuous emission lasers are suitable light sources for this temporal treatment mode. The exposure time can be controlled either with intensity modulators — acoustooptic, electrooptic, mechanical choppers— or with the electronic shutter of some cameras.

The intensity modulation function is (figure 8)

$$s_n(t) = \begin{cases} 1 & t_{1,n} \le t \le t_{2,n} \\ 0 & \text{otherwise} \end{cases} \tag{4.11}$$

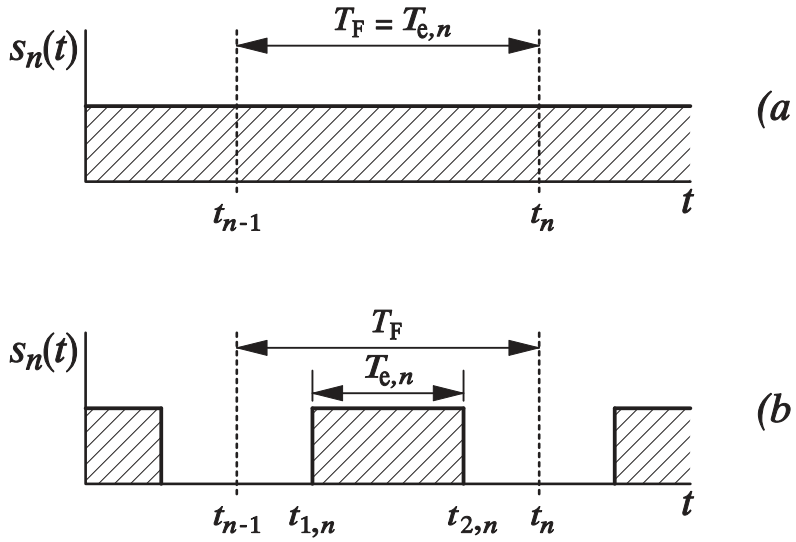

Figure 8 Shutter functions for time-average techniques: a) continuous illumination, b) illumination during a limited interval.

and the fringe function

$$M_n(\mathbf{x}) = \frac{1}{T_{\mathrm{e},n}} \int_{t_{1,n}}^{t_{2,n}} \exp\{\mathrm{i}[\phi_\mathrm{o}(\mathbf{x};t') - \phi_\mathrm{r}(t')]\} dt' \tag{4.12}$$

4.1.1 Static measurands

When the changes of the measurand are slow enough to assume that the object phase-difference ϕ_o is constant during the exposure period and the reference phase-difference ϕ_r is kept also constant, the fringe function results

$$M_n(\mathbf{x}) = \exp\{\mathrm{i}[\phi_\mathrm{o}(\mathbf{x}) - \phi_\mathrm{r}]\} \tag{4.13}$$

and, according to (4.7), primary correlgrams are

$$I_n(\mathbf{x}) = g\mathcal{I}_0(\mathbf{x})\{1 + \mathcal{V}(\mathbf{x})\cos[\psi_\mathrm{p}(\mathbf{x}) - \phi_\mathrm{r} + \phi_\mathrm{o}(\mathbf{x})]\} \tag{4.14}$$

4.1.2 Harmonic oscillation

When the object phase-difference experiments a sinusoidal oscillation it can be written

$$\phi_\mathrm{o}(\mathbf{x};t) = \phi_\mathrm{om}(\mathbf{x})\sin[\omega_\mathrm{o} t + \varphi_\mathrm{o}(\mathbf{x})] \tag{4.15}$$

where $\phi_\mathrm{om}(\mathbf{x};t)$ is the amplitude in terms of optical phase, ω_o is the angular frequency of oscillation and $\varphi_\mathrm{o}(\mathbf{x})$ is the mechanical phase.

Several variants are defined according to the relationship between the exposure interval $T_{\mathrm{e},n}$ and the mechanical oscillation period T_o, and to the type of modulation of the reference phase-difference ϕ_r.

4.1.2.1 Standard time-average

The exposure interval is much longer than the oscillation period ($T_{e,n} >> T_o = 2\pi/\omega_o$) and ϕ_r is kept constant during each exposure. The fringe function takes then the approximate value (e.g., Ref. [33, pp 107-109])

$$M_n(\mathbf{x}) \approx \exp(-i\phi_r) J_0[\phi_{om}(\mathbf{x})] \tag{4.16}$$

and therefore

$$I_n(\mathbf{x}) = g\mathcal{I}_0(\mathbf{x})\{1 + \mathcal{V}(\mathbf{x})\cos[\psi_p(\mathbf{x}) - \phi_r] J_0[\phi_{om}(\mathbf{x})]\} \tag{4.17}$$

The fringe function does not depend of the mechanical phase $\varphi_o(\mathbf{x})$, this information is lost. The reference phase-difference ϕ_r can be used to modify the phase noise of speckle, but has no effect on the argument of the Bessel's $J_0(\cdot)$ function that contains the usable information. These two drawbacks can be overcome using phase modulation techniques [121]; the most widely used in TVH are described in §4.1.2.4 and §4.1.2.5.

The exposure interval is usually the whole frame ($T_{e,n} = T_F$) or field ($T_{e,n} = T_f = T_F/2$) period of the video camera; although, if the oscillation frequency is high enough, it is possible to reduce it to make measurements on unstable objects or in noisy environments.

4.1.2.2 Reduced exposure time-average

The exposure interval $T_{e,n}$ is comparable to or shorter than the oscillation period T_o. This situation is typically reached when the oscillation frequency is close to the frame frequency of the camera, or when the exposure interval is reduced to a minimum in order to gain stability.

If the reference phase difference is kept constant during each exposure, the fringe function results [122, 123]

$$M_n(\mathbf{x}) = \exp(-\mathrm{i}\phi_\mathrm{r}) \sum_{q=-\infty}^{\infty} \left\{ \mathrm{J}_q[\phi_\mathrm{om}(\mathbf{x})] \exp\{\mathrm{i}q[\varphi_{\mathrm{m},n} + \varphi_\mathrm{o}(\mathbf{x})]\} \operatorname{sinc}\left(q \frac{T_{\mathrm{e},n}}{T_\mathrm{o}} \right) \right\} \tag{4.18}$$

where

$$\varphi_{\mathrm{m},n} = \frac{2\pi}{T_\mathrm{o}} \frac{t_{1,n} + t_{2,n}}{2} \tag{4.19}$$

is the average mechanical phase during the exposure interval.

4.1.2.3 Extended exposure time-average

For very low frequency oscillations —comparable to or lower than the frame frequency of the camera—, several images corresponding to primary correlgrams $I_n(\mathbf{x})$ obtained with the maximum exposure interval —typically $T_{\mathrm{e},n} = T_\mathrm{F}$— and randomly distributed average mechanical phase $\varphi_{\mathrm{m},n}$ can be averaged to get

$$\hat{I}_n(\mathbf{x}) = \frac{1}{N} \sum_{i=0}^{N} I_{n-i}(\mathbf{x}) \tag{4.20}$$

whose fringe function [123] is

$$M_n(\mathbf{x}) = \exp(-\mathrm{i}\phi_\mathrm{r}) \sum_{q=-\infty}^{\infty} \left\{ \mathrm{J}_q[\phi_\mathrm{om}(\mathbf{x})] \operatorname{sinc}\left(q \frac{T_{\mathrm{e},n}}{T_\mathrm{o}} \right) \right\} \tag{4.21}$$

4.1.2.4 Time-average with homodyne phase modulation

The reference phase-difference $\phi_\mathrm{r}(t)$ is sinusoidally modulated during the exposure interval with the same frequency of the object according to expression

$$\phi_\mathrm{r}(t) = \phi_\mathrm{rA} + \phi_\mathrm{rm} \cos(\omega_\mathrm{r} t + \varphi_\mathrm{r}) \tag{4.22}$$

where ϕ_rA is a phase offset that is kept constant during the exposure period, ϕ_rm is the amplitude of the modulation in terms of optical phase, $\omega_\mathrm{r} = \omega_\mathrm{o}$ its angular frequency and φ_r its mechanical phase.

The resulting fringe function is [121, 124]

$$M_n(\mathbf{x}) \approx \exp(-\mathrm{i}\phi_{\mathrm{rA}})\,\mathrm{J}_0\left(\left\{\phi_{\mathrm{om}}^2(\mathbf{x}) + \phi_{\mathrm{rm}}^2 - 2\phi_{\mathrm{om}}(\mathbf{x})\phi_{\mathrm{rm}}\cos[\varphi_{\mathrm{o}}(\mathbf{x}) - \varphi_{\mathrm{r}}]\right\}^{1/2}\right) \tag{4.23}$$

A particularly interesting case arises when the modulation is in phase with the oscillation of the object —$\varphi_{\mathrm{r}} = \varphi_{\mathrm{o}}(\mathbf{x})$, $\forall\mathbf{x}$—. The fringe function is then simplified to

$$M_n(\mathbf{x}) \approx \exp(-\mathrm{i}\phi_{\mathrm{rA}})\,\mathrm{J}_0[\phi_{\mathrm{om}}(\mathbf{x}) - \phi_{\mathrm{rm}}] \tag{4.24}$$

Homodyne modulation makes possible:

— To get fringes with sensitivity to both amplitude and phase of the oscillation of the object, and to shift them by means of the modulation parameters ϕ_{rm} and φ_{r} [125].

— To control the sensitivity of the fringe function to the amplitude of oscillation. This is achieved shifting the zero order fringe with an appropriate value of ϕ_{rm} in expression (4.24), and can be used to detect oscillations with either very small [124] or very large [126, 127] amplitudes.

— The implementation of phase shifting evaluation techniques [128] on time-average correlgrams.

The modulation of the reference phase-difference is usually derived from the signal used to excite the oscillation of the object. It is also possible to generate it from the measurand itself by optical [129] or optoelectronic [130, 131] means.

Homodyne modulation has been combined with reduced exposure (§4.1.2.2) to increase the immunity to object and environment instabilities. The fringe function [129, 132] becomes then more complicated than (4.23).

4.1.2.5 Time-average with heterodyne phase modulation

The reference phase-difference $\phi_{\mathrm{r}}(t)$ is sinusoidally modulated with an angular frequency $\omega_{\mathrm{r}} = \omega_{\mathrm{o}} + \delta\omega$ slightly different to the object's. Expression (4.22) is then

$$\omega_{\mathrm{r}} = \omega_{\mathrm{o}} + \delta\omega \quad \Rightarrow \quad \phi_{\mathrm{r}}(t) = \phi_{\mathrm{rA}} + \phi_{\mathrm{rm}}\sin[\omega_{\mathrm{r}}t + (\varphi_{\mathrm{r}} + \delta\omega t)] \tag{4.25}$$

The practical interest of such modulation arises when the difference between these frequencies $\delta\omega$ is so small that the term ($\varphi_r+\delta\omega t$) can be considered constant during each exposure period and the fringe function results

$$M_n(\mathbf{x}) \approx \exp(-\mathrm{i}\phi_{rA})\,\mathrm{J}_0\left(\left\{\phi_{om}^2(\mathbf{x})+\phi_{rm}^2-2\phi_{om}(\mathbf{x})\phi_{rm}\cos\left[\varphi_o(\mathbf{x})-(\varphi_r+\delta\omega t_n)\right]\right\}^{1/2}\right) \qquad (4.26)$$

Even if all the parameters —of the object oscillation and of the phase modulation— are constant, the value of the fringe function changes periodically with a frequency $\delta f = \delta\omega/2\pi$ wherever the amplitude of oscillation is not zero ($\phi_{om} \neq 0$). This allows the detection and measurement of extremely low amplitude oscillations. Sensitivity limits of 20 Å with visual observation and 0,1 Å with lock-in detection have been reported [120, 133].

4.1.3 General periodic measurands

General periodic oscillations can be expressed as Fourier series and the corresponding object phase-difference is

$$\phi_o(\mathbf{x};t) = \sum_{k=1}^{\infty} \phi_{om,k}(\mathbf{x})\cos\left[k\omega_o t + \varphi_{o,k}(\mathbf{x})\right] \qquad (4.27)$$

4.1.3.1 Standard time-average

Substituting expression (4.27) in (4.12) and considering an exposure interval much longer than the oscillation period ($T_{e,n} >> T_o = 2\pi/\omega_o$) results the following fringe function [134]

$$M_n(\mathbf{x}) \approx \mathrm{e}^{-\mathrm{i}\phi_r} \prod_{k=1}^{\infty} \mathrm{J}_0\left[\phi_{om,k}(\mathbf{x})\right] \qquad (4.28)$$

4.1.3.2 Time-average with phase modulation

When the reference phase-difference ϕ_{r} is sinusoidally modulated according to expression (4.22) with the frequency of the *j*-th harmonic $\omega_{\mathrm{r}} = j\omega_o$ the resulting fringe function is [134]

$$M_n(\mathbf{x}) \approx \exp(-\mathrm{i}\phi_{\mathrm{rA}})\,\mathrm{J}_0\left(\left\{\phi_{\mathrm{om},j}^2(\mathbf{x}) + \phi_{\mathrm{rm}}^2 - 2\phi_{\mathrm{om},j}(\mathbf{x})\phi_{\mathrm{rm}}\cos\left[\varphi_{\mathrm{o},j}(\mathbf{x}) - \varphi_{\mathrm{r}}\right]\right\}^{1/2}\right)\frac{\prod_{k=1}^{\infty}\mathrm{J}_0\left[\phi_{\mathrm{om},k}(\mathbf{x})\right]}{\mathrm{J}_0\left[\phi_{\mathrm{om},j}(\mathbf{x})\right]} \tag{4.29}$$

that reveals the amplitude and mechanical phase of that harmonic as well as the amplitudes of all the remainder harmonics. The information about the harmonic of interest can be extracted dividing expression (4.29) by (4.28). This allows to analyse general oscillations on a harmonic base, to apply them sensitivity control techniques and to evaluate the resulting fringes with phase-shifting techniques [135].

4.1.4 Non-periodic dynamic measurands

The applicability of time-average TVH to the measurement of non-periodic measurands is highly limited, although it is possible to analyse transient phenomena with such slow evolution that can be considered static (§4.1.1) during the exposure interval and oscillations with a damping factor low enough to assume that their amplitude, phase and frequency are constant during the exposure [10].

It is also possible to measure movements with constant speed during the exposure interval. As suggested in reference [122], the fringe function for this case is similar to its holographic interferometry counterpart [136, pp 93-94]. It can be found that

$$M_n(\mathbf{x}) = \exp(-\mathrm{i}\phi_{\mathrm{r}})\exp\left[\mathrm{i}\frac{\phi_{\mathrm{o}}(\mathbf{x};t_{1,n}) + \phi_{\mathrm{o}}(\mathbf{x};t_{2,n})}{2}\right]\frac{\sin\left(\frac{T_{\mathrm{e},n}}{2}\dot{\phi}_{\mathrm{o}}(\mathbf{x})\right)}{\frac{T_{\mathrm{e},n}}{2}\dot{\phi}_{\mathrm{o}}(\mathbf{x})} \tag{4.30}$$

with

$$\dot{\phi}_o(\mathbf{x}) = \frac{d\phi_o}{dt}(\mathbf{x}) \tag{4.31}$$

4.2 Stroboscopic illumination

The nature of stroboscopic techniques make them only useful for periodic or repetitive measurands. The object is illuminated with a train of light pulses synchronised to its oscillation —the width of these pulses T_p is shorter than the oscillation period ($T_p<T_o$)— resulting in a synchronous temporal sampling of the oscillation.

One of the main advantages of these techniques is that the instantaneous value of the measurand appears "frozen" as if it were static; this means that the fringe function is sinusoidal and, therefore, easier to interpret and evaluate than the Bessel's function that arises from time-average. Furthermore, the mechanical phase of the pulses can be controlled thus providing temporal resolution to scan the vibration cycle. The price for these benefits is a higher complexity in the interferometer and a lower economy of the available light power.

Pulsed lasers would seem ideal to provide this kind of illumination (figure 9-a), but in their current state of development they are only capable to operate in very limited frequency ranges and they are too expensive for most applications. It is more usual to modulate the intensity of continuous emission lasers with mechanical light choppers, acoustooptic and electrooptic modulators to generate finite width pulses (figure 9-b).

If the width of the pulses T_p is comparable to the oscillation period T_o, the stroboscopic method is equivalent to the superposition of multiple reduced exposure time-average correlgrams (§4.1.2.2) with the same average mechanical phase φ_m. The fringe function is then (4.18).

The width of the pulses must be conveniently short to consider that the object phase-difference is constant during it. Most of authors [30, 34, 137] assume that for

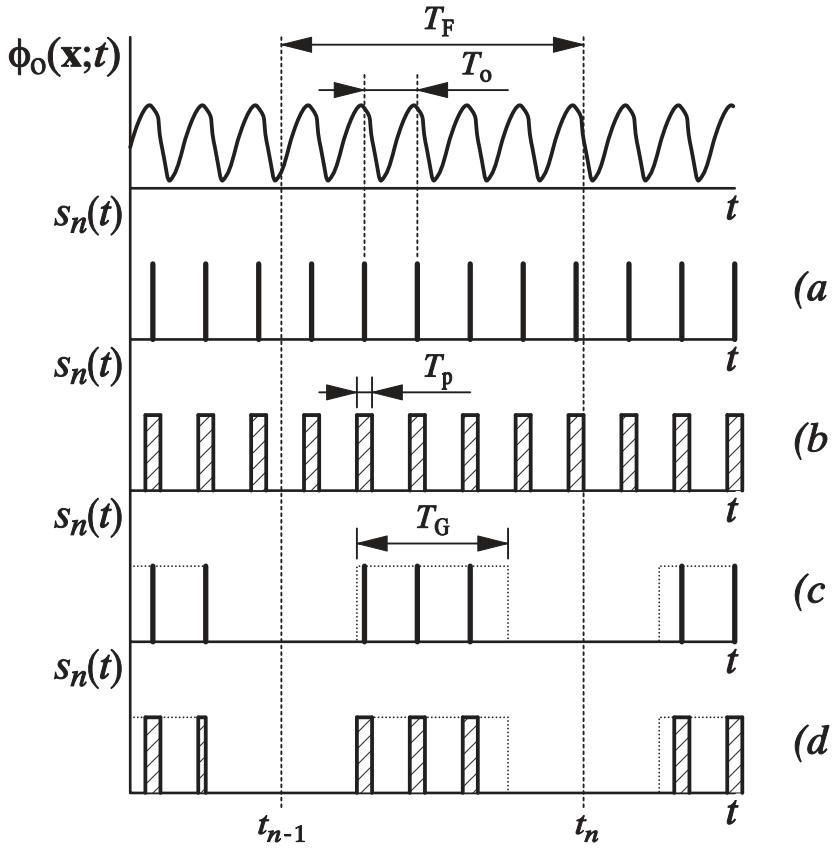

Figure 9 Shutter functions for stroboscopic illumination: a) ideal pulses (pulsed laser), b) finite length pulses (chopped laser), gated illumination with c) ideal and d) finite length pulses.

$T_p \leq T_o/10$ and moderate amplitudes the oscillation is effectively "frozen" in the mean instant of the pulses t_p and they can be reasonably represented as Dirac's delta functions

$$I(t) = \mathcal{I}_0 \delta(t - t_p) \tag{4.32}$$

The length of the stroboscopic pulse trains is usually the whole frame period of the video camera T_F; but illumination gates of shorter duration $T_G < T_F$ (figures 9-c and d) may be used for the measurement of unstable objects or in hostile environments, although with an even lower light economy.

4.2.1 General periodic measurands

When the measurand experiments a general oscillation with period T_o, the object phase-difference verifies

$$\phi_o(\mathbf{x}; t + kT_o) = \phi_o(\mathbf{x}; t) \tag{4.33}$$

Being $T_o < T_F$, in every primary correlgram a given number N of oscillation cycles are recorded and in each of them q light pulses are fired. When expression (4.32) is applicable, the intensity modulation function results

$$s_n(t) = \sum_{j=1}^{q} \mathrm{comb}\left(\frac{t - t_{pj,n}}{T_o} \right) \tag{4.34}$$

with [138]:

$$\mathrm{comb}(x) = \sum_{k=-\infty}^{+\infty} \delta(x - k) \tag{4.35}$$

the function "train of pulses" and $0 \leq t_{pj,n} \leq T_o$ the delays of the q light pulses with respect to the beginning of each oscillation cycle ($t = kT_o$).

The effective exposure time is, according to expression (4.9), $T_{e,n} = qN$. Considering expression (4.33) and assuming that the reference phase-difference ϕ_r and the oscillation are stable during each frame period, the fringe function results

$$M_n(\mathbf{x}) = \exp(-\mathrm{i}\phi_\mathrm{r})\frac{1}{q}\sum_{j=1}^{q}\exp\left[\mathrm{i}\phi_\mathrm{o}\left(\mathbf{x};t_{\mathrm{p}j,n}\right)\right] \tag{4.36}$$

To the best of our knowledge, only techniques with one or two pulses per oscillation cycle have been implemented in TVH, although the use of multiple pulses has been suggested [42] and its theoretical background is well known [121].

4.2.1.1 Single exposure

Only one light pulse with a delay $t_{\mathrm{p},n}$ (figure 10-a) is fired in each oscillation cycle. The fringe function is

$$M_n(\mathbf{x}) = \exp\left\{\mathrm{i}\left[\phi_\mathrm{o}\left(\mathbf{x};t_{\mathrm{p},n}\right) - \phi_\mathrm{r}\right]\right\} \tag{4.37}$$

and the intensity of the primary correlgram, according to expression (4.7), results

$$I_n(\mathbf{x}) = g\mathcal{I}_0(\mathbf{x})\left\{1 + \mathcal{V}(\mathbf{x})\cos\left[\psi_\mathrm{p}(\mathbf{x}) - \phi_\mathrm{r} + \phi_\mathrm{o}\left(\mathbf{x};t_{\mathrm{p},n}\right)\right]\right\} \tag{4.38}$$

that is equivalent to an static displacement (4.14) corresponding to the state of the object at the sampling instants $t = t_{\mathrm{p},n}+kT_\mathrm{o}$.

4.2.1.2 Double exposure

4.2.1.2.1 Standard double-exposure

Two pulses with different delays $t_{\mathrm{p1},n}$ and $t_{\mathrm{p2},n}$ are fired within each oscillation cycle (figure 10-b) or two bursts, with the same number of single light pulses but different delays, are fired alternately within the integration period of the camera [139]. The resulting fringe function is

$$M_n(\mathbf{x}) = \exp(-\mathrm{i}\phi_\mathrm{r})\frac{1}{2}\left\{\exp\left[\mathrm{i}\phi_\mathrm{o}\left(\mathbf{x};t_{\mathrm{p1},n}\right)\right] + \exp\left[\mathrm{i}\phi_\mathrm{o}\left(\mathbf{x};t_{\mathrm{p2},n}\right)\right]\right\} \tag{4.39}$$

that can be also written as

$$M_n(\mathbf{x}) = \exp(-\mathrm{i}\phi_\mathrm{r})\exp\left[\mathrm{i}\frac{\phi_\mathrm{o}\left(\mathbf{x};t_{\mathrm{p1},n}\right)+\phi_\mathrm{o}\left(\mathbf{x};t_{\mathrm{p2},n}\right)}{2}\right]\cos\left[\frac{\phi_\mathrm{o}\left(\mathbf{x};t_{\mathrm{p1},n}\right)-\phi_\mathrm{o}\left(\mathbf{x};t_{\mathrm{p2},n}\right)}{2}\right] \tag{4.40}$$

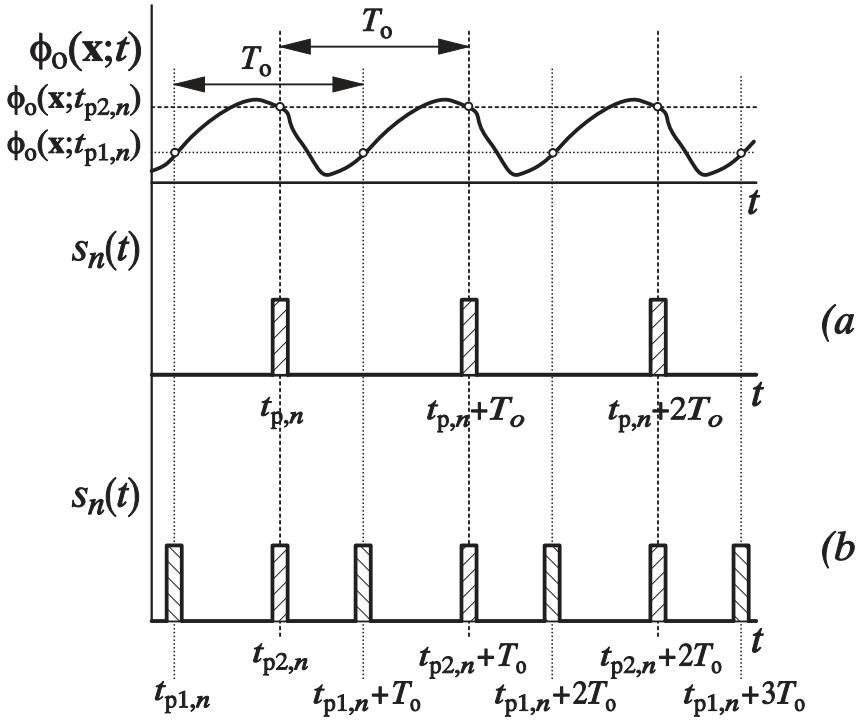

Figure 10 Shutter functions for a) single exposure and b) double exposure stroboscopic illumination.

Therefore, the intensity of the primary correlgrams depends sinusoidally of the change experimented by the object phase-difference between light pulses $\Delta\phi_o(\mathbf{x}) = \phi_o(\mathbf{x};t_{p1,n})-\phi_o(\mathbf{x};t_{p2,n})$.

4.2.1.2.2 Double exposure with synchronous phase-modulation

The reference phase-difference is modulated between each pair of pulses. The shape of the modulation is not as relevant as the value of the phase when the pulses are fired. The resulting fringe function is then [140, 141]

$$M_n(\mathbf{x}) = \cos\left[\frac{\Delta\phi_{o,n}(\mathbf{x})}{2} - \phi_{rS,n}\right]\exp\left\{i\left[\bar{\phi}_{o,n}(\mathbf{x}) - \phi_{rA,n}\right]\right\} \tag{4.41}$$

where $\Delta\phi_{o,n}(\mathbf{x})$ and $\bar{\phi}_{o,n}(\mathbf{x})$ are, respectively, the change between pulses and the average value of the object phase-difference, $\phi_{rS,n}$ is the amplitude of the phase modulation between pulses and $\phi_{rA,n}$ its mean value.

A pseudo-heterodyne effect [142] can be also achieved if the amplitude of the modulation is slightly increased between consecutive correlgrams.

4.2.2 Harmonic oscillation

When the object phase-difference follows a sinusoidal expression as (4.15), it is more convenient to speak in terms of mechanical phase φ_p rather than of pulse delays t_p; the relation between both parameters is trivial

$$\varphi_p = \frac{2\pi}{T_o}t_p = \omega_o t_p \tag{4.42}$$

and, therefore, at the sampling instant

$$\phi_o(\mathbf{x};t_p) = \phi_{om}(\mathbf{x})\sin\left[\varphi_p + \varphi_o(\mathbf{x})\right] \tag{4.43}$$

4.2.2.1 Single exposure

The expression of the primary correlgrams is obtained combining (4.43) and (4.38). When the light pulses are synchronised to the maxima —$\varphi_{\mathrm{p},n} = -\varphi_{\mathrm{o}}(\mathbf{x})$— or minima —$\varphi_{\mathrm{p},n} = \pi - \varphi_{\mathrm{o}}(\mathbf{x})$— the correlgram measures the amplitude of oscillation ϕ_{om}

$$I_n(\mathbf{x}) = g\mathcal{I}_0(\mathbf{x})\left\{1 + \mathcal{V}(\mathbf{x})\cos\left[\psi_{\mathrm{p}}(\mathbf{x}) - \phi_{\mathrm{r}} \pm \phi_{\mathrm{om}}(\mathbf{x})\right]\right\} \tag{4.44}$$

4.2.2.2 Double exposure

The combination of (4.43), (4.40) and (4.7) gives the expression of the primary correlgrams. It is specially interesting the case of equally spaced light pulses: $t_{\mathrm{p2},n} = t_{\mathrm{p1},n} + T_{\mathrm{o}}/2 \;\Leftrightarrow\; \varphi_{\mathrm{p2},n} = \varphi_{\mathrm{p1},n} + \pi \;\Leftrightarrow\; \phi_{\mathrm{o}}(\mathbf{x};t_{\mathrm{p2},n}) = -\phi_{\mathrm{o}}(\mathbf{x};t_{\mathrm{p1},n})$, then

$$I_n(\mathbf{x}) = gI_{\mathrm{m}}(\mathbf{x})\left(1 + V(\mathbf{x})\cos\left[\psi_{\mathrm{p}}(\mathbf{x}) - \phi_{\mathrm{r}}\right]\cos\left\{\phi_{\mathrm{om}}(\mathbf{x})\cos\left[\varphi_{\mathrm{p1},n} + \varphi_{\mathrm{o}}(\mathbf{x})\right]\right\}\right) \tag{4.45}$$

As in single exposure, when the pulses are matched to the extrema of the oscillation [49] —$\varphi_{\mathrm{p1},n} = -\varphi_{\mathrm{o}}(\mathbf{x})$— the primary correlgram shows the amplitude of oscillation

$$I_n(\mathbf{x}) = g\mathcal{I}_0(\mathbf{x})\left\{1 + \mathcal{V}(\mathbf{x})\cos\left[\psi_{\mathrm{p}}(\mathbf{x}) - \phi_{\mathrm{r}}\right]\cos\left[\phi_{\mathrm{om}}(\mathbf{x})\right]\right\} \tag{4.46}$$

but with ϕ_{om} made independent of the speckle phase noise as in time-average techniques (4.17).

4.2.3 General measurands

Stroboscopic techniques have been applied [143] to the measurement of transient events that are shorter than the frame period of the camera and can be accurately repeated. The transient is re-excited after its extinction at regular intervals, thus converting it in a periodic measurand (§4.2.1).

4.3 Pulsed illumination

The exposure of each video frame is achieved with a reduced number of high energy light pulses, typically one or two. The measurement time is very short and, therefore, these techniques are highly immune to object instability and environmental disturbance as required for industrial applications. Furthermore, being able of recording the state of the object in just one or two instants, this is the only TVH technique suitable for the analysis of transient events that, in general, are not repeatable as required for stroboscopic techniques (§4.2.3).

Light pulses with the required properties for TVH —i.e.: coherence, very small width (tens of nanoseconds) and high energy (several millijoule)— can be only obtained with pulsed lasers. Nevertheless, some authors [42] have used continuous emission lasers with acoustooptic or electrooptic intensity modulators, although with serious restrictions imposed by the lack of energy (small objects) and the length of the pulses (relatively slow measurands).

Ruby lasers have been traditionally used in TVH [62, 144 145], but the current trend is to use Nd:YAG lasers optimised for operation at video frame rates [13, 146, 147] —25 Hz Europe/30 Hz America— and also at field rates [148, 149] —50 Hz/60 Hz—. A few research groups have even used double cavity lasers to get very small pulse separations [150-152].

Very short light pulses can be represented by Dirac's delta functions and therefore

$$s_n(t) = \sum_{j=1}^{q} \delta\left(t - t_{\mathrm{p}j,n}\right) \tag{4.47}$$

where q is the number of pulses fired during the integration period of the video camera —T_F for frame integration cameras or T_f for field integration [153, 154]— and $t_{\mathrm{p}j,n}$ are the respective pulse delays. The effective exposure time is, according to (4.9), $T_{\mathrm{e},n} = q$ and the fringe function results

$$M_n(\mathbf{x}) = \exp(-\mathrm{i}\phi_\mathrm{r}) \frac{1}{q} \sum_{j=1}^{q} \exp\left[\mathrm{i}\phi_\mathrm{o}(\mathbf{x}; t_{\mathrm{p}j,n})\right] \tag{4.48}$$

This is the same expression found for stroboscopic illumination (4.36), but in this case no assumptions about the dynamics of the measurand or its stability are needed.

Several operating variants may be established according to the number of pulses fired during the integration period, as well as to their distribution respect to the video fields for interlaced scanning cameras [155].

4.3.1 Single exposure

The laser is fired at video frame rate, thus yielding a single pulse for each image (figure 11-a). The state of the measurand at the exposure time $t_{\mathrm{p},n}$ is recorded. The expressions of the fringe function and the primary correlgrams are the same of stroboscopic single exposure: (4.37) and (4.38).

4.3.2 Double exposure

Two pulses are fired at different instants $t_{\mathrm{p1},n}$ and $t_{\mathrm{p2},n}$ during the exposure interval (figure 11-b), therefore, the pulse frequency must be twice the frame frequency. The expressions of the fringe function (4.39) and the primary correlgrams are the same that for stroboscopic double exposure.

4.3.3 Combined exposure

4.3.3.1 Double single exposure

Field integration interline transfer CCD cameras with interlaced scanning [153, 154] have non overlapped integration periods for both image fields. Therefore, when they are illuminated with a single light pulse the image is present in just one half of the lines, even or odd ones. Some authors [156, 157] have used this operating particularity

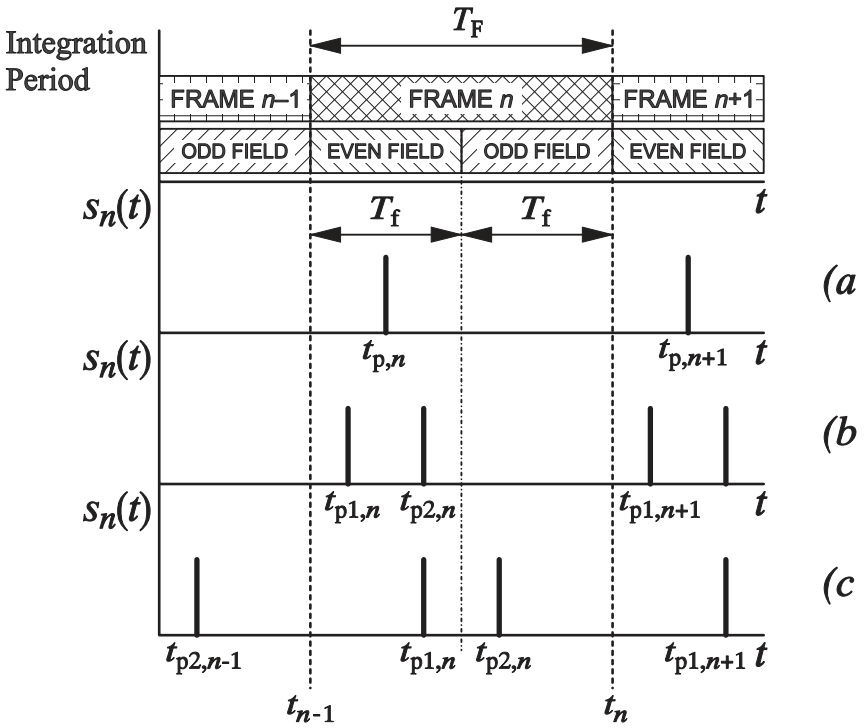

Figure 11 Shutter functions for pulsed TVH: a) single exposure, b) double exposure, c) double single-exposure.

to get two single exposure primary correlgrams corresponding to different instants $t_{\mathrm{p1},n}$ and $t_{\mathrm{p2},n}$ within a single image, one in each field (figure 11-c); this requires a pulsed laser operating at video field frequency.

4.3.3.2 Double exposure + double single exposure

Frame integration interline transfer CCD cameras with interlaced scanning [153, 154] have overlapped integration periods for both image fields. This kind of cameras has been used to get, with only two light pulses, a double exposure correlgram and the single exposure ones corresponding to both pulses in three consecutive video fields [155].

5 Secondary-fringe generation

One of the most noticeable characteristics of primary correlgrams is their random appearance, due to the distinctive spatial distribution of irradiance and phase of the speckle patterns. The information related to the measurand —i.e., the object phase-difference $\phi_{\mathrm{o}}(\mathbf{x};t)$— is contained in the fringe function $M_n(\mathbf{x})$ that modulates the speckle.

The fringe function can be expressed in terms of its modulus and argument

$$M_n(\mathbf{x}) = \mathrm{mod}[M_n(\mathbf{x})]\exp\{\mathrm{i}\,\arg[M_n(\mathbf{x})]\} \tag{5.1}$$

and the primary correlgrams (4.7) become

$$I_n(\mathbf{x}) = g\mathcal{I}_0(\mathbf{x})\{1+\mathcal{V}(\mathbf{x})\mathrm{mod}[M_n(\mathbf{x})]\mathrm{Re}(\exp[\mathrm{i}\,\psi_{\mathrm{p}}(\mathbf{x})]\exp\{\mathrm{i}\,\arg[M_n(\mathbf{x})]\})\} \tag{5.2}$$

$$I_n(\mathbf{x}) = g\mathcal{I}_0(\mathbf{x})(1+\mathcal{V}(\mathbf{x})\mathrm{mod}[M_n(\mathbf{x})]\cos\{\psi_{\mathrm{p}}(\mathbf{x})+\arg[M_n(\mathbf{x})]\}) \tag{5.3}$$

Speckle is present in two ways, with radically different behaviour: *intensity noise* and *phase noise*. Intensity noise is caused by the original irradiance distributions of the interfering speckle patterns and appears in both the average local intensity $\mathcal{I}_0(\mathbf{x})$ and in the visibility $\mathcal{V}(\mathbf{x})$ that are random variables with positive values and, consequently,

non-zero spatial mean values. Phase noise $\psi_p(\mathbf{x})$, already defined in §3, appears added to the argument of the fringe function; it is related to the random component of the phase in the interfering patterns and its spatial mean is zero, because its value is uniformly distributed between $-\pi$ and π.

This last fact implies that the mean value of $\cos\{\psi_p(\mathbf{x})+\arg[M_n(\mathbf{x})]\}$ is also zero and, hence, the *mean brightness* —i.e., the local spatial mean of the intensity— of the primary correlgrams is independent of the fringe function and, consequently, of the measurand. When one of these correlgrams is observed, no intensity fringes but random fluctuations of the speckle pattern are noticed.

To get a *secondary fringe pattern* revealing the changes of ϕ_o it is necessary to remove, as far as possible, the speckle carrier and extract the fringe function. The procedure to generate such secondary pattern can be understood as a spatial demodulation and allows several variants with different degrees of compromise between resulting fringe quality, processing time, simplicity of implementation, etc.

5.1 Types of primary correlgrams

Two kinds of primary correlgrams can be identified attending to the modulus of the fringe function. We call these two kinds: *phase modulated (PM) correlgrams* and *amplitude modulated (AM) correlgrams*.

Phase modulated correlgrams have a constant value for the modulus of their fringe function, typically: $\mathrm{mod}[M_n(\mathbf{x})] = 1$. The information related to the measurand is encoded in its argument and appears as local changes of the intensity distribution, not normally noticeable, that are evidenced only when at least two primary correlgrams with a change in the object phase-difference $\Delta\phi_o$ are compared. Correlgrams of this kind are obtained with the temporal treatment techniques where the interferogram does not experiment changes during the exposure period i.e.: time-average with static measurands and single exposure stroboscopic and pulsed techniques.

Amplitude modulated correlgrams have a fringe function whose modulus depends on the changes experimented by the object phase-difference during the exposure period: $\mathrm{mod}[M_n(\mathbf{x})] = f(\Delta\phi_o)$. The variation of $\mathrm{mod}[M_n(\mathbf{x})]$ yields primary correlation fringes of additive nature, that are present in the primary correlgram as changes in the contrast of speckle that can be seen with the naked eye, although with certain difficulty. AM correlgrams result from time-average techniques applied on measurands that change during the exposure period as well as from double exposure stroboscopic and pulsed techniques, where the interferograms corresponding to different states of the object are incoherently added.

Table 1 resumes the expressions of the modulus and the argument of the fringe functions corresponding to the main temporal treatment techniques used in TVH, indicating the kind of primary correlgrams provided by each of them.

For real-time displaying, primary correlgrams have to be electronically processed —either analogic or digitally— to transform the local changes of intensity or contrast of speckle in local variations of the mean brightness with some kind of demodulation process to get secondary correlgrams with well contrasted fringes. The secondary fringe generation process is very often used also as a first step for automatic evaluation of the object phase-difference, although this can be also implemented directly on primary correlgrams.

Fringe generation may also incorporate techniques to reduce the phase and intensity speckle noise either as a part of the secondary correlgram generation process or as a further filtering of the correlgrams.

5.2 Basic secondary-fringe generation techniques

The elementary techniques for the generation of secondary correlgrams can be classified in two families: those using a single primary correlgram and those using two of them.

Table 1 Primary correlgrams obtained with different temporal treatment techniques.

Temporal Treatment	Measurand	Exposure/ Modulation	Type	$M_{\mathrm{n}}(\mathbf{x})$	mod$[M_{\mathrm{n}}(\mathbf{x})]$	arg $[M_{\mathrm{n}}(\mathbf{x})]$
Time-Average	Static	Standard	PM	(4.13)	1	$\phi_{\mathrm{o}}(\boldsymbol{x})-\phi_{\mathrm{r}}$
	Harmonic	Standard	AM	(4.16)	$\mathrm{J}_0\left[\phi_{\mathrm{om}}(\boldsymbol{x})\right]$	$-\phi_{\mathrm{r}}$
		Homodyne	AM	(4.23)	$\mathrm{J}_0\left(\left\{\phi_{\mathrm{om}}^2(\mathbf{x})+\phi_{\mathrm{rm}}^2-2\phi_{\mathrm{om}}(\mathbf{x})\phi_{\mathrm{rm}}\cos\left[\varphi_{\mathrm{o}}(\mathbf{x})-\varphi_{\mathrm{r}}\right]\right\}^{1/2}\right)$	$-\phi_{\mathrm{rA}}$
	General Periodic	Standard	AM	(4.28)	$\prod_{k=1}^{\infty}\mathrm{J}_0\left[\phi_{\mathrm{om},k}(\boldsymbol{x})\right]$	$-\phi_{\mathrm{r}}$
		Homodyne with j-th Harmonic	AM	(4.29)	$\mathrm{J}_0\left(\left\{\phi_{\mathrm{om},j}^2(\mathbf{x})+\phi_{\mathrm{rm}}^2-2\phi_{\mathrm{om},j}(\mathbf{x})\phi_{\mathrm{rm}}\cos\left[\varphi_{\mathrm{o},j}(\mathbf{x})-\varphi_{\mathrm{r}}\right]\right\}^{1/2}\right)\times \frac{\prod_{k=1}^{\infty}\mathrm{J}_0\left[\phi_{\mathrm{om},k}(\mathbf{x})\right]}{\mathrm{J}_0\left[\phi_{\mathrm{om},j}(\mathbf{x})\right]}$	$-\phi_{\mathrm{rA}}$
	Constant Speed	Standard	AM	(4.30)	$\dfrac{\sin\left(\frac{T_{\mathrm{e},n}}{2}\dot{\phi}_{\mathrm{o}}(\boldsymbol{x})\right)}{\frac{T_{\mathrm{e},n}}{2}\dot{\phi}_{\mathrm{o}}(\boldsymbol{x})}$	$\dfrac{\phi_{\mathrm{o}}(\boldsymbol{x};t_{1,n})+\phi_{\mathrm{o}}(\boldsymbol{x};t_{2,n})}{2}-\phi_{\mathrm{r}}$
Stroboscopic (Pulsed)	General Periodic (General)	Single Exposure	PM	(4.37)	1	$\phi_{\mathrm{o}}(\boldsymbol{x};t_{\mathrm{p},n})-\phi_{\mathrm{r}}$
		Double Exposure Standard	AM	(4.40)	$\cos\left[\dfrac{\phi_{\mathrm{o}}(\boldsymbol{x};t_{\mathrm{p1},n})-\phi_{\mathrm{o}}(\boldsymbol{x};t_{\mathrm{p2},n})}{2}\right]$	$\dfrac{\phi_{\mathrm{o}}(\boldsymbol{x};t_{\mathrm{p1},n})+\phi_{\mathrm{o}}(\boldsymbol{x};t_{\mathrm{p2},n})}{2}-\phi_{\mathrm{r}}$
		Homodyne modulation	AM	(4.41)	$\cos\left[\dfrac{\Delta\phi_{\mathrm{o},n}(\mathbf{x})}{2}-\phi_{\mathrm{rS},n}\right]$	$\bar{\phi}_{\mathrm{o},n}(\mathbf{x})-\phi_{\mathrm{rA},n}$

In any case, the process comprises two stages. First, the continuous component of the primary correlgram —$g\,\mathcal{I}_0(\mathbf{x})$ in expression (5.3)— is removed and the local changes of intensity are converted in variations of the contrast of speckle. Second, square-law demodulation is applied to transform the local changes of contrast in secondary fringes of mean brightness. For real-time displaying this last stage is often approximated by a full wave rectification —i.e. the calculation of the absolute value—, easier to implement, whilst for automatic evaluation true square-law demodulation is preferred because of its lower harmonic distortion.

5.2.1 Spatial filtering of a single primary correlgram

This technique is only applicable to AM primary correlgrams, where contrast fringes are already present. The continuous component is removed by high pass (HP) spatial filtering. This is usually implemented on the video signal with dedicated analogue circuits.

High pass filtering is, up to a point, equivalent to subtract from the primary correlgram its average level —$\langle I_n(\mathbf{x})\rangle = g\langle \mathcal{I}_0(\mathbf{x})\rangle$—, and its result [37] can be schematised as follows

$$\mathrm{HP}[I_n(\mathbf{x})] = g\Big(\big[\mathcal{I}_0(\mathbf{x}) - \langle \mathcal{I}_0(\mathbf{x})\rangle\big] + \mathcal{I}_0(\mathbf{x})\mathcal{V}(\mathbf{x})\,\mathrm{mod}[M_n(\mathbf{x})]\cos\{\psi_{\mathrm{p}}(\mathbf{x}) + \arg[M_n(\mathbf{x})]\}\Big) \tag{5.4}$$

The secondary correlgram is obtained by square-law demodulation

$$\begin{aligned}\tilde{I}_n(\mathbf{x}) &= \{\mathrm{HP}[I_n(\mathbf{x})]\}^2 = \\ &= g^2\Big(\big[\mathcal{I}_0(\mathbf{x}) - \langle \mathcal{I}_0(\mathbf{x})\rangle\big]^2 + [\mathcal{I}_0(\mathbf{x})\mathcal{V}(\mathbf{x})]^2\,\mathrm{mod}[M_n(\mathbf{x})]^2\cos^2\{\psi_{\mathrm{p}}(\mathbf{x}) + \arg[M_n(\mathbf{x})]\} + \\ &\qquad + 2\big[\mathcal{I}_0(\mathbf{x}) - \langle \mathcal{I}_0(\mathbf{x})\rangle\big]\,\mathcal{I}_0(\mathbf{x})\mathcal{V}(\mathbf{x})\,\mathrm{mod}[M_n(\mathbf{x})]\cos\{\psi_{\mathrm{p}}(\mathbf{x}) + \arg[M_n(\mathbf{x})]\}\Big)\end{aligned} \tag{5.5}$$

and its local mean brightness can be easily found [33]

$$\begin{aligned}B_n(\mathbf{x}) = \langle \tilde{I}_n(\mathbf{x})\rangle &= g^2\left\{\sigma_0^2 + \frac{1}{2}\langle [\mathcal{I}_0(\mathbf{x})\mathcal{V}(\mathbf{x})]^2\rangle\,\mathrm{mod}[M_n(\mathbf{x})]^2\right\} \\ &= g^2\{\sigma_1^2 + \sigma_2^2 + 2\langle I_1(\mathbf{x})\rangle\langle I_2(\mathbf{x})\rangle\,\mathrm{mod}[M_n(\mathbf{x})]^2\}\end{aligned} \tag{5.6}$$

where $\langle\cdot\rangle$ represents the spatial averaging extended to a region where $M_n(\mathbf{x})$ has a constant value —such region must be much larger than the average size of speckle to get a significant average, i.e., fringes must be much wider than speckle—, and σ_0, σ_1 and σ_2 are the standard deviations of the local average intensity and of the intensities of the interfering beams, respectively. For the second identity it is assumed that I_1 and I_2 are statistically independent.

When this kind of secondary correlgrams are displayed in a monitor or when they are low pass filtered for automatic evaluation, a background level —$g^2\,(\sigma_1^2+\sigma_2^2)$— related to the contrast of the original speckle patterns appear superimposed to the changes of the mean brightness that are proportional to the modulus of the fringe function. The contrast of the secondary-fringe pattern is hence reduced as the contrast of the interfering patterns increases.

This fringe-generation technique requires neither storage nor numerical processing of the correlgrams (figure 12) and can be implemented in real-time with very simple analogue electronic circuits connected between the video camera and the monitor. It was the first to be used in TVH by Butters and Leendertz [1, 2]. Originally designed for time-average correlgrams of vibrating objects [93, 158], it has been also applied to double-exposure stroboscopic [159] and pulsed [153] correlgrams.

5.2.2 Subtraction of two primary correlgrams

PM correlgrams encode information related to the object phase-difference ϕ_o corresponding to a single state of the measurand that appears mixed with phase noise ψ_p. It is necessary to compare at least two of such correlgrams with a change $\Delta\phi_o$ of the object phase difference to get a secondary-fringe pattern. The easiest way to do this and, by far, the most commonly used is to subtract two primary correlgrams and apply then the square-law demodulation. Subtraction has two effects: on one hand yields a random

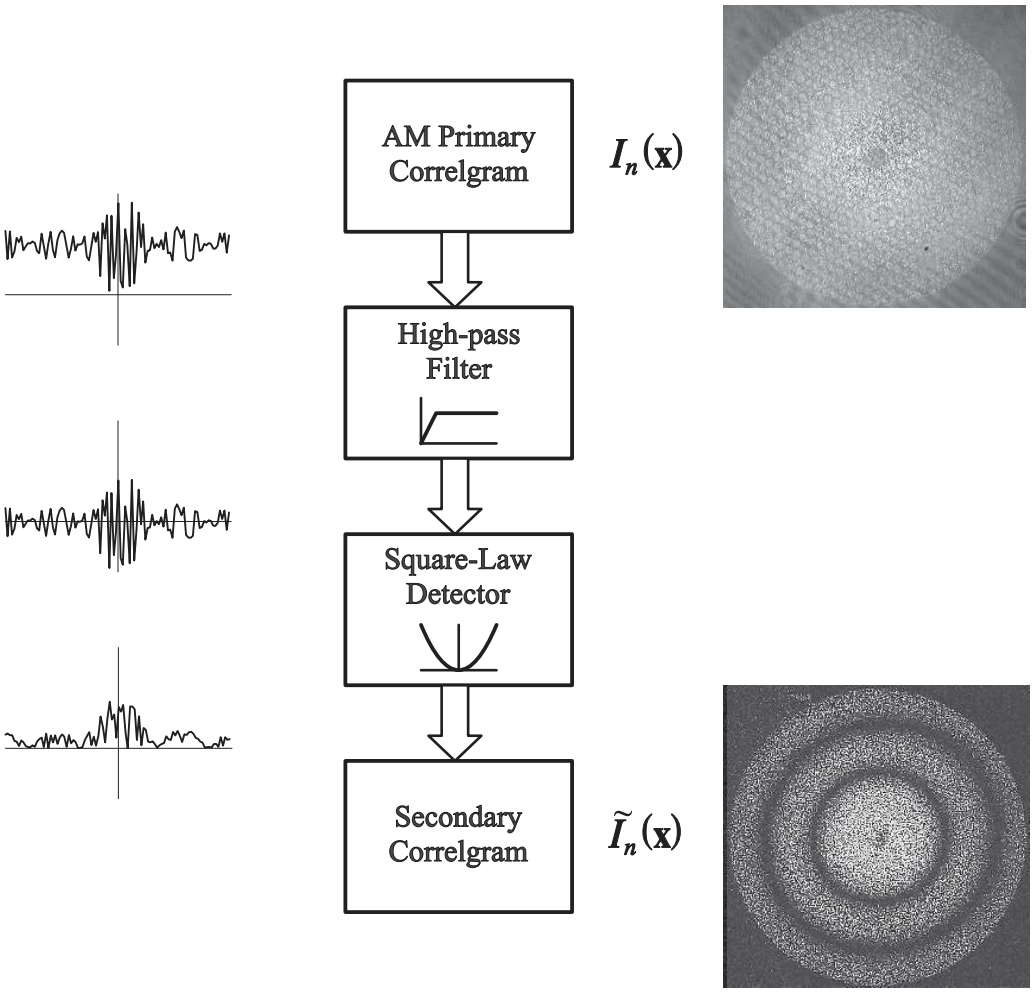

Figure 12 Scheme of the secondary-fringe generation process by spatial filtering of a single AM primary correlgram. Centre: block diagram, right: images of real correlgrams, left: sketch of the profiles of the central line of the correlgrams.

intensity pattern with local contrast related to the argument of the fringe function and, on the other, removes the continuous component $g\,\mathcal{I}_0$.

Subtraction technique is also applicable to AM primary correlgrams. In this case only to remove the continuous component as contrast fringes are already present. The two correlgrams that are subtracted must be different; this is achieved either changing conveniently the argument of the fringe function by means of the reference phase-difference ϕ_r or —what is much less usual— comparing AM primary correlgrams corresponding to different states of the measurand.

Subtractive secondary-fringe generation admits a general analytic formulation comprising both types of correlgrams, AM and PM. Let us take two generic primary correlgrams —$I_a(\mathbf{x})$ and $I_b(\mathbf{x})$— following expression (5.3). Secondary correlgrams are obtained by subtraction and square-law demodulation

$$\begin{aligned}\tilde{I}_b(\mathbf{x}) = \left[I_b(\mathbf{x}) - I_a(\mathbf{x})\right]^2 = g^2\left[\mathcal{I}_0(\mathbf{x})\mathcal{V}(\mathbf{x})\right]^2\big(&\mathrm{mod}\left[M_b(\mathbf{x})\right]\cos\left\{\psi_\mathrm{p}(\mathbf{x}) + \arg\left[M_b(\mathbf{x})\right]\right\} - \\ &- \mathrm{mod}\left[M_a(\mathbf{x})\right]\cos\left\{\psi_\mathrm{p}(\mathbf{x}) + \arg\left[M_a(\mathbf{x})\right]\right\}\big)^2\end{aligned} \tag{5.7}$$

Considering that typically $\mathrm{mod}\left[M_a(\mathbf{x})\right] = \mathrm{mod}\left[M_b(\mathbf{x})\right]$ and using simple trigonometric relations, results [140]

$$\begin{aligned}\tilde{I}_b(\mathbf{x}) = g^2\left[\mathcal{I}_0(\mathbf{x})\mathcal{V}(\mathbf{x})\right]^2\mathrm{mod}\left[M_b(\mathbf{x})\right]^2\big(&1 - \cos\left\{\arg\left[M_b(\mathbf{x})\right] - \arg\left[M_a(\mathbf{x})\right]\right\}\big)\times \\ &\times\big(1 - \cos\left\{2\psi_\mathrm{p}(\mathbf{x}) + \arg\left[M_b(\mathbf{x})\right] + \arg\left[M_a(\mathbf{x})\right]\right\}\big)\end{aligned} \tag{5.8}$$

where the term containing the speckle phase-noise ψ_p has zero average and the local mean brightness is

$$B_b(\mathbf{x}) = \left\langle \tilde{I}_b(\mathbf{x}) \right\rangle = g^2\left\langle \left[\mathcal{I}_0(\mathbf{x})\mathcal{V}(\mathbf{x})\right]^2 \right\rangle \mathrm{mod}\left[M_b(\mathbf{x})\right]^2\big(1 - \cos\left\{\arg\left[M_b(\mathbf{x})\right] - \arg\left[M_a(\mathbf{x})\right]\right\}\big) \tag{5.9}$$

Unlike spatial filtering (5.6), this technique does not yield any background brightness and, hence, its secondary fringes are intrinsically more contrasted.

There are several variants of the basic technique regarding the choosing of the primary correlgrams to be subtracted, that will be treated in succeeding.

5.2.2.1 Sequential acquiring

This is the most usual operating mode. The two correlgrams are acquired in different instants, storing the first until the second is available. In the first prototypes using this fringe generation techniques the storage of the correlgrams was implemented with analogue devices as magnetic video tapes and disks [4, 5, 93] or scan converter memories [160]; nowadays, they have been completely replaced by computer based digital image processing systems.

5.2.2.1.1 Subtraction of a reference correlgram

A reference primary correlgram $I_q(\mathbf{x}) = I_{\text{ref}}(\mathbf{x})$ is acquired with the measurand in a given state and stored. The reference correlgram is then subtracted (figure 13) from the next primary correlgrams $I_b(\mathbf{x}) = I_n(\mathbf{x})$. The resulting secondary correlgrams reveal the deviation of the measurand from the reference state.

$$\tilde{I}_n(\mathbf{x}) = \left[I_n(\mathbf{x}) - I_{\text{ref}}(\mathbf{x})\right]^2 \tag{5.10}$$

This technique is typically used with PM correlgrams [4, 5], where $\text{mod}[M_n(\mathbf{x})] = 1$ and expression (5.9) becomes

$$B_n(\mathbf{x}) = \left\langle \tilde{I}_n(\mathbf{x}) \right\rangle = g^2 \left\langle \left[\mathcal{I}_0(\mathbf{x})\mathcal{V}(\mathbf{x})\right]^2 \right\rangle \left(1 - \cos\left\{\arg\left[M_n(\mathbf{x})\right] - \arg\left[M_{\text{ref}}(\mathbf{x})\right]\right\}\right) \tag{5.11}$$

It has been also applied to AM correlgrams, taking as reference a correlgram with the measurand at rest, either with time-average [79, 161] or with double-exposure stroboscopic [141] and pulsed illumination [162, 163]; it is also practical to acquire the reference with the measurand in other states [151, 164, 165]. Other variants are to get a reference correlgram with the modulus of the fringe function forced to be zero by sinusoidal [164] or triangular [166] modulation of the reference phase-difference during time average, or to subtract the reference beam [155] instead of a correlgram when the state of the measurand is not repeatable.

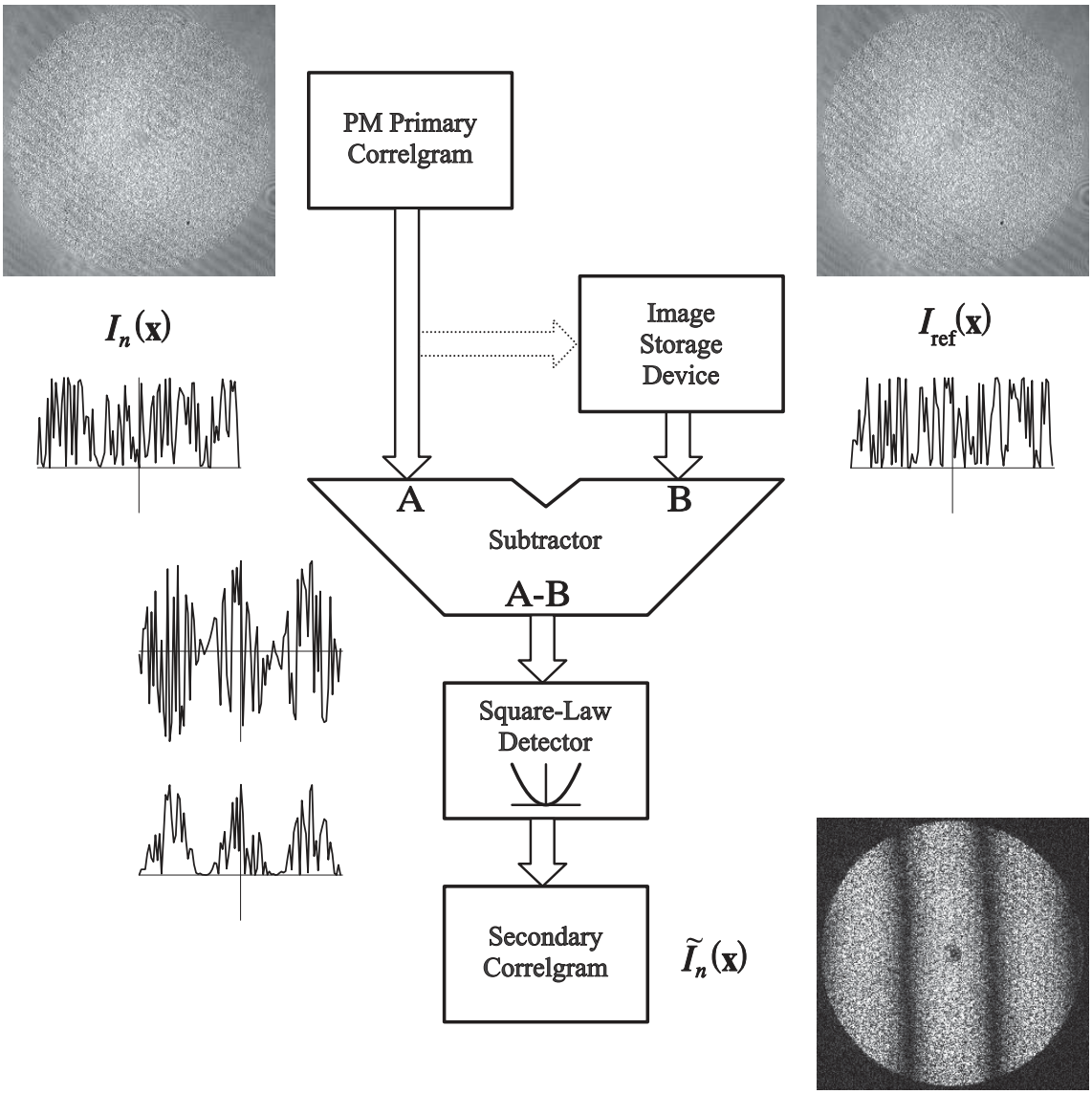

Figure 13 Scheme of the secondary-fringe generation process by subtraction of a reference applied to PM primary correlgrams. Real correlgrams and sketched line profiles are shown as in figure 13.

5.2.2.1.2 Sequential subtraction

The last two primary correlgrams recorded by the video camera —$I_b(\mathbf{x}) = I_n(\mathbf{x})$ and $I_a(\mathbf{x}) = I_{n-1}(\mathbf{x})$— are subtracted, usually in real-time. The first $I_{n-1}(\mathbf{x})$ is stored and, once the subtraction is performed, it is replaced by the next $I_n(\mathbf{x})$ until a new correlgram $I_{n+1}(\mathbf{x})$ is acquired and subtracted, an so on (figure 14).

The resulting secondary correlgrams can be expressed

$$\tilde{I}_n(\mathbf{x}) = \left[I_n(\mathbf{x}) - I_{n-1}(\mathbf{x})\right]^2 \tag{5.12}$$

This technique is typically applied to AM correlgrams, changing the reference phase-difference among each video frame and the next to make $\left|\arg\left[M_n(\mathbf{x})\right] - \arg\left[M_{n-1}(\mathbf{x})\right]\right| = \pi$. Expressions (5.8) and (5.9) become then

$$\tilde{I}_n(\mathbf{x}) = 2g^2\left[\mathcal{I}_0(\mathbf{x})\mathcal{V}(\mathbf{x})\right]^2 \operatorname{mod}\left[M_n(\mathbf{x})\right]^2\left[1 + \cos\left(2\left\{\psi_p(\mathbf{x}) + \arg\left[M_n(\mathbf{x})\right]\right\}\right)\right] \tag{5.13}$$

$$B_n(\mathbf{x}) = \left\langle \tilde{I}_n(\mathbf{x}) \right\rangle = 2g^2\left\langle \left[\mathcal{I}_0(\mathbf{x})\mathcal{V}(\mathbf{x})\right]^2 \right\rangle \operatorname{mod}\left[M_n(\mathbf{x})\right]^2 \tag{5.14}$$

Sequential subtraction was originally applied to time-average correlgrams [129, 167, 168] and recently extended to double-exposure stroboscopic [140, 142, 169, 170].

Some authors have proposed to use other values for the increment of the argument of the fringe function among correlgrams —e.g. $\pi/2$ [168, 171]—, to induce random changes in the reference phase-difference with a moving diffuser [49], or even to rely on air turbulence and mechanical instability [167]. It has been proven [172] that the optimum contrast of the secondary fringes is obtained with a phase increment of π, although any value between 30º and 330º is acceptable.

Sequential subtraction can be also applied to PM correlgrams; secondary fringes appear when the object phase-difference changes from one frame to the next. It has been used with single-exposure stroboscopic [49], alternating the position of the pulses among frames, and also with single-exposure pulsed illumination [155]; in both approaches, the secondary correlgrams map the change of ϕ_o between pulses.

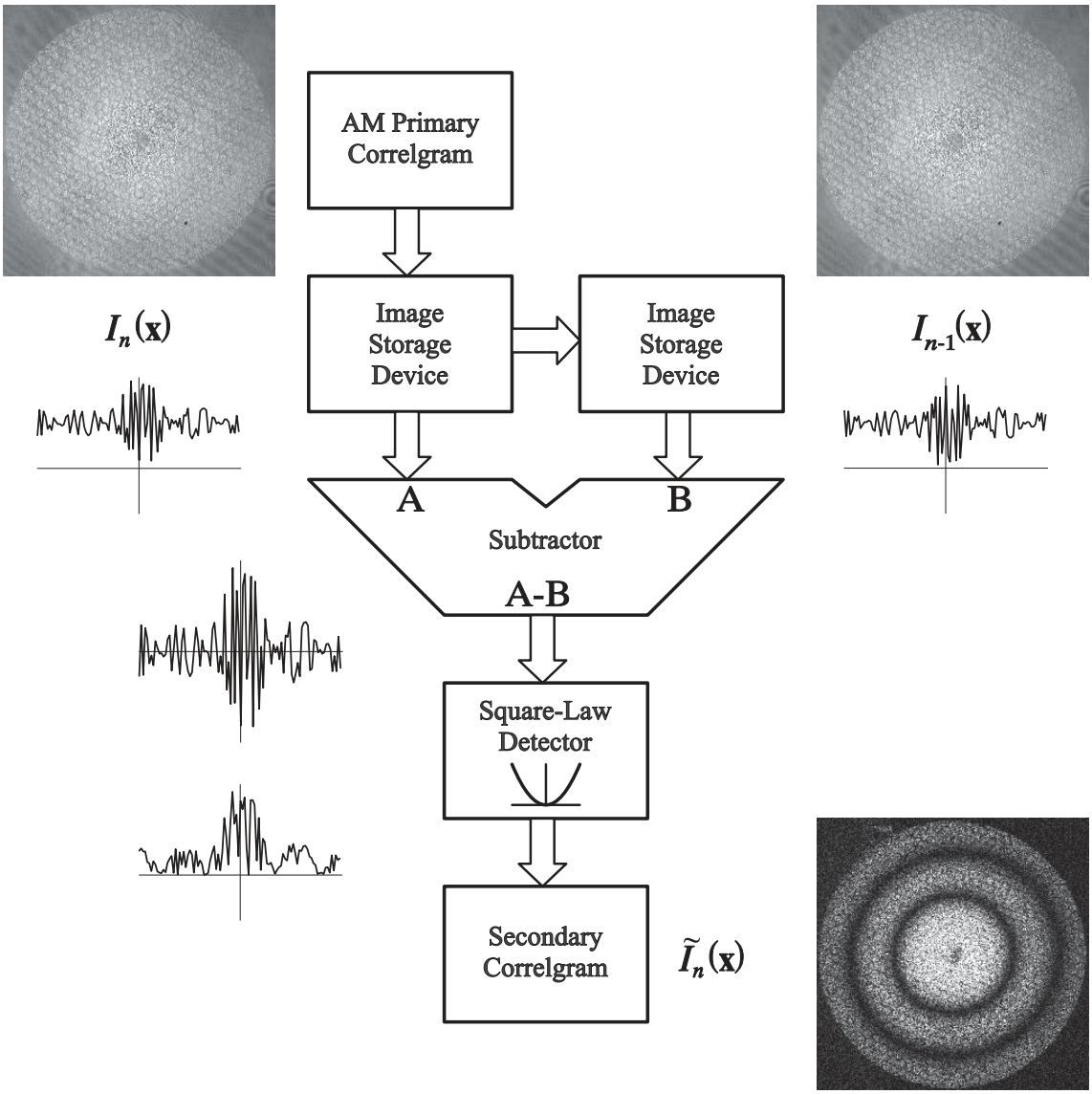

Figure 14 Scheme of the secondary-fringe generation process by sequential subtraction of AM primary correlgrams. Real correlgrams and sketched line profiles are shown as in figure 13.

5.2.2.1.3 Interval subtraction

This is an extension of sequential subtraction [173] where each primary correlgram is subtracted from one acquired d video frames before —$I_b(\mathbf{x}) = I_n(\mathbf{x})$ and $I_a(\mathbf{x}) = I_{n-d}(\mathbf{x})$—, the secondary correlgrams result

$$\tilde{I}_n(\mathbf{x}) = \left[I_n(\mathbf{x}) - I_{n-d}(\mathbf{x})\right]^2 \tag{5.15}$$

It is applied to PM correlgrams that change very slowly, compared to the video frame rate. The secondary fringes contour points with the same change of the object phase-difference between exposures —i.e., with the same average speed—. Sensitivity is controlled by the delay $d \cdot T_F$ between the correlgrams being compared.

5.2.2.2 Simultaneous acquiring

Wizinowich and Colucci [174, 175] developed a technique to record two interferograms in the even and odd video fields, respectively, during the same frame period. This technique has been adapted to TVH for double-single exposure pulsed illumination [156] and also for time-average [26]. It is also possible, by optical means, to obtain simultaneously two or more correlgrams each with a different value of the reference phase-difference that are recorded by independent cameras [176].

5.3 Secondary-fringe contrast

The contrast of the secondary fringe patterns is defined as the ratio between the excursion of the local mean brightness and its average value

$$C = \frac{B_{\max} - B_{\min}}{B_{\max} + B_{\min}} = \frac{SNR}{2 + SNR} \tag{5.16}$$

where $B_{\max}$ and $B_{\min}$ are the extreme values of the local mean brightness in the correlgram and SNR is the signal to noise ratio, considering that the signal is the component of the local mean brightness related to the fringe function.

The mean brightness of the secondary correlgrams can be expressed as

$$B = S + N_{\mathrm{o}} + N_{\mathrm{e}} \tag{5.17}$$

being S the signal, N_{o} the optical noise and N_{e} the electronic noise. This last appears at the output of the video camera, combined with the primary correlgrams $I_{\mathrm{n}}(\mathbf{x})$, and its effect is characterised by its standard deviation σ_{e}, that is usually approximated [158] by

$$\sigma_{\mathrm{e}}^2 = \sigma_{\mathrm{ed}}^2 + k\langle I_n(\boldsymbol{x})\rangle \tag{5.18}$$

where σ_{ed} is the standard deviation of the darkness noise, that is independent of the illumination level, and k is a constant value determined by the constructive and operating characteristics of the sensor, the gain of the amplifiers, etc.

Table 2 summarises the expressions of the *SNR* for the main secondary correlgram generation techniques, that have been derived by Slettemoen [37, 158] for spatial filtering and Joenathan [172] for correlgram subtraction. It is assumed that the intensity distributions of the beams are statistically independent. The effect of the limited resolution of the video camera is taken into account [37] through the *contrast* of the beams (γ_1 and γ_2) and the *resolution degree* (γ_{12}) of the *fringe carrier*, i.e., of the speckle pattern resulting of their interference. When the speckle pattern is fully resolved by the camera $\gamma_1 = \gamma_2 = \gamma_{12} = 1$; but if the size of speckle is similar or smaller than the dimensions of the pixels, then $\gamma_1 \leq 1$, $\gamma_2 \leq 1$ and $\gamma_{12} \leq 1$.

5.3.1 Factors determining the contrast of the secondary fringes

The contrast of the secondary fringes is directly related to the SNR of the secondary correlgrams. Every factor with influence on the SNR has a similar effect on fringe contrast. These factors can be classified in those that set the maximum attainable value of contrast and those determining its actual value in a given operating conditions. In any case, their effects can be quantified using the expressions of table 2.

Table 2 Expressions of the signal to noise ratio (SNR) for the main fringe generation techniques

Primary correlograms	Fringe generation	SNR
PM	Subtraction of Reference	$\frac{4g^2\gamma_{12}^2\langle I_1(\boldsymbol{x})\rangle\langle I_2(\boldsymbol{x})\rangle}{\sigma_e^2}$
AM	Spatial Filtering	$\frac{2g^2\gamma_{12}^2\langle I_1(\boldsymbol{x})\rangle\langle I_2(\boldsymbol{x})\rangle \operatorname{mod}[M_n]_{\max}^2}{g^2\left[\gamma_1^2\langle I_1(\boldsymbol{x})\rangle^2+\gamma_2^2\langle I_2(\boldsymbol{x})\rangle^2\right]+\sigma_e^2}$
	Sequential Subtraction	$\frac{4g^2\gamma_{12}^2\langle I_1(\mathbf{x})\rangle\langle I_2(\mathbf{x})\rangle \operatorname{mod}[M_n]_{\max}^2}{\sigma_e^2}$

Among the factors that set the maximum attainable contrast, there are many related to the design and the physical implementation of the interferometer as the maximum available light power, the sensitivity, electronic SNR, linearity [177], spatial resolution and automatic gain control of the video camera, the quantization noise of the image digitizer if present, the degree, relative state of polarisation and type —speckled or uniform— of the beams, and the shape and alignment of their pupils. Other factors are connected to the operating mode of the TVH system as the expression of the fringe function, given by the temporal treatment technique, the secondary-fringe generation technique, that decides which of the expressions in table 2 gives the SNR, and the de-correlation of speckle due to the operation mode, specially present in contouring [96, 178, 179].

Once established the design of the interferometer, the operating mode, the fringe formation technique and the illumination conditions, the maximum value of contrast that can be attained is completely determined. But the actual value of the contrast of the secondary fringes is set by other factors. Some of them depend of the adjustment of the interferometer can be optimised according to the working conditions; other, related to the object, to the value of the measurand or to environmental factors, cannot be controlled and often lead to a reduction of the contrast.

Optimisable parameters are the intensity balance between the interfering beams, generally represented by the *beam ratio* $\kappa = I_2/I_1$ [36, p 31; 180], and the relative aperture (*F/#*) of the objective; whilst non-optimisable ones are the reflectivity of the object, the de-polarisation of light in certain surfaces, the presence of ambient light, the de-correlation of speckle due to transversal displacements and tilts of the object induced by the measurand, and the density of the secondary fringes [39].

5.3.2 Optimisation of the secondary-fringe contrast

Although in practice it is usual to adjust the average intensity of the illumination beam $\langle I_1(\mathbf{x})\rangle$ (or $\langle I_2(\mathbf{x})\rangle$), the F number of the objective and the beam ratio κ by "trial and error", several authors [37, 39, 158, 177, 180] have derived analytically the values of these parameters that maximise the SNR for different types of interferometers and in diverse operating conditions.

The first condition for the optimisation of contrast is that the dynamic range of the camera must be completely used. For fully developed speckle patterns, the condition

$$\left\langle I_n(\mathbf{x})\right\rangle + 2\sigma_{I_n} = I_{\text{sat}} \tag{5.19}$$

ensures that 95% of the pixels in primary correlgrams are under the saturation level, being $\langle\cdot\rangle$ the average extended to a set of macroscopically identical but microscopically different diffusing objects and σ_{In} the standard deviation of the intensity of the primary correlgrams in the same conditions. Expression (5.19) can be written [33, 180]

$$\left\langle I_1(\mathbf{x})\right\rangle\left\{1+\kappa+2\left[\gamma_1^2+\kappa\gamma_2^2+2\kappa\gamma_{12}^2\,\text{mod}(M_n)_{\max}^2\right]^{1/2}\right\}=I_{\text{sat}} \tag{5.20}$$

that, for a camera with a given saturation intensity I_{sat}, establishes a relation between the values of $\langle I_1(\mathbf{x})\rangle$ and κ that is conditioned by the resolution degree of the fringe carrier and the contrasts of the beams.

To optimise contrast, in principle, the F number must be set to the minimum value F_{res} that makes $\gamma_{12} = 1$, i.e.: provides a fringe carrier coarse enough to be fully resolved by the camera whilst maximises the irradiance at the sensor. In these conditions, expression (5.20) can be used to find the value of the beam ratio $\kappa_{\max}$ that maximises contrast and then calculate the corresponding values of the average intensities of the beams $\langle I_1(\mathbf{x})\rangle_{\max}$ and $\langle I_2(\mathbf{x})\rangle_{\max}$.

At this stage, two situations may be found in practice: the optimisation is made *"with unlimited power"* if the power of the laser is high enough to reach the intensities

$\langle I_1(\mathbf{x})\rangle_{\max}$ and $\langle I_2(\mathbf{x})\rangle_{\max}$ at the sensor of the camera with the lens closed to F_{res} and a given object, otherwise the optimisation is made *"with limited power"*.

When optimising with unlimited power the beam ratio is set to $\kappa_{\max}$, usually adjusting the intensity of the reference beam —in geometries with double illumination [39] it is always $\kappa_{\max} = 1$— and then the illumination intensity must be set according to the characteristics of each object to reach $\langle I_1(\mathbf{x})\rangle_{\max}$ and $\langle I_2(\mathbf{x})\rangle_{\max}$.

With limited power, the laser have to be used at full power and the lens must be open to a compromise value $F_{\text{opt}} < F_{\text{res}}$ where the better use of the dynamic range of the camera amply compensates the loose of carrier resolution degree. To find such optimum value of the F number, equation (5.20) must be considered together with the dependence of $\langle I_1(\mathbf{x})\rangle_{\max}$, $\langle I_2(\mathbf{x})\rangle_{\max}$ and γ_{12} with *F/#*. As this is influenced by the size and reflectivity of the object, the values F_{opt} and κ_{opt} that optimise the contrast are different for each object.

5.4 Speckle-noise reduction techniques

In the secondary correlgrams generated with basic techniques (§5.2), the fringes appear corrupted by speckle. This is present as both intensity noise, in $\mathcal{I}_0(\mathbf{x})\,\mathcal{V}(\mathbf{x})$, and phase noise, in the term $\cos\{\psi_{\text{p}}(\mathbf{x})+\arg[M_n(\mathbf{x})]\}$.

The contrast of these secondary speckle patterns [181] is

$$C = \sqrt{2+3\tau} \tag{5.21}$$

where τ is a parameter that depends of the type of beams used, the size and relative positions of their pupils and of the spatial resolution of the camera.

In TVH systems with uniform reference beams $\tau = 0$ and $C = \sqrt{2}$. When two speckle patterns interfere and the camera resolves the interferogram $\tau = 1$ and $C = \sqrt{5}$, but if resolution is only partial they take intermediate values: $0 < \tau < 1$ and $\sqrt{2} < C < \sqrt{5}$.

In any case, the contrast of speckle noise in the secondary correlgrams is even higher than in fully developed speckle patterns ($C = 1$) so that it is, at least, uncomfortable for direct observation of the secondary-fringe patterns and interferes with their automatic analysis. Several techniques have been developed to reduce it, either modifying the process to generate secondary correlgrams or by numerical processing of these. Such techniques can be classified as follows.

5.4.1 Speckle-phase shift based methods

This type of techniques is characterised by the use of more than two primary correlgrams where speckle-phase shift is introduced between them through controlled changes of the reference phase-difference, ϕ_r or ϕ_{rA} (table 1). The resulting secondary correlgrams are almost completely free of phase noise but intensity noise, in general, is still present.

The most popular of these techniques is "electro-optic holography" (EOH), proposed by Stetson and Brohinsky [15], that implements algorithms related to temporal phase-shift fringe pattern evaluation techniques to eliminate the terms affected by the phase-noise. The initial version used four primary correlgrams, but variants with three of them have been also proposed [182, 183]. EOH can be applied to both PM and AM correlgrams [184, 185]. For the first case it is necessary to compare with a reference state, this involves the use of twice the number of primary correlgrams, but provides simultaneously two noise-reduced secondary correlgrams that depend on the sine and cosine of the object phase-difference respectively, thus allowing phase evaluation with no extra cost.

A similar scheme is followed in techniques as max-min scanning [186] —also applied to phase evaluation— and the averaging of several secondary correlgrams with shifted speckle phase [187, 188] that, although do not remove phase noise completely, show very high immunity to environmental disturbance.

The use of a large number of primary correlgrams generally redounds to the increment of the SNR thus improving the contrast of the secondary fringes [172, 189], but intensity noise is still present. To reduce it up to a point, some authors have developed "normalised" versions of EOH [15, 161, 182, 190] and max-min scanning [186] that lie in the division of the secondary correlgrams by one without fringes, typically obtained with the measurand at rest.

5.4.2 Speckle de-correlation based methods

In view of the random character of speckle noise, the average of a given number N of secondary correlgrams corresponding to the same state of the measurand but with statistically independent speckle patterns, leads to a reduction of the typical deviation of the final intensity distribution and, therefore, of the contrast of speckle [32] according to the expression

$$C_N = \frac{1}{\sqrt{N}} C = \left(\frac{2+3\tau}{N} \right)^{\frac{1}{2}} \tag{5.22}$$

It is necessary to average a large number of correlgrams —typically between ten and fifty— to get a noticeable reduction of speckle noise, although a similar effect can be achieved with less correlgrams if phase noise is removed *a priori* by phase shift techniques [184, 185] as described in §5.4.1.

Correlgram averaging also helps to the reduction of electronic noise [191] and, therefore, increases marginally the contrast of the secondary fringes.

Speckle must be completely de-correlated between secondary correlgrams to obtain statistically independent patterns. Several methods have been proposed and demonstrated [192] as tilting the illumination beam —either with a moving mirror [193] or with a rotating plane parallel window [40, 185]—, changing observation direction by rotation of an eccentric diaphragm [50] or illuminating the object through a moving or rotating diffuser [192].

Averaging may be analogue —e.g. displaying the secondary correlgrams in a high-persistence monitor [50, 192]—, although it is usual to apply it numerically in digital computers [194].

The implementation of this kind of techniques is specially simple with AM correlgrams; speckle is de-correlated after the generation of each secondary corelogram and just the average have to be stored. For PM correlgrams, conversely, it is necessary to acquire and store N speckle de-correlated primary correlgrams with the measurand in a reference state and then N more, correlated one to one to the firsts, with the measurand in a second state; this requires a de-correlating device with very high repeatability and a huge amount of computer memory.

5.4.3 Spatial filtering of secondary correlgrams

Spatial filtering of secondary correlgrams, often performed numerically, reduces the phase and intensity speckle noise at once though, contrary to the techniques that combine a large number of images, the contrast of the correlation fringes is also reduced.

As evidenced in the preceding sections, speckle behaves as a multiplicative noise. Its power spectrum, usually covering the full range of spatial frequencies that the camera can resolve, appears mixed with the correlation fringes' and it is specially complicated to filter it out. The merit of a filter for speckle removal in TVH is given not only by its ability to reduce the contrast of noise but by the extent that the fringe pattern, the edges, the details of the object, etc remain unaffected.

Linear low-pass convolution filters —mean, gaussian, etc.— are the most widely used for this purpose because they are very easy to implement and render acceptable results, provided that the spatial frequency of fringes is low. To avoid the loose of fringe contrast, "smooth" mean filters —i.e., with a small kernel, typically 3×3 pixels— applied repeatedly [127, 195] are often preferred to perform a single step with a larger

window. Low-pass filters with recursive formulation [196] and with windows fitted to the shape of the fringes [197] have been proposed with the same aim.

Low-pass filtering can be also applied on the Fourier Transform of the correlgrams; the shape of the filter may be then tailored for each particular situation [198], although the automation of this process is very difficult. An alternative technique is the "spectral subtraction image-restoration" method [163, 199], consisting in the subtraction of the power spectrum of a primary correlgram without fringes from that of a secondary correlgram.

Other frequently used filters are the median [200], truncated median and mode [201] that, for gaussian noise as speckle, are even more efficient than linear ones [202]. These filters can be also used with tailored windows [197] to improve the final contrast of the fringes.

Special filters originally designed for speckle reduction in synthetic aperture radar (SAR) have been applied to TVH [203, 204]. These filters are of diverse natures: adaptive [205], based on the local statistical properties of the correlgrams as sigma (Lee 1986), variance [207] and geometric [208] filters, based on information theory and statistical mechanics [209], etc. All of them exhibit better noise rejection and detail preservation characteristics than classical filters.

6 Fringe analysis in TV-holography

Generally speaking, a *fringe pattern* is any distribution of light and dark areas, the fringes. The dependence of intensity i with spatial coordinates $\mathbf{x}$ in this type of distributions is formalised by the general expression

$$i(\mathbf{x}) = i_0(\mathbf{x})\{1 + v(\mathbf{x}) f[\phi(\mathbf{x})]\} \tag{6.1}$$

where $i_0(\mathbf{x})$ is the *local average intensity*, $v(\mathbf{x})$ the *visibility* or *contrast* of the pattern and f a periodic or quasi-periodic unidimensional function that defines the *profile* of the fringes and whose argument $\phi(\mathbf{x})$ is the *phase of the pattern*.

According to this definition, there are three types of fringe patterns in TVH: speckle interferograms, primary and secondary correlgrams. Only the correlgrams, however, are of practical interest in this context as they are electronic images susceptible of further processing.

TVH fringe patterns are characterised by the random distribution of $i_0(\mathbf{x})$ and $v(\mathbf{x})$ due to speckle noise. Their profile is typically sinusoidal for PM correlgrams, whilst for AM correlgrams it can be sinusoidal, follow Bessel's or sinc functions, or even a combination of them according to the particular expression of the modulus of the fringe function (table 1). The profile of secondary correlgrams may be slightly influenced by the fringe generation technique, but its essential characteristics are established by those of the corresponding primary correlgrams.

The phase of the pattern $\phi(\mathbf{x})$ is directly related to the object phase-difference $\phi_o(\mathbf{x})$ or to its changes $\Delta\phi(\mathbf{x})$ and, therefore, to the measurand. It may also depend of the reference phase-difference $\phi_r(\mathbf{x})$, its variation $\Delta\phi_r(\mathbf{x})$ and also of the random component of the phase of speckle, i.e., the phase noise $\psi_p(\mathbf{x})$.

6.1 The process of fringe pattern analysis

Automatic fringe pattern analysis, in its most general conception, comprises four stages [210]:

Phase evaluation

Consisting in the calculation of the spatial distribution of the phase of the pattern from one or more conveniently chosen and sampled fringe patterns —i_1, i_2,…, i_N— corresponding to the same state of the measurand. The resulting array of values $\phi(\mathbf{x})$ is the *phase map*.

Phase unwrapping

Most of phase evaluation techniques yield its main value —i.e., modulo 2π—, hence, an ambiguity $\pm 2n\pi$ of is present in the resulting phase, being n an integer number called *fringe order*. This uncertainty has to be solved by determining the fringe order at each point to build an unwrapped phase map ${}^{R}\phi(\mathbf{x}) = \phi(\mathbf{x}) \pm 2n\pi$ free of 2π discontinuities.

A living interest has arisen on the problem of phase unwrapping in the most diverse conditions during the last years. The result has been a great number of techniques, many of them specifically devised for the analysis of speckle-corrupted patterns. Several authors as, for example, Robinson [211], Judge and Bryanston-Cross [212] and Takeda [214] have published excellent compilations on the subject.

Removal of additional terms

During both the fringe generation process and the evaluation stage, terms not related to the measurand —typically constant or linearly dependent of the spatial coordinates— may be added to the phase of the pattern. Their value, that may be known *a priori* or estimated by least squares fitting [214] or any other process, is subtracted from the phase map at this stage.

Re-scaling

The preceding stages yield a map of the phase as a function of the coordinates of the fringe pattern space. It is often necessary to transform it in a map of the measurand in terms of the coordinates of the object space. The relations between both sets of parameters are, in general, known for each measurement method used to generate fringe patterns. In our case, image-plane TVH, the correspondence between object and fringe pattern coordinates is given by the object-image transform determined by the objective and the working distance; the relation between the phase of the pattern and the

measurand results of the choice of methods used in the three first stages of our approach: the fringe formation technique (§5) establishes the relation between the phase of the pattern $\phi(\mathbf{x})$ and the fringe function $M_n(\mathbf{x})$, the temporal treatment (§4) fixes the relation between $M_n(\mathbf{x})$ and the object optical phase-difference $\phi_o(\mathbf{x})$ or its changes $\Delta\phi_o(\mathbf{x})$ and, finally, the geometry of the speckle interferometer (§3) determines the relation between $\phi_o(\mathbf{x})$ and the measurand.

Figure 15 illustrates this sequence of operations and their possible combinations. Only the first step, phase evaluation, is indispensable; the others are optional and sometimes unnecessary. The use of these steps have to be decided according to the characteristics of each particular case and the way that the final result must be presented.

TVH uses the same phase evaluation techniques than any other interferometric technique, but the speckled nature of TVH fringes introduces some peculiarities that must be taking into account in their implementation; we will treat these particularities in succeeding. Once the phase map has been calculated, unwrapping, additional term removal and re-scaling can be performed with general techniques, not specifically designed for TVH but for noisy phase maps.

6.2 Correlgram-fringe pattern identification

Speckle noise appears in TVH correlgrams as intensity and phase noise. Intensity noise is present in the random distributions of $\mathcal{I}_0(\mathbf{x})$ and $\mathcal{V}(\mathbf{x})$, consequently, the average intensity $i_0(\mathbf{x})$ and the visibility $v(\mathbf{x})$ of such patterns have also random distributions with the potential appearing of *low modulation* —$i_0(\mathbf{x})v(\mathbf{x}) \to 0$— and *saturation* — $i(\mathbf{x}) > i_{sat}$— points where phase cannot be evaluated. Phase noise $\psi_p(\mathbf{x})$ may appear embedded in the phase of the pattern and also affecting the values of the average intensity and the visibility; this depends on the type of correlgrams, the fringe

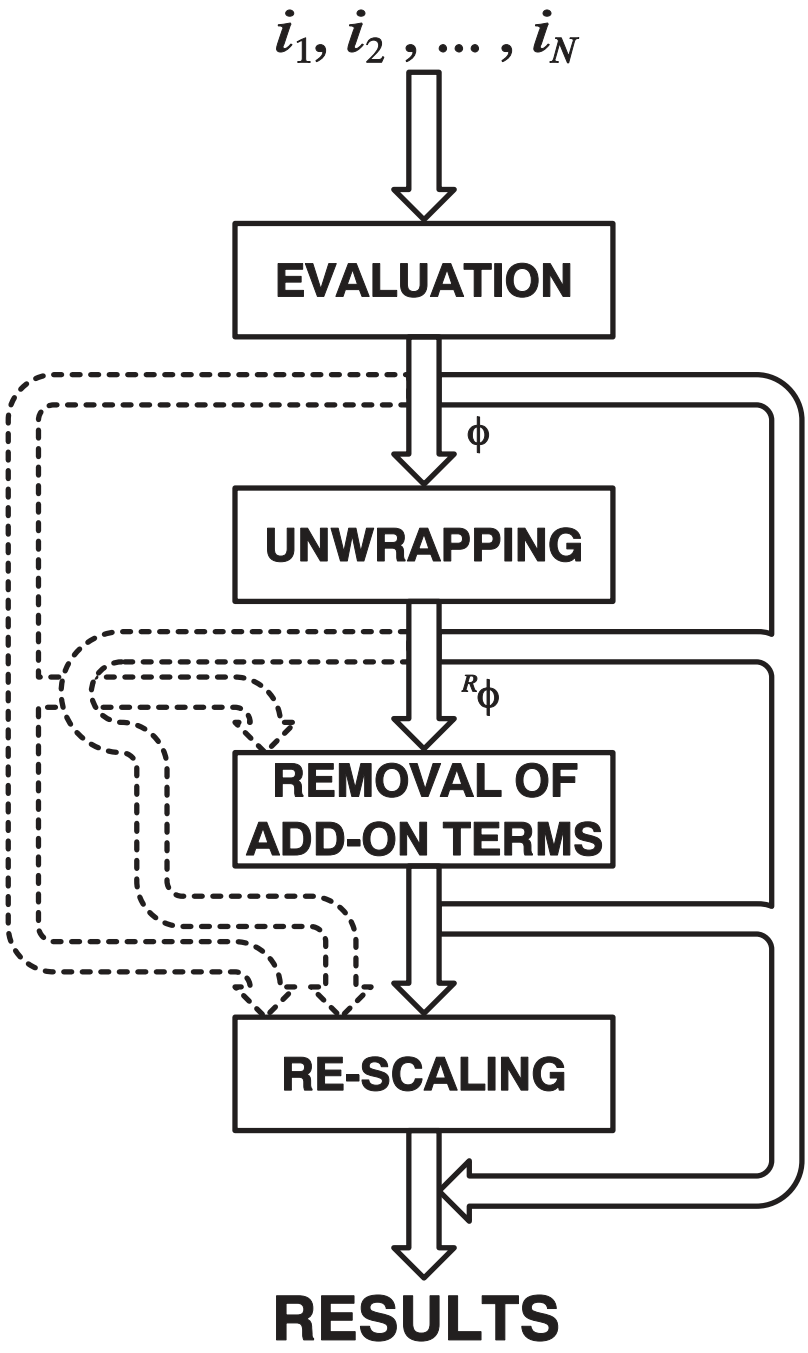

Figure 15 Stages of the process of fringe pattern analysis.

generation technique an even on how the fringe pattern is identified, i.e., on which term is considered to represent the fringes.

On the other hand, there are two kinds of fringe patterns: primary and secondary correlgrams, and their respective phases can be evaluated. The main benefit of using secondary correlgrams is the possibility of reducing speckle noise with techniques as those pointed out in §5.4 before phase evaluation. This is generally impracticable with primary correlgrams because speckle removal would lead to the suppression of the fringes.

In any case, the measurand is encoded in the changes of the object phase-difference $\Delta\phi_o(\mathbf{x})$ and this is the first measurement to be extracted from the fringe pattern. At this stage two situations become apparent [34, pp. 306-307;215]:

6.2.1 The fringe pattern depends on $\phi_o(\mathbf{x})$, but not on $\Delta\phi_o(\mathbf{x})$.

This is the case of primary PM correlgrams where, moreover, $\phi_o(\mathbf{x})$ appears added to the phase noise $\psi_p(\mathbf{x})$. Considering that, in general, mod$[M_n(\mathbf{x})] = 1$ the identification of the terms in the expression of these correlgrams (5.3) with a general fringe pattern (6.1) is established as follows

$$I_n(\mathbf{x}) = \underbrace{g\mathcal{I}_0(\mathbf{x})}_{i_0(\mathbf{x})}\left(1 + \underbrace{\mathcal{V}(\mathbf{x})}_{v(\mathbf{x})}\underbrace{\cos}_{f}\left\{\underbrace{\psi_p(\mathbf{x}) + \arg[M_n(\mathbf{x})]}_{\phi(\mathbf{x})}\right\}\right) \tag{6.2}$$

where arg$[M_n(\mathbf{x})]$ is proportional to $\phi_o(\mathbf{x})$ (table 1).

The most usual method to obtain $\Delta\phi_o(\mathbf{x})$ is to evaluate two primary correlgrams corresponding to different states of the measurand, one of them taken as a reference, and then subtract the resulting phase maps. If the speckle pattern does not experiment de-correlation between both states —i.e., $\psi_p(\mathbf{x})$ is constant— the difference

$$\Delta\phi(\boldsymbol{x}) = \phi_n(\boldsymbol{x}) - \phi_{\text{ref}}(\boldsymbol{x}) = \arg[M_n(\boldsymbol{x})] - \arg[M_{\text{ref}}(\boldsymbol{x})] \tag{6.3}$$

is proportional to $\Delta\phi_{o,n}(\mathbf{x}) = \phi_{o,n}(\mathbf{x}) - \phi_{o,\text{ref}}(\mathbf{x})$.

It also feasible to use differential phase evaluation methods [16, 166, 216, 217], specifically designed for this particular case of TVH, to calculate the increment of the phase $\Delta\phi(\mathbf{x})$ from two series of primary correlgrams corresponding to two states of the measurand neither explicitly evaluating their respective phase nor generating secondary correlgrams.

6.2.2 The fringe pattern directly depends on $\Delta\phi_o(\mathbf{x})$.

This situation corresponds to AM primary correlgrams and all the secondary correlgrams.

In AM primary correlgrams (table 1), $\Delta\phi_o(\mathbf{x})$ is encoded in the modulus of the fringe function. Thus, identifying the terms of (5.3) with (6.1) results

$$I_n(\mathbf{x}) = \underbrace{g\mathcal{I}_0(\mathbf{x})}_{i_0(\mathbf{x})}\Big(1+\underbrace{\mathcal{V}(\mathbf{x})\cos\{\psi_p+\arg[M_n(\mathbf{x})]\}}_{v(\mathbf{x})}\underbrace{\mathrm{mod}[M_n(\mathbf{x})]}_{f[\phi(\mathbf{x})]}\Big) \tag{6.4}$$

where $\phi(\mathbf{x})$ is normally proportional to $\Delta\phi_{o,n}(\mathbf{x})$ and f is a cosine, Bessel's or $\sin(x)/x$ function.

As stated in §5.2.2.1.1, the most usual method to generate secondary fringes from PM primary correlgrams is the subtraction of a reference correlgram. The expression of this kind of secondary correlgrams can be obtained particularising (5.8) according to (5.10), and the resulting terms can be identified with (6.1) as follows

$$\begin{aligned}\tilde{I}_n(\mathbf{x}) = \underbrace{g^2[\mathcal{I}_0(\mathbf{x})\mathcal{V}(\mathbf{x})]^2\big(1-\cos\{2\psi_p(\mathbf{x})+\arg[M_n(\mathbf{x})]+\arg[M_{\mathrm{ref}}(\mathbf{x})]\}\big)}_{i_0(\mathbf{x})}\times \\ \times\Big(1+\underbrace{\{-1\}}_{v(\mathbf{x})}\underbrace{\cos}_{f}\underbrace{\{\arg[M_n(\mathbf{x})]-\arg[M_{\mathrm{ref}}(\mathbf{x})]\}}_{\phi(\mathbf{x})}\Big)\end{aligned} \tag{6.5}$$

therefore, the profile of these patterns is sinusoidal and its phase is proportional to $\Delta\phi_{o,n}(\mathbf{x})$.

Sequential subtraction (§5.2.2.1.2) is normally used to generate secondary correlgrams from AM primary ones. The resulting expression (5.13) is identified with (6.1) in the following terms

$$\tilde{I}_n(\mathbf{x}) = \underbrace{2g^2[\mathcal{I}_0(\mathbf{x})\mathcal{V}(\mathbf{x})]^2\left[1+\cos\left(2\left\{\psi_{\mathrm{p}}(\mathbf{x})+\arg[M_n(\mathbf{x})]\right\}\right)\right]}_{i_0(\mathbf{x})}\underbrace{\mathrm{mod}[M_n(\mathbf{x})]^2}_{1+\nu(\mathbf{x})f[\phi(\mathbf{x})]} \tag{6.6}$$

and therefore, the profile of the pattern and the dependence of its phase $\phi(\mathbf{x})$ with $\Delta\phi_{\mathrm{o},n}(\mathbf{x})$ are given by the expression of mod$[M_{\mathrm{n}}(\mathbf{x})]$, that is characteristic of the temporal treatment technique used to generate the primary correlgram (see §4 and table 1).

When using secondary correlgrams, it is possible to apply speckle noise reduction techniques before the phase evaluation process. Speckle phase-shift based methods (§5.4.1) only remove phase noise and, therefore, the mean intensity of the fringe patterns represented by (6.5) and (6.6) is reduced to

$$i_0(\mathbf{x}) = 2g^2[\mathcal{I}_0(\mathbf{x})\mathcal{V}(\mathbf{x})]^2 \tag{6.7}$$

where intensity noise is still present in $\mathcal{I}_0(\mathbf{x})$ and $\mathcal{V}(\mathbf{x})$. Whilst with speckle de-correlation (§5.4.2) and spatial filtering (§5.4.3) methods it results

$$i_0(\mathbf{x}) \approx 2g^2\left\langle[\mathcal{I}_0(\mathbf{x})\mathcal{V}(\mathbf{x})]^2\right\rangle \tag{6.8}$$

6.3 Phase evaluation

Phase evaluation of TVH fringe patterns is essentially performed with the same well-known methods used for other whole-field interferometric techniques. The most relevant particularity is that the presence of speckle noise leads to the appearance of a significant amount of defective points where it is not possible to calculate the phase with acceptable precision. The percentage of these points in the whole of the phase map's depends of the statistical properties of the intensity distribution of the fringe pattern and also of the phase evaluation technique that is used. Some authors [218, 219] have derived analytic expressions to calculate the expected ratio of valid points, that may be used to optimise the adjustment of the interferometer.

Defective points are usually identified and marked during the phase evaluation process either to bypass them in further stages or to estimate their phase by interpolation

[220] or low-pass filtering techniques. These last are the most commonly used; their variants are characterised by the type of filter —convolution [221], median [222], spectral [223], etc— and by the stage of the analysis process where they are applied — on the unwrapped phase map [222], on the wrapped map [224] or even in the last step of some phase evaluation methods [43].

6.3.1 Phase evaluation methods

There are many phase evaluation methods, most of them have been originally designed to be used with smooth sinusoidal fringe patterns as those generated by classical double-beam interferometry. Nevertheless, they can be applied to other fringe profiles, usually by approximation, and also to speckled patterns as those obtained in TVH.

Many authors have reviewed and classified the phase evaluation methods according to diverse criterions: local vs. global [225], intensity based vs. phase based [226, 227], temporal vs. spatial [227, 228], electronic vs. analytic [229, 230], phase-shifting vs. Fourier transform methods [34, 210], methods with vs. without spatial carrier [231], etc.

In general [231], most of the evaluation methods use some kind of phase modulation where an auxiliary phase-shift $\alpha_k(\mathbf{x})$ is added to the phase of interest to generate the set of fringe patterns (i_1, i_2,..., i_N) necessary to apply the corresponding phase calculation algorithm. It is usually assumed that the profile of the patterns is sinusoidal and, then, they can be written as

$$i_k(\mathbf{x}) = i_0(\mathbf{x})\{1 + v(\mathbf{x})\cos[\phi(\mathbf{x}) + \alpha_k(\mathbf{x})]\}; k = 1,2,\cdots,N \tag{6.9}$$

It is not within the scope of this review to classify and describe the formulation of the phase evaluation algorithms —the aforementioned literature constitutes an excellent reference, in particular the review on the subject that our colleagues Dorrío and

Fernández [231] have recently published in MEASUREMENT SCIENCE AND TECHNOLOGY is very well matched to the approach taken in this article—, but to explain how the auxiliary phase-shift is introduced in TVH fringe patterns.

Phase modulation can be applied in either the *temporal* or the *spatial* domains. In temporal methods the phase-shift is usually the same at every point of the pattern but different for each pattern of the evaluation sequence $\alpha_k(\mathbf{x}) = \alpha_k$; this is the case of the temporal phase-shift methods (TPSM) [230, 232] and the temporal Fourier transform method (TFTM) [233]. On the other hand, in spatial methods the phase shift is different for each point of the pattern $\alpha_k(\mathbf{x}) = \alpha(\mathbf{x})$ —usually with a linear dependence of the coordinates $\alpha(\mathbf{x}) = 2\pi\mathbf{f}_c\mathbf{x}$, where $\mathbf{f}_c = (f_{cx}, f_{cy})$ can be interpreted as the frequency of a spatial carrier— whilst a single pattern, rather than a set of them, is often enough to perform the evaluation process; the spatial-carrier phase-shift methods (SCPSM) [234], the spatial synchronous detection method (SSDM) [235] and the spatial Fourier transform method (SFTM) [236] are of this type.

In TVH, as in many other interferometric techniques, the phase-shift is introduced by modulation of the reference phase-difference $\phi_r(\mathbf{x},t)$ although sometimes it is also possible to add an extra term to the object phase-difference $\phi_o(\mathbf{x},t)$. According to the model established for the generation of primary correlgrams in §4, the effects of phase-difference modulation appear in the expression of the fringe function, where the integration of the irradiance in both time —during the exposure interval— and space —over each pixel— is taken into account. The appropriate identification of the terms $i_0(\mathbf{x})$, $v(\mathbf{x})$ y $\phi(\mathbf{x})$ (§6.2) allows to establish the relation between the shape and magnitude of the modulation of the reference phase-difference $\phi_r(\mathbf{x},t)$ and the resulting phase-shift $\alpha_k(\mathbf{x})$; from this point, the corresponding phase-evaluation algorithms can be applied with independence of the type of correlgrams and fringe generation methods that had been used.

6.3.2 Temporal phase-shift generation

Temporal modulation of the reference phase-difference is implemented in TVH with the same methods used in other interferometric techniques [34, 229, 231, 232, 237] as, for example: mirrors and optical fibres attached to piezoelectric devices, translating or rotating wedges and prisms, diffraction gratings, polarising elements, liquid crystal devices (LCD), current and temperature modulation of laser diodes, etc.

Optical phase-difference modulation affects both the modulus and the argument of the fringe function, but in different ways according to the temporal treatment technique used to generate the primary correlgrams, as evidenced in table 1. Generally speaking, the part of the reference phase-difference that remains constant during the exposure interval T_e modifies the argument of the fringe function $\arg[M_n(\mathbf{x})]$, whilst its change during that period appears in $\mathrm{mod}[M_n(\mathbf{x})]$.

6.3.2.1 PM correlgrams

According to the usual identification of terms (§6.2), in primary PM correlgrams (6.2) as well as in the secondary correlgrams obtained from them (6.5) the phase of the pattern is the argument of the fringe function —plus the phase noise $\psi_\mathrm{p}(\mathbf{x})$ in primary correlogams— that for the most usual techniques (table 1) is given by

$$\arg\left[M_n(\boldsymbol{x})\right] = \phi_\mathrm{o}(\boldsymbol{x}) - \phi_\mathrm{r} \tag{6.10}$$

Phase shift is then achieved modulating the reference phase-difference between exposure intervals, i.e., adding to $\arg[M_n(\mathbf{x})]$ a value $\Delta\phi_{\mathrm{r},n}$ that is kept constant during the whole exposure interval $T_{\mathrm{e},n}$ of each primary correlgram

$$\arg\left[M_n(\boldsymbol{x})\right] = \phi_\mathrm{o}(\boldsymbol{x}) - \left(\phi_\mathrm{r} + \Delta\phi_{\mathrm{r},n}\right) \tag{6.11}$$

As pointed in §6.2.1, when phase evaluation is performed on primary PM correlgrams by standard TPSM [221, 222] it is necessary to subtract the phase maps corresponding to two states of the measurand. This implies the acquisition of two sets,

one for each state, of N phase-shifted correlgrams. But only N patterns, $N/2$ for each state of the measurand, are needed with differential TPSM [166, 216] or a sequence of correlgrams with slightly different states for TFTM [238-241].

When secondary correlgrams are used (§6.2.2), on the other hand, it is enough to acquire just one set of N phase-shifted patterns. Three strategies become apparent to generate such set:

a) 1+N

The same reference primary-correlgram is used to generate all the secondary correlgrams. N more primary correlgrams are then acquired with the measurand in the second state and shifting their phases by $\Delta\phi_{\mathrm{r},k} = -\alpha_k$ [45]. Using expressions (6.3), (6.5) and (6.11), the resulting set of secondary correlgrams is

$$\tilde{I}_k(\mathbf{x}) = \underbrace{g^2[\mathcal{I}_0(\mathbf{x})\mathcal{V}(\mathbf{x})]^2\{1-\cos[2\psi_{\mathrm{p}}(\mathbf{x})+\Sigma\phi_{\mathrm{o},k}(\mathbf{x})-2\phi_{\mathrm{r}}+\alpha_k]\}}_{i_{0,k}(\mathbf{x})}\times \\ \times\{1+\underbrace{[-1]}_{v(\mathbf{x})}\underbrace{\cos}_{f}\underbrace{[\Delta\phi_{\mathrm{o},k}(\mathbf{x})+\alpha_k]}_{\phi(\mathbf{x})+\alpha_k}\} \tag{6.12}$$

b) N+1

N reference primary-correlgrams with their phases shifted by $\Delta\phi_{\mathrm{r},k} = \alpha_k$ are acquired. Just one additional primary-correlgram with the measurand in the second state is thus needed [242, 243]. The set of secondary correlgrams is obtained subtracting this last from each of the firsts, and can be expressed

$$\tilde{I}_k(\mathbf{x}) = \underbrace{g^2[\mathcal{I}_0(\mathbf{x})\mathcal{V}(\mathbf{x})]^2\{1-\cos[2\psi_{\mathrm{p}}(\mathbf{x})+\Sigma\phi_{\mathrm{o},k}(\mathbf{x})+2\phi_{\mathrm{r}}-\alpha_k]\}}_{i_{0,k}(\mathbf{x})}\times \\ \times\{1+\underbrace{[-1]}_{v(\mathbf{x})}\underbrace{\cos}_{f}\underbrace{[\Delta\phi_{\mathrm{o},k}(\mathbf{x})+\alpha_k]}_{\phi(\mathbf{x})+\alpha_k}\} \tag{6.13}$$

c) N+N

N primary correlgrams are acquired with the measurand in the reference state with one half of the phase-shift ($\Delta\phi_{\mathrm{r},k} = \alpha_k/2$) and other N with the remainder

($\Delta\phi_{r,k} = -\alpha_k/2$) are taken in the second state. The secondary correlgram sequence is generated subtracting both sets

$$\tilde{I}_k(\mathbf{x}) = \underbrace{g^2[\mathcal{I}_0(\mathbf{x})\mathcal{V}(\mathbf{x})]^2\{1-\cos[2\psi_p(\mathbf{x})+\Sigma\phi_{o,k}(\mathbf{x})+2\phi_r]\}}_{i_{0,k}(\mathbf{x})}\times \\ \times\{1+\underbrace{[-1]}_{v(\mathbf{x})}\underbrace{\cos}_{f}\underbrace{[\Delta\phi_{o,k}(\mathbf{x})+\alpha_k]}_{\phi(\mathbf{x})+\alpha_k}\} \tag{6.14}$$

In these three expressions, $\Sigma\phi_{o,k}(\mathbf{x})$ and $\Delta\phi_{o,k}(\mathbf{x})$ represent the sum and difference, respectively, of the object phase-differences of the two primary PM correlgrams used to generate each secondary correlgram $\tilde{I}_k(\mathbf{x})$.

When TPSM are used, $\Delta\phi_{o,k}(\mathbf{x})$ must have the same value for the whole set of N correlgrams to ensure the accuracy of the phase evaluation process. This implies that only the perturbation of the measurand must be stable for the first of the strategies, only the reference state must be stable for the second —therefore, this option can be applied to transient events— and both reference and perturbed states must be stable for the last.

Moreover, the local average intensity must also be the same for the set of N patterns. This is ensured with the third strategy, but not in the two firsts where $i_{0,k}(\mathbf{x})$ is sinusoidally dependent of the phase-shift α_k. In this last case, the speckle noise must be removed (vid. §5.4) before proceeding to evaluate the phase or, alternatively, an algorithm allowing a variable average-intensity [215] may be used.

6.3.2.2 AM correlgrams

In AM primary (6.4) and the corresponding secondary correlgrams (6.6) the value of the phase is related to the modulus of $M_n(\mathbf{x})$. Then, the phase-shift must be introduced by a modulation of the reference phase-difference, somehow synchronised to the changes of the measurand, during the exposure interval.

In practice, phase evaluation have been only implemented on secondary AM correlgrams of periodic measurands obtained with time-average or double-exposure stroboscopic illumination and homodyne phase modulation.

In the sinusoidal patterns produced with double-exposure stroboscopic illumination (4.41) the phase-shift is controlled by the amplitude of the synchronous reference phase-difference modulation. The primary correlgrams can be identified to a general fringe pattern as follows

$$I_k(\mathbf{x}) = \underbrace{g\mathcal{I}_0(\mathbf{x})}_{i_0(\mathbf{x})}\left\{1+\underbrace{\mathcal{V}(\mathbf{x})\cos\left[\psi_{\mathrm{p}}(\mathbf{x})+\bar{\phi}_{\mathrm{o},k}(\mathbf{x})-\phi_{\mathrm{rA},k}\right]}_{v(\mathbf{x})}\underbrace{\cos}_{f}\left[\underbrace{\frac{\Delta\phi_{\mathrm{o},k}(\mathbf{x})}{2}}_{\phi(\mathbf{x})}-\underbrace{\phi_{\mathrm{rS},k}}_{\alpha_k}\right]\right\} \tag{6.15}$$

And also the corresponding secondary correlgrams [140, 141]

$$\tilde{I}_k(\mathbf{x}) = \underbrace{g^2\left[\mathcal{I}_0(\mathbf{x})\mathcal{V}(\mathbf{x})\right]^2\left(1+\cos\left\{2\left[\psi_{\mathrm{p}}(\mathbf{x})+\bar{\phi}_{\mathrm{o},k}(\mathbf{x})\right]\right\}\right)}_{i_0(\mathbf{x})}\left\{1+\underbrace{\cos}_{f}\left[\underbrace{\Delta\phi_{\mathrm{o},k}}_{\phi(\mathbf{x})}-\underbrace{2\phi_{\mathrm{rS},k}}_{\alpha_k}\right]\right\} \tag{6.16}$$

On the other hand, time-average with sinusoidal homodyne reference phase-difference modulation applied to harmonic measurands (§4.1.2.4) yields non-sinusoidal primary AM correlgrams (4.23), and the secondary ones resulting of sequential subtraction (6.6) follow the expression

$$\begin{aligned}\tilde{I}_n(\mathbf{x}) = &\underbrace{2g^2\left[\mathcal{I}_0(\mathbf{x})\mathcal{V}(\mathbf{x})\right]^2\left(1+\cos\left\{2\left[\psi_{\mathrm{p}}(\mathbf{x})-\phi_{\mathrm{rA}}\right]\right\}\right)}_{i_0(\mathbf{x})}\times \\ &\times\underbrace{\mathrm{J}_0^2\left(\left\{\phi_{\mathrm{om}}^2(\mathbf{x})+\phi_{\mathrm{rm}}^2-2\phi_{\mathrm{om}}(\mathbf{x})\phi_{\mathrm{rm}}\cos\left[\varphi_{\mathrm{o}}(\mathbf{x})-\varphi_{\mathrm{r}}\right]\right\}^{1/2}\right)}_{1+v(\mathbf{x})f[\phi(\mathbf{x})]}\end{aligned} \tag{6.17}$$

To apply the usual phase evaluation algorithms, designed for sinusoidal patterns, this expression must be transformed by approximation in one of the type $1+v(\mathbf{x})\cos[\phi(\mathbf{x})+\alpha_k]$. Two alternative solutions have been proposed:

Pryputniewicz and Stetson [244] take the approximation $\mathrm{J}_0(x) \approx \cos(x)$ and apply reference phase modulation *in phase* with the oscillation of the measurand $\varphi_{\mathrm{o}}(\mathbf{x}) = \varphi_{\mathrm{r}}$. Consequently, this technique can be only used when all the points of the object oscillate in phase. In this conditions, the approximated expression of the secondary correlgrams results

$$\tilde{I}_k(\mathbf{x}) \approx \underbrace{g^2\left[\mathcal{I}_0(\mathbf{x})\mathcal{V}(\mathbf{x})\right]^2\left(1+\cos\left\{2\left[\psi_{\mathrm{p}}(\mathbf{x})-\phi_{\mathrm{rA}}\right]\right\}\right)}_{i_0(\mathbf{x})}\left\{1+\underbrace{\cos}_{f}\left[\underbrace{2\phi_{\mathrm{om}}(\mathbf{x})}_{\phi(\mathbf{x})}-\underbrace{2\phi_{\mathrm{rm}}}_{\alpha_k}\right]\right\} \tag{6.18}$$

and the phase shift is controlled with the amplitude ϕ_{rm} of the reference phase-difference modulation. In principle, this approximation is only valid for very small values of $[\phi_{\mathrm{om}}(\mathbf{x})-\phi_{\mathrm{rm}}]$ and, consequently, of the range of amplitudes of oscillation in the object but, nevertheless, for relatively wide amplitude ranges it is possible to apply correction tables once the erroneous phase has been evaluated and unwrapped.

For very small values of $\phi_{\mathrm{om}}(\mathbf{x})$, it is possible to shift the working point to the centre of the most linear region of the Bessel's function choosing appropriately the amplitude of the sinusoidal reference phase-difference modulation ϕ_{rm} [120, 127]. It is then possible to make the approximation

$$\begin{aligned} &\mathrm{J}_0^2\left(\left\{\phi_{\mathrm{om}}^2(\mathbf{x})+\phi_{\mathrm{rm}}^2-2\phi_{\mathrm{om}}(\mathbf{x})\phi_{\mathrm{rm}}\cos\left[\varphi_{\mathrm{o}}(\mathbf{x})-\varphi_{\mathrm{r}}\right]\right\}^{1/2}\right)\approx \\ &\quad\approx \mathrm{J}_0^2(\phi_{\mathrm{rm}})-\frac{\mathrm{d}}{\mathrm{d}\,\phi_{\mathrm{rm}}}\left[\mathrm{J}_0^2(\phi_{\mathrm{rm}})\right]\phi_{\mathrm{om}}(\mathbf{x})\cos\left[\varphi_{\mathrm{o}}(\mathbf{x})-\varphi_{\mathrm{r}}\right] \end{aligned} \tag{6.19}$$

that substituted in (6.17) results

$$\begin{aligned} \tilde{I}_k(\mathbf{x}) \approx \underbrace{2g^2\left[\mathcal{I}_0(\mathbf{x})\mathcal{V}(\mathbf{x})\right]^2\left(1+\cos\left\{2\left[\psi_{\mathrm{p}}(\mathbf{x})-\phi_{\mathrm{rA}}\right]\right\}\right)\mathrm{J}_0^2\left(\phi_{\mathrm{rm}}\right)}_{i_0(\mathbf{x})}\times \\ \times\left\{1-\underbrace{\breve{k}\phi_{\mathrm{om}}(\mathbf{x})}_{v(\mathbf{x})}\underbrace{\cos}_{f}\left[\underbrace{\varphi_{\mathrm{o}}(\mathbf{x})}_{\phi(\mathbf{x})}-\underbrace{\varphi_{\mathrm{r},k}}_{\alpha_k}\right]\right\} \end{aligned} \tag{6.20}$$

where $\breve{k}$ is a constant that only depends of ϕ_{rm} and is usually experimentally optimised and measured through a calibration process [127]. The phase-shift is controlled with the mechanical phase φ_{r} of the sinusoidal modulation. The result of the phase evaluation process is the local phase of oscillation $\varphi_{\mathrm{o}}(\mathbf{x})$ of the measurand. To obtain the amplitude of oscillation $\phi_{\mathrm{om}}(\mathbf{x})$, the visibility of the pattern $v(\mathbf{x}) = \breve{k}\ \phi_{\mathrm{om}}(\mathbf{x})$ has to be calculated and divided by the scale factor $\breve{k}$.

6.3.3 Spatial carrier generation

Two types of techniques have been proposed in TVH to generate the spatial carrier that methods as SCPSM, SSDM and SFTM require; the most usual is to tilt the

reference beam off the optical axis, although a technique based on a degenerated version of contouring has been recently introduced.

6.3.3.1 Off-axis reference beam

This technique is applied in out-of-plane sensitive interferometers with a, generally uniform, reference beam. When the reference beam is tilted respect to the object beam, the reference phase-difference $\phi_r(\mathbf{x})$ becomes different at each point of the interferogram; if the tilt angle is the same for every point, the dependence of $\phi_r(\mathbf{x})$ with the coordinates is linear and then

$$\phi_{r,k}(\mathbf{x}) = \phi_r + 2\pi\mathbf{f}_c\mathbf{x} = \phi_r + \Delta\phi_{r,k}(\mathbf{x}) \tag{6.21}$$

where ϕ_r is a constant.

For the evaluation of primary PM correlgrams —that has been implemented with SCPSM [21, 245] and SFTM [43, 246]— the tilt of the reference beam is permanent, therefore

$$I_n(\mathbf{x}) = \underbrace{g\mathcal{I}_0(\mathbf{x})}_{i_0(\mathbf{x})}\left\{1 + \underbrace{\mathcal{V}(\mathbf{x})}_{v(\mathbf{x})}\underbrace{\cos}_{f}\left[\underbrace{\psi_p(\mathbf{x}) + \phi_o(\mathbf{x}) + \phi_r}_{\phi(\mathbf{x})} + \underbrace{2\pi\mathbf{f}_c\mathbf{x}}_{\alpha(\mathbf{x})}\right]\right\} \tag{6.22}$$

When secondary PM correlgrams are used [247], the reference beam is tilted between the reference and the succeeding primary correlgrams. Once again, two strategies are apparent:

a) Unidirectional tilt

The reference primary correlgram is acquired with an in-line reference beam — $\Delta\phi_{r,ref} = 0$—and then it is tilted to produce $\Delta\phi_{r,k} = -2\pi\mathbf{f}_c\mathbf{x} = -\alpha(\mathbf{x})$. Substituting in (6.3) and (6.5), the resulting secondary correlgrams are

$$\tilde{I}_k(\mathbf{x}) = \underbrace{g^2[\mathcal{I}_0(\mathbf{x})\mathcal{V}(\mathbf{x})]^2\{1-\cos[2\psi_\mathrm{p}(\mathbf{x})+\Sigma\phi_{\mathrm{o},k}(\mathbf{x})-2\phi_\mathrm{r}+2\pi\mathbf{f}_\mathrm{c}\mathbf{x}]\}}_{i_{0,k}(\mathbf{x})}\times \\ \times\{1+\underbrace{[-1]}_{v(\mathbf{x})}\underbrace{\cos}_{f}[\underbrace{\Delta\phi_{\mathrm{o},k}(\mathbf{x})}_{\phi(\mathbf{x})}+\underbrace{2\pi\mathbf{f}_\mathrm{c}\mathbf{x}}_{\alpha(\mathbf{x})}]\} \tag{6.23}$$

b) Symmetrical tilt

The reference primary correlgram is acquired with one half of the tilt and, therefore, with an spatial carrier $\Delta\phi_{\mathrm{r,ref}} = \pi\mathbf{f}_\mathrm{c}\mathbf{x} = \alpha(\mathbf{x})/2$; the reference beam is then symmetrically tilted in the opposite direction to get $\Delta\phi_{\mathrm{r},k} = -\pi\mathbf{f}_\mathrm{c}\mathbf{x} = -\alpha(\mathbf{x})/2$. The resulting secondary correlgrams

$$\tilde{I}_k(\mathbf{x}) = \underbrace{g^2[\mathcal{I}_0(\mathbf{x})\mathcal{V}(\mathbf{x})]^2\{1-\cos[2\psi_\mathrm{p}(\mathbf{x})+\Sigma\phi_{\mathrm{o},k}(\mathbf{x})+2\phi_\mathrm{r}]\}}_{i_{0,k}(\mathbf{x})}\times \\ \times\{1+\underbrace{[-1]}_{v(\mathbf{x})}\underbrace{\cos}_{f}[\underbrace{\Delta\phi_{\mathrm{o},k}(\mathbf{x})}_{\phi(\mathbf{x})}+\underbrace{2\pi\mathbf{f}_\mathrm{c}\mathbf{x}}_{\alpha(\mathbf{x})}]\} \tag{6.24}$$

are free of carrier noise in their local mean intensity and can be directly evaluated.

Finally, when this technique is applied to AM correlgrams the reference beam is tilted during the exposure of each primary correlgram. For example, with double-exposure pulsed illumination [248] the reference beam is tilted between the light pulses.

6.3.3.2 Degenerate contouring

In this variant, the carrier is introduced through the changes of the object phase-difference $\Delta\phi_\mathrm{o}(\mathbf{x})$ tilting the illumination beam between exposures; being this tilt symmetrical with respect to the observation direction (§3.3.3) it is equivalent to a degenerate shape-measurement technique where the contouring planes are parallel to the observation direction and produce a set of equally-spaced parallel fringes that is used as spatial carrier. The change of the object phase-difference among exposures can be expressed as

$$\Delta\phi_{o,k}(\mathbf{x}) = \Delta\phi_{oo,k}(\mathbf{x}) + \Delta\phi_{oc,k}(\mathbf{x}) = \Delta\phi_{oo,k}(\mathbf{x}) + 2\pi\mathbf{f}_c\mathbf{x} \tag{6.25}$$

where $\Delta\phi_{oo,k}(\mathbf{x})$ is the increment due to the changes of the measurand and $\Delta\phi_{oc,k}(\mathbf{x})$ is the increment induced by degenerate contouring.

This technique has been demonstrated with secondary PM correlgrams for contouring [249], shearing [250, 251], out-of-plane[152, 252] and in-plane [253] geometries.

6.3.4 Simultaneous phase-shift

Whenever the number *N* of phase-shifted primary correlgrams needed to evaluate the phase with TPSM is small, they can be generated at once and recorded with individual video cameras —generally three to comply with the input requirements of RGB standard digitisers— to produce phase maps in almost real-time. This requires a rigorous alignment of the cameras as long as, in general, the speckle size has to be comparable to the size of the pixels to maximise the contrast of the fringes.

The phase-shift among the correlgrams is induced with either polarising elements [176] or diffraction gratings [228, 254].

7 Concluding remarks

Image-plane TV-holography is now a well established branch of this field of optical metrology. Most of its variants have been investigated and, consequently, it can be considered with a global perspective that permits the systematisation of its procedures and techniques. The development of the other branch, Fresnel/Fourier TVH, is just beginning and many of its potential methods are, at present, unexplored. It would be, therefore, somewhat speculative to propose at the time being a common scheme for both of them.

Our approach to TVH can accommodate the techniques of Fresnel/Fourier TVH that have been reported to date, but this does not mean that all the techniques reported

for the first branch have to be applicable to the second, some of then may work an others not.

All the Fresnel/Fourier TVH techniques that have been established use interferometers with a smooth reference beam that provide sensitivity to displacements out-of-plane (§3.1.1), in general directions (§3.1.3) [18, 21, 22], in multiple directions (§3.1.4) [255] or to the shape (§3.3.1) [25, 26]. The use of interferometers with two speckle beams as, for example, double-illumination (§3.1.2, §3.3.3.2) and shearing ones (§3.2) has not been reported.

Apparently, all the temporal treatment techniques that yield PM correlgrams can be used in Fresnel/Fourier TVH. Time average with a static measurand (§4.1.1) [22, 23], single exposure (§4.3.1) [20, 25] and double-single exposure (§4.3.3.1) [21, 24] pulsed illumination have been demonstrated, and single exposure stroboscopic illumination can be used in similar conditions. Nothing has been published about the techniques that yield true AM correlgrams but, according to the results obtained by Schnars and Jüptner [23] with synthetic AM correlgrams produced by the addition of two PM correlgrams, they must be also applicable in this branch of TVH.

The main difference between image-plane and Fresnel/Fourier TVH is that in the last the analysis of the fringe pattern is always necessary in order to calculate the complex amplitude —i.e., the local average intensity and the phase— of the hologram (primary correlgram); then the corresponding complex amplitude at the object plane has to be *reconstructed* simulating the back-propagation of light by use of the diffraction integral in Fresnel's or Fourier's (Fraunhoffer's) approximation [19, 24, 256, 257]. The phase of the resulting complex amplitude is the phase-difference of the interfering beams corresponding to each point of the object and its magnitude can be used to render secondary-fringe patterns.

In most of the Fresnel/Fourier TVH systems that have been reported [18-27] an off-axis reference beam is used to introduce an spatial carrier and the reconstruction is

performed directly from the primary correlgrams simulating the optical reconstruction of classic holograms, i.e., the diffraction of the reference beam through the hologram. This procedure is equivalent [258] to calculate the complex amplitude of the primary correlgram using the spatial Fourier transform method [236] —that involves the Fourier transform, filtering and inverse Fourier transform— and then perform the reconstruction with the diffraction integral —a further Fourier transform with a weighting function [24]. It has been demonstrated that other evaluation methods as, for example, temporal phase-shifting can also be used to calculate that complex amplitude [259] although they cannot be merged with the reconstruction process as the SFTM.

Secondary-fringe generation techniques can be applied to the reconstructed intensity fields [21], but also to the primary correlgrams before the reconstruction [23], in this case omitting the square-law demodulation that is implicitly performed when calculating the intensity of the reconstructed field.

The new Fresnel/Fourier techniques that, beyond the shadow of a doubt, are due to appear in the next years will ultimately determine whether our approach to TV-holography is fully applicable to both branches or has to be modified to embrace them.

References

[1] Butters J N 1971 Speckle pattern interferometry using video techniques *SPIE Journal* **10** 5–9

[2] Butters J N and Leendertz J A 1971 Speckle pattern and holographic techniques in engineering metrology *Optics and Laser Technology* **3** 26–30

[3] Butters J N and Leendertz J A 1971 Reasons and methods for electronic processing in coherent light systems for engineering measurement *Proceedings of the Technical Program Electro-Optics'71 International Conference* (Brighton, England) 189–193

[4] Butters J N and Leendertz J A 1971 Holographic and video techniques applied to engineering measurement *Transactions of the Institute of Measurement and Control* **4** 349–354

[5] Macovski A, Ramsey S D and Schaefer L F 1971 Time-lapse interferometry and contouring using television systems *Applied Optics* **10** 2722–2727

[6] Schwomma O 1972 Holographisch-interferometrisches oder moirémetrisches Verfahren *Osterreichisches Patent no. 298 830*

[7] Köpf U 1972 *Messtechnik* **4** p 105

[8] Gåsvik K 1980 Vibration analysis of a circular saw blade by means of moiré technique and TV-holography *OSA Technical Digest of the Topical Meeting on Hologram Interferometry and Speckle Metrology (June 1980)* WA6-1

[9] Gåsvik K J 1987 *Optical Metrology* (Chichester:John Wiley & Sons) 108–113

[10] Nakadate S , Yatagai T and Saito H 1980 Electronic speckle pattern interferometry using digital image processing techniques *Applied Optics* **19** 1879–1883

[11] Nakadate S , Yatagai T and Saito H 1983 Computer-aided speckle pattern interferometry *Applied Optics* **22** 237–243

[12] Oreb B F , Sharon B and Hariharan P 1984 Electronic speckle pattern interferometry with a microcomputer *Applied Optics* **23** 3940–3941

[13] Hirai A , Akatsu T and Horii Y 1985 Dynamic motion measurement using digital TV speckle interferometry *Proc. SPIE* **549** 86–93

[14] Creath K 1984 Digital speckle pattern interferometry (DSPI) using a 100x100 imaging array *Proc. SPIE* **501** 292–298

[15] Stetson K A and Brohinsky W R 1985 Electrooptic holography and its application to hologram interferometry *Applied Optics* **24** 3631–3637

[16] Stetson K A 1990 Theory and applications of electronic holography *Proc. SEM. Conference on Hologram Interferometry and Speckle Metrology* (Baltimore) 294–300

[17] Malmo J T and Vikhagen E 1988 Vibration analysis of a car body by means of TV holography *Experimental Techniques* **12** 28–30

[18] Schnars U and Jüptner W 1993 Principles of direct holography for interferometry *Fringes'93. Proceedings of the 2nd International Workshop on Automatic Processing of Fringe Patterns* (Bremen:Akademie Verlag (Berlin)) 115–120

[19] Schnars U and Jüptner W 1994 Direct recording of holograms by a CCD target and numerical reconstruction *Applied Optics* **33** 179–181

[20] Schnars U , Kreis T M and Jüptner W P O 1996 Digital recording and numerical reconstruction of holograms: reduction of the spatial frequency spectrum *Optical Engineering* **35** 977–982

[21] Pedrini G , Tiziani H J and Zou Y 1997 Digital double pulse-TV-holography *Optics and Lasers in Engineering* **26** 199–219

[22] Schnars U 1994 Direct phase determination in hologram interferometry with use of digitally recorded holograms *J. Opt. Soc. Am. A* **11** 2011–2015

[23] Schnars U and Jüptner W P O 1994 Digital recording and reconstruction of holograms in hologram interferometry and shearography *Applied Optics* **33** 4373–4377

[24] Pedrini G , Zou Y L and Tiziani H J 1995 Digital double-pulsed holographic interferometry for vibration analysis *Journal of Modern Optics* **42** 367–374

[25] Zou Y -L , Pedrini G and Tiziani H 1996 Two-wavelength contouring with a pulsed ruby laser by employing TV-holography *Journal of Modern Optics* **43** 639–646

[26] Zou Y , Pedrini G and Tiziani H 1996 Surface contouring in a video frame by changing the wavelength of a diode laser *Optical Engineering* **35** 1074–1079

[27] Pomarico J , Schnaars U , Hartmann H-J and Jüptner W 1995 Digital recording and numerical reconstruction of holograms: a new method for displaying light in flight *Applied Optics* **34** 8095–8099

[28] Butters J N , Jones R and Wykes C 1978 Electronic speckle pattern interferometry *Speckle metrology* ed Erf R K (London:Academic Press) 111–158

[29] Løkberg O J 1980 Electronic speckle pattern interferometry *Phys. Technol.* **11** 16–22

[30] Løkberg O J 1984 ESPI - The ultimate holographic tool for vibration analysis? *Journal of the Acoustics Society of America* **75** 1783–1791

[31] Løkberg O J 1993 Recent developments in video speckle interferometry *Speckle Metrology* ed Sirohi R S (New York:Marcel Dekker) 157–194

[32] Løkberg O J and Slettemoen G Å 1987 Basic electronic speckle pattern interferometry *Applied Optics and Optical Engineering* **10** eds Shannon R and Wyant J C (San Diego:Academic Press) 455–504

[33] Jones R and Wykes C 1989 *Holographic and speckle interferometry* (Cambridge:Cambridge University Press)

[34] Davies J C and Buckberry C H 1993 Television holography and its applications *Optical methods in engineering metrology* ed Williams D C (London:Chapman & Hall) 275–338

[35] Born M and Wolf E 1993 *Principles of optics* (Oxford:Pergamon Press) 505-508

[36] Goodman J W 1984 Statistical properties of laser speckle patterns *Laser speckle and related phenomena (Second edition)* ed Dainty J C (Berlin:Springer-Verlag) 9–75

[37] Slettemoen G Å 1979 General analysis of fringe contrast in electronic speckle pattern interferometry *Optica Acta* **26** 313–327

[38] Butters J N 1976 Electronic speckle pattern interferometry: a general review background to subsequent papers *The engineering uses of coherent optics* ed Robertson E R (Cambridge:Cambridge University Press) 155–169

[39] Jones R and Wykes C 1981 General parameters for the design and optimization of electronic speckle pattern interferometers *Optica Acta* **28** 949–972

[40] Virdee M S , Williams D C , Banyard J E and Nassar N S 1990 A simplified system for digital speckle interferometry *Optics and Laser Technology* **22** 311–316

[41] Løkberg O J , Seeberg B E and Vestli K 1997 Microscopic video speckle interferometry *Optics and Lasers in Engineering* **26** 313–330

[42] Soares O D D , Lage A L V S and Sakowski H 1987 Improvements on electronic speckle pattern interferometry *Optical metrology* ed Soares O D D (Dordrecht:Martinus Nijhoff Publishers) 587–605

[43] Saldner H O , Molin N -E and Stetson K A 1996 Fourier-transform evaluation of phase data in spatially phase-biased TV holograms *Applied Optics* **35** 332–336

[44] Biedermann K and Ek L 1975 A recording and display system for hologram interferometry with low resolution imaging devices *Journal of Physics E: Sci. Instrum.* **8** 571–576

[45] Nakadate S and Saito H 1985 Fringe scanning speckle-pattern interferometry *Applied Optics* **24** 2172–2180

[46] Peng S , Joenathan C and Khorana B M 1992 Quasi-equal-path electronic speckle pattern interferometric system *Optics Letters* **17** 1040–1042

[47] Joenathan C and Khorana B M 1993 Quasi-equal-path electronic speckle pattern interferometric system *Applied Optics* **32** 5724–5726

[48] Schultz B 1994 Electronic speckle-pattern-interferometrie through shearography *Proc. SPIE* **2358** 153–157

[49] Pouet B F and Krishnaswamy S 1993 Additive/subtractive decorrelated electronic speckle pattern interferometry *Optical Engineering* **32** 1360–1369

[50] Slettemoen G Å 1980 Electronic speckle pattern interferometric system based on a speckle reference beam *Applied Optics* **19** 616–623

[51] Joenathan C and Khorana B M 1991 A simple and modified ESPI system *Optik* **88** 169–171

[52] Joenathan C and Torroba R 1991 Modified electronic speckle pattern interferometer employing an off-axis reference beam *Applied Optics* **30** 1169–1171

[53] Petrov V and Lau B 1996 Electronic speckle pattern interferometry with a holographically generated reference wave *Optical Engineering* **35** 2363–2370

[54] Løkberg O J 1985 Mapping of in-plane vibration modes by electronic speckle pattern interferometry *Optical Engineering* **24** 356–359

[55] Joenathan C , Sohmer A and Bürkle L 1995 Increased sensitivity to in-plane displacements in electronic speckle pattern interferometry *Applied Optics* **34** 2880–2885

[56] Butters J N and Leendertz J A 1971 A double exposure technique for speckle pattern interferometry *Journal of Physics E: Sci. Instrum.* **4** 277–279

[57] Duffy D E 1972 Moiré gauging of in-plane displacement using double aperture imaging *Applied Optics* **11** 1178–1181

[58] Sirohi R S and Krishna Mohan N 1993 In-plane displacement measurement configuration with twofold sensitivity *Applied Optics* **32** 6387–6390

[59] Sohmer A and Joenathan C 1996 Twofold increase in sensitivity with a dual-beam illumination arrangement for electronic speckle pattern interferometry *Optical Engineering* **35** 1943–1948

[60] Joenathan C , Franze B and Tiziani H J 1994 Oblique incidence and observation electronic speckle-pattern interferometry *Applied Optics* **33** 7307–7311

[61] Hung Y Y 1978 Displacement and strain measurement *Speckle Metrology* ed Erf R K (London:Academic Press) 51–71

[62] Pedrini G and Tiziani H J 1994 Double-pulse electronic speckle pattern interferometry for vibration analysis *Applied Optics* **33** 7857–7863

[63] Mendoza-Santoyo F , Shellabear M C and Tyrer J R 1991 Whole field in-plane vibration analysis using pulsed phase-stepped ESPI *Applied Optics* **30** 717–721

[64] Shellabear M C and Tyrer J R 1988 Three-dimensional vibration analysis using electronic speckle pattern interferometry (ESPI) *Proc. SPIE* **952** 251–259

[65] Moore A J and Tyrer J R 1990 An electronic speckle pattern interferometer for complete in-plane displacement measurement *MEASUREMENT SCIENCE AND TECHNOLOGY* **1** 1024–1030

[66] Shellabear M C and Tyrer J R 1991 Application of ESPI to three-dimensional vibration measurements *Optics and Lasers in Engineering* **15** 43–56

[67] Winther S 1988 3D strain measurements using ESPI *Optics and Lasers in Engineering* **8** 45–57

[68] Bhat G K 1995 Measurement of strains in turbine blades vibrating at resonance using electro-optic holography *Journal of Modern Optics* **42** 667–677

[69] Arizaga R , Rabal H and Trivi M 1994 Simultaneous multiple-viewpoint processing in digital speckle pattern interferometry *Applied Optics* **33** 4369–4372

[70] Wang L-S , Janbunathan K , Dobbins B N and He S-P 1996 Measurement of three-dimensional surface shape and deformations using phase stepping speckle interferometry *Optical Engineering* **35** 2333–2340

[71] Ganesan A R , Joenathan C and Sirohi R S 1987 Real-time comparative digital speckle pattern interferometry *Optics Communications* **64** 501–506

[72] Ganesan A R , Meinlschmidt P and Hinsch K D 1994 Vibration mode separation using comparative electronic speckle pattern interferometry (ESPI) *Optics Communications* **107** 28–34

[73] Saldner H O , Krishna Mohan N and Molin N-E 1995 Comparative TV holography for vibration analysis *Optical Engineering* **34** 486–492

[74] Aebischer H A and Waldner S 1997 Strain distributions made visible with image-shearing speckle pattern interferometry *Optics and Lasers in Engineering* **26** 407–420

[75] Tyrer J R and Petzing J N 1997 In-plane electronic speckle pattern shearing interferometry *Optics and Lasers in Engineering* **26** 395–406

[76] Mantravadi M V 1992 Lateral shearing interferometers *Optical Shop Testing* ed Malacara D 123–172

[77] Leendertz J A and Butters J N 1973 An image-shearing speckle-pattern interferometer for measuring bending moments *Journal of Physics E: Sci. Instrum.* **6** 1107–1110

[78] Hung Y Y , Tang S and Hovanesian J D 1994 Real-time shearography for measuring time-dependent displacement derivatives *Experimental Mechanics* **34** 89–92

[79] Nakadate S , Yatagai T and Saito H 1980 Digital speckle-pattern shearing interferometry *Applied Optics* **19** 4241–4246

[80] Rabal H , Henao R and Torroba R 1996 Digital speckle pattern shearing interferometry using diffraction gratings *Optics Communications* **126** 191–196

[81] Joenathan C and Bürkle L 1997 Electronic speckle pattern shearing interferometer using holographic gratings *Optical Engineering* **36** 2473–2477

[82] Krishna Murthy R , Sirohi R S and Kothiyal M P 1982 Speckle shearing interferometry: a new method *Applied Optics* **21** 2865–2867

[83] Joenathan C and Torroba R 1990 Simple electronic speckle-shearing-pattern interferometer *Optics Letters* **15** 1159–1161

[84] Krishna Mohan N , Masalkar P J and Sirohi R S 1992 Electronic speckle pattern interferometry with holo-optical element *Proc. SPIE* **1821** 234–242

[85] Valera J D and Jones J D C 1994 Phase stepping in fiber-based speckle shearing interferometry *Optics Letters* **19** 1161–1163

[86] Valera J D R , Jones J D C , Towers D P and Buckberry C H 1997 Strain and vibration analysis by fibre based speckle shearing interferometry *Optics and Lasers in Engineering* **26** 361–376

[87] Krishna Murthy R , Mohanty R K , Sirohi R S and Kothiyal M P 1984 Radial speckle shearing interferometer and its engineering aplications *Optik* **67** 85–94

[88] Mohanty R K , Joenathan C and Sirohi R S 1986 High sensitivity tilt measurement by speckle shear interferometry *Applied Optics* **25** 1661–1664

[89] Ganesan A R , Sharma D K and Kothiyal M P 1988 Universal digital speckle shearing interferometer *Applied Optics* **27** 4731–4734

[90] Krishna Mohan N , Saldner H and Molin N -E 1993 Electronic speckle pattern interferometry for simultaneous measurement of out-of-plane displacement and slope *Optics Letters* **18** 1861–1863

[91] del Carreto P and Perlo P 1994 Compact multi-beam shearography for deformation and vibration observation *Proc. SPIE* **2358** 140–144

[92] Denby D , Quintanilla G E and Butters J N 1976 Contouring by electronic speckle pattern interferometry *The engineering uses of coherent optics* ed Robertson E R (Cambridge:Cambridge University Press) 171–197

[93] Butters J N and Leendertz J A 1974 Component inspection using speckle pattern *Proc. of the Technical Program Electro-Optics'73 International Conference* (Brighton:Kiver Communications) 43–50

[94] Jones R and Butters J N 1975 Some observations on the direct comparison of the geometry of two objects using speckle pattern interferometric contouring *Journal of Physics E: Sci. Instrum.* **8** 231–234

[95] Jones R and Wykes C 1978 The comparison of complex object geometries using a combination of electronic speckle pattern inteferometric difference contouring and holographic illumination elements *Optica Acta* **25** 449–472

[96] Wykes C 1977 De-correlation effects in speckle-pattern interferometry. 1. Wavelength change dependent de-correlation with application to contouring and surface roughness measurement *Optica Acta* **24** 517–532

[97] Tatam R P , Davies J C , Buckberry C H and Jones J D C 1990 Holographic surface contouring using wavelength modulation of laser diodes *Optics & Laser Technology* **22** 317–321

[98] Peng X , Zou Y L , Diao H Y and Tiziani H J 1992 A simplified multi-wavelength ESPI contouring technique based on a diode laser system *Optik* **91** 81–85

[99] Rastogi P K 1993 Techniques of displacement and deformation measurements in speckle metrology *Speckle Metrology* ed Sirohi R S (New York:Marcel Dekker) 41–98

[100] Winther S and Slettemoen G Å 1984 An ESPI contouring technique in strain analysis *Proc. SPIE* **473** 44–47

[101] Rodríguez-Vera R , Kerr D and Mendoza-Santoyo F 1992 Electronic speckle contouring *J. Opt. Soc. Am. A* **9** 2000–2008

[102] Rodríguez-Vera R 1997 Optical gauging of diffuse surfaces by electronic speckle contouring *Optics and Lasers in Engineering* **26** 101–114

[103] Diao H , Zou Y , Peng X , Tiziani H J and Chen L 1992 Calibration of the inclined contour planes formed on ESPI and optimization of ESPI optical system for contouring *Optik* **91** 71–75

[104] Peng X , Diao H Y , Zou Y L and Tiziani H J 1992 Contouring by modified dual-beam ESPI based on tilting illumination beams *Optik* **90** 61–64

[105] Ganesan A R and Sirohi R S 1988 New method of contouring using digital speckle pattern interferometry (DSPI) *Proc. SPIE* **954** 327–332

[106] Joenathan C , Pfister B and Tiziani H J 1990 Contouring by electronic speckle pattern interferometry employing dual beam illumination *Applied Optics* **29** 1905–1911

[107] Zou Y , Diao H , Peng X and Tiziani H 1992 Geometry for contouring by electronic speckle pattern interferometry based on shifting illumination beams *Applied Optics* **31** 6616–6621

[108] Diao H , Zou Y and Tiziani H J 1993 Design considerations of a dual-beam ESPI optical system for contouring *Optik* **93** 45–51

[109] Zou Y , Diao H , Peng X and Tiziani H 1992 Contouring by electronic speckle pattern interferometry with quadruple-beam illumination *Applied Optics* **31** 6599–6602

[110] Bolognini N , Rabal H and Torroba R 1992 Single-beam digital holographic contouring *Applied Optics* **31** 1009–1011

[111] Zou Y , Pedrini G and Tiziani H 1994 Contouring by electronic speckle pattern interferometry employing divergent dual beam illumination *Journal of Modern Optics* **41** 1637–1652

[112] Arizaga R , Rabal H , Trivi M , Alanís E and Romero G 1994 Single fringe contouring *Optics Communications* **108** 209–213

[113] Lu B , Yang X , Abendroth H , Eggers H and Ziolkowski E 1988 Measurement of a three-dimensional temperature field applying ESPI and CT techniques *Optics Communications* **69** 6–10

[114] Løkberg O J , Espeland M and Pedersen H M 1995 Tomographic reconstruction of sound fields using TV holography *Applied Optics* **34** 1640–1645

[115] Løkberg O J , Rustad R and Espeland M 1996 Tomographic reconstruction of sound fields in air using TV-holography *Optics and Lasers in Engineering* **25** 361–372

[116] Rustad R , Løkberg O J , Pedersen H M , Klepsvik K and Støren T 1996 Full field tomographic reconstruction of acoustic fields using TV-holography theory, developments and possibilities *Proc. SPIE* **2782** 302–312

[117] Løkberg O J 1994 Sound in flight: measurement of sound fields by use of TV holography *Applied Optics* **33** 2574–2584

[118] Dupont O , Dewandel J L and Legros J C 1995 Use of electronic speckle pattern inteferometry for temperature distribution measurements through liquids *Optics Letters* **20** 1824–1826

[119] Stetson K A 1969 A rigorous treatment of the fringes of hologram interferometry *Optik* **29** 386–400

[120] Høgmoen K and Pedersen H M 1977 Measurement of small vibrations using electronic speckle pattern interferometry: Theory *J. Opt. Soc. Am.* **67** 1578–1583

[121] Aleksoff C C 1974 Temporal modulation techniques *Holographic nondestructive testing* ed Erf R K (Orlando:Academic Press) 247–263

[122] Løkberg O J 1979 Use of chopped laser light in electronic speckle pattern interferometry *Applied Optics* **18** 2377–2384

[123] Rosvold G O and Løkberg O J 1993 Effect and use of exposure control in vibration analysis using TV holography *Applied Optics* **32** 684–691

[124] Løkberg O J and Høgmoen K 1976 Use of modulated reference wave in electronic speckle pattern interferometry *Journal of Physics E: Scientific Instruments* **9** 847–851

[125] Løkberg O J and Høgmoen K 1976 Vibration phase mapping using electronic speckle pattern interferometry *Applied Optics* **15** 2701–2704

[126] Løkberg O J and Høgmoen K 1977 Holographic methods made useful by phase modulated ESPI *Proc. SPIE* **136** 222–225

[127] Ellingsrud S and Rosvold G O 1992 Analysis of a data-based TV-Holography system used to measure small vibration amplitudes *J. Opt. Soc. Am. A* **9** 237–251

[128] Stetson K A and Brohinsky W R 1988 Fringe-shifting technique for numerical analysis of time-average holograms of vibrating objects *J. Opt. Soc. Am. A* **5** 1472–1476

[129] Moran S E , Law R L , Craig P N and Goldberg W M 1987 Optically phase-locked electronic speckle pattern interferometer *Applied Optics* **26** 475–491

[130] Valera Robles J D , Harvey D and Jones J D C 1992 Automatic heterodyning in fiber optic speckle pattern interferometry using laser velocimetry *Optical Engineering* **31** 1646–1653

[131] Valera J D , Doval A F and Jones J D C 1993 Combined fibre optic laser velocimeter and electronic speckle pattern interferometer with a common reference beam *MEASUREMENT SCIENCE AND TECHNOLOGY* **4** 578–582

[132] Moran S E , Luganani R , Craig P N and Law R L 1989 Optically phase-locked electronic speckle pattern interferometer system performance for vibration measurement in random displacement fields *J. Opt. Soc. Am. A.* **6** 252–269

[133] Høgmoen K and Løkberg O J 1977 Detection and measurement of small vibrations using electronic speckle pattern interferometry *Applied Optics* **16** 1869–1875

[134] Pedersen H M , Løkberg O J , Valo H and Wang G 1994 Detection of nonsinusoidal periodic vibrations using phase-modulated TV-holography *Optics Communications* **104** 271–276

[135] Løkberg O J , Pedersen H M , Valo H and Wang G 1994 Measurement of higher harmonics in periodic vibrations using phase-modulated TV holography with digital image processing *Applied Optics* **33** 4997–5002

[136] Waters J P 1974 Interferometric Holography *Holographic Nondestructive Testing* ed Erf R K (Orlando:Academic Press) 87–103

[137] Steinbichler H and Gehring G 1996 TV-holography and holographic interferometry: industrial applications *Optics and Lasers in Engineering* **24** 111–127

[138] Gaskill J D 1978 *Linear systems, Fourier transforms and optics* (New York:John Wiley & Sons) 60-63

[139] Alén J M, Doval A F, Bugarín J, Dorrío B V, López C, Fernández A, Blanco-García J, Pérez-Amor M and Fernández J L 1997 Phase-shifted double single-pulse additive stroboscopic TV-holography for the measurement of high-frequency vibrations using low-bandwidth phase modulation devices *Proc. SPIE* **3098** 166-175

[140] Doval A F , Fernández J L , Pérez-Amor M , Valera J D and Jones J D C 1994 Phase-stepped additive stroboscopic fibre optic TV holography for vibration analysis *Proc. SPIE* **2248** 229–240

[141] Wang L -S and Krishnaswamy S 1996 Additive-subtractive speckle interferometry: extraction of phase data in noisy environments *Optical Engineering* **35** 794–801

[142] Doval A F , Fernández J L , Pérez-Amor M , Valera J D R and Jones J D C 1996 Contrast enhanced and phase controlled stroboscopic additive fibre optic TV-holography for whole field out-of-plane vibration analysis *Optics and Lasers in Engineering* **25** 323–342

[143] Chatters T , Pouet B and Krishnaswamy S 1992 ESPI with synchronized pressure stressing *Proc. SPIE* **1821** 38–45

[144] Hughes R G 1976 The determination of vibration patterns using a pulsed laser with holographic and electronic speckle pattern interferometry techniques *The engineering uses of coherent optics* ed Robertson E R (Cambridge:Cambridge University Press) 199–218

[145] Cookson T J , Butters J N and Pollard H C 1978 Pulsed lasers in electronic speckle pattern interferometry *Optics and Laser Technology* **10** 119–124

[146] Tyrer J R 1985 Application of pulsed holography and double pulsed electronic speckle pattern interferometry to large vibrating engineering structures *Proc. SPIE* **599** 181–188

[147] Mendoza-Santoyo F , Tyrer J R , West T C and Kerr D 1989 Vibration analysis using phase stepped pulsed electronic speckle pattern interferometry *Proc. SPIE* **1084** 262–278

[148] Spooren R 1990 TV-holography using a double pulsed single oscillator Nd:YAG laser; restrictions and possibilities *Proc. SEM Conference on Hologram Interferometry and Speckle Metrology* eds Stetson K A and Pryputniewicz R J (Baltimore) 260–267

[149] Spooren R 1992 Double-pulse characteristics of a single-oscillator Nd:YAG laser affecting its performance in TV holography *Applied Optics* **31** 208–216

[150] Shellabear M C , Mendoza Santoyo F and Tyrer J R 1990 Processing of addition and subtraction fringes from pulsed ESPI for the study of vibrations *Proc. SEM Conference on Hologram Interferometry and Speckle Metrology* eds Stetson K A and Pryputniewicz R J (Baltimore) 238–244

[151] Mendoza-Santoyo F , Moore A J , Tyrer J R and Alcalá-Ochoa N 1994 Noise reduction in twin-pulsed addition electronic speckle pattern interferometry fringe patterns *Optical Engineering* **33** 1712–1716

[152] Fernández A, Blanco-García J, Doval A F, Bugarín J, Dorrío B V, López C, Alén J M, Pérez-Amor M and Fernández J L 1998 Transient deformation measurement by double-pulsed-subtraction TV holography and the Fourier transform method *Applied Optics* **37** 3440-3446

[153] Spooren R 1994 Standard charge-coupled device cameras for video speckle interferometry *Optical Engineering* **33** 889–896

[154] Holst G C 1996 *CCD arrays, cameras and displays* (Bellingham WA/USA:SPIE Optical Engineering Press) 55-65

[155] Spooren R 1991 Fringe quality in pulsed TV-holography *Proc. SPIE* **1508** 118–127

[156] Spooren R 1992 Double-pulse subtraction TV holography *Optical Engineering* **31** 1000–1007

[157] Pedrini G , Pfister B and Tiziani H 1993 Double pulse-electronic speckle interferometry *Journal of Modern Optics* **40** 89–96

[158] Slettemoen G Å 1977 Optimal signal processing in electronic speckle pattern interferometry *Optics Communications* **23** 213–216

[159] Pedersen H M , Løkberg O J and Forre B M 1974 Holographic vibration measurement using a TV speckle interferometer with silicon target vidicon *Optics Communications* **12** 421–426

[160] Løkberg O J , Holje O M and Pedersen H M 1976 Scan converter memory used in TV-speckle interferometry *Optics and Laser Technology* **8** 17–20

[161] Nakadate S 1986 Vibration measurement using phase-shifting speckle-pattern interferometry *Applied Optics* **25** 4162–4167

[162] Davila A , Kaufmann G H and Kerr D 1993 Digital processing of ESPI addition fringes *Proc. FASIG, "Fringe'93"* eds Jüptner W and Osten W (Bremen:Akademie Verlag) 339–346

[163] Davila A , Kerr D and Kaufmann G H 1994 Digital processing of electronic speckle pattern interferometry addition fringes *Applied Optics* **33** 5964–5969

[164] Creath K and Slettemoen G A 1985 Vibration-observation techniques for digital speckle-pattern interferometry *J. Opt. Soc. Am. A* **2** 1629–1636

[165] Kaufmann G H , Kerr D and Halliwell N A 1994 Contrast enhancement of pulsed ESPI addition fringes *Optics and Lasers in Engineering* **20** 25–34

[166] Facchini M , Albrecht D and Zanetta P 1993 Phase detection algorithm in ESPI fringes with speckle noise reduction by using preliminary time averaging *Proc. FASIG, "Fringe'93"* eds Jüptner W and Osten W (Bremen:Akademie Verlag) 45–50

[167] Davies J C , Buckberry C H , Jones J D C and Panell C N 1987 Development and application of a fibre optic electronic speckle pattern interferometer (ESPI) *Proc. SPIE* **863** 194–207

[168] Davies J C , Buckberry C H , Jones J D C and Pannell C N 1988 Developments in electronic speckle pattern interferometry for automotive vibration analysis *Proc. SPIE* **952** 260–274

[169] Pouet B F and Krishnaswamy S 1994 Additive-subtractive phase-modulated electronic speckle interferometry: analysis of fringe visibility *Applied Optics* **33** 6609–6616

[170] Chatters T C , Pouet B F and Krishnaswamy S 1995 Additive-subtractive phase-modulated shearography with synchronized acoustic stressing *Experimental Mechanics* **35** 159–165

[171] Lu B , Yang X , Abendroth H and Eggers H 1989 Time-average subtraction method in electronic speckle pattern interferometry *Optics Communications* **70** 177–180

[172] Joenathan C 1991 Vibration fringes by phase stepping on an electronic speckle pattern interferometer: an analysis *Applied Optics* **30** 4658–4665

[173] Qin Y and Dai J 1994 Real-time interval technique for electronic shearing speckle pattern interferometry *Optics and Lasers in Engineering* **21** 241–248

[174] Wizinowich P L 1990 Phase shifting interferometry in the presence of vibration: a new algorithm and system *Applied Optics* **29** 3271–3279

[175] Colucci D , Wizinowich P 1992 Millisecond phase acquisition at video rates *Appied Optics* **31** 5919–5925

[176] van Haasteren A J P and Frankena H J 1994 Real-time displacement measurement using a multicamera phase-stepping speckle interferometer *Applied Optics* **33** 4137–4142

[177] Joenathan C 1990 Effect of the non-linearity of the TV camera in electronic speckle pattern interferometry *Optik* **85** 33–37

[178] Jones R and Wykes C 1977 De-correlation effects in speckle-pattern interferometry. 2. Displacement dependent de-correlation and applications to the observation of machine-induced strain *Optica Acta* **24** 533–550

[179] Owner-Petersen M 1991 Decorrelation and fringe visibility: on the limiting behavior of various electronic speckle-pattern correlation interferometers *J. Opt. Soc. Am. A* **8** 1082–1089

[180] Wykes C 1987 A theoretical approach to the optimization of electronic speckle pattern interferometry with limited laser power *Journal of Modern Optics* **34** 539–554

[181] Slettemoen G Å 1981 First-order statistics of displayed speckle patterns in electronic speckle pattern interferometry *J. Opt. Soc. Am.* **71** 474–482

[182] Williams D C and Robinson D W 1987 Electro-optic holography *Non-Destructive Testing, Proc. of the 4th European Conference* 588–596

[183] Pouet B F and Krishnaswamy S 1995 Technique for the removal of speckle phase in electronic speckle interferometry *Optics Letters* **20** 318–320

[184] Stetson K A 1989 An electronic system for real-time display and quantitative analysis of hologram interference fringes *Proc. SPIE (L.I.A.-ICALEO'89)* **1375** 78–85

[185] Bushman T 1989 Development of a holographic computing system *Proc. SPIE* **1162** 66–77

[186] Vikhagen E 1989 Vibration measurement using phase shifting TV-holography and digital image processing *Optics Communications* **69** 214–218

[187] Lu B , Hu Z , Abendroth H , Eggers H and Ziolkowski E 1989 Improvement of time-average subtraction technique applied to the vibration analysis with TV-holography *Optics Communications* **78** 217–221

[188] Rosenthal D M , Trolinger J D and Weber D C 1991 The use of double pulsed ESPI for earthquake mitigation of large structures *Proc. SPIE* **1553** 175–184

[189] Joenathan C and Khorana B M 1992 Contrast of the vibration fringes in time-averaged electronic speckle-pattern interferometry: effect of speckle averaging *Applied Optics* **31** 1863–1870

[190] Johansson S and Predko K G 1989 Performance of a phase-shifting speckle interferometer for measuring deformation and vibration *J. Phys. E: Sci. Instrum.* **22** 289–292

[191] O'Shea M and O'Mongain E 1992 Charge-coupled devices: frame adding as an alternative to long integration times and cooling *Optical Engineering* **31** 522–526

[192] Løkberg O J and Slettemoen G Å 1984 Improved fringe definition by speckle averaging in ESPI *Proceedings of ICO-13 Conference* (Sapporo) 116–117

[193] Creath K 1985 Averaging double-exposure speckle interferograms *Optics Letters* **10** 582–584

[194] Montgomery P and Bergquist B D 1985 Contrast enhancement of ESPI patterns by specke averaging in a video frame store *Proc. SPIE* **599** 201–206

[195] Towers D P , Judge T R and Bryanston-Cross P J 1991 Automatic interferogram analysis techniques applied to quasi-heterodine holography and ESPI *Optics and Lasers in Engineering* **14** 239–281

[196] Qin Y, Dai J and Wang J 1994 Recursive filtering technique for electronic speckle fringe patterns *Optical Engineering* **33** 1708–1711

[197] Yu E, Cha S S and Joo W 1995 Use of interferometric directionality for noise reduction *Optical Engineering* **34** 173–182

[198] Kerr D , Mendoza-Santoyo F and Tyrer J R 1989 Manipulation of the Fourier components of speckle fringe patterns as part of an interferometric analysis process *Journal of Modern Optics* **36** 195–203

[199] Lim J S 1981 Techniques for speckle noise removal *Optical Engineering* **20** 670–678

[200] González R C and Wintz P 1987 *Digital image processing* (Reading, MA:Addison-Wesley) 162-163

[201] Davies E R 1990 *Machine vision: theory, algorithms, practicalities* (London:Academic Press) 47-54

[202] Davies E R 1992 The relative effects of median and mean filters on noisy signals *Journal of Modern Optics* **39** 103–113

[203] Davila A , Kaufmann G H and Kerr D 1995 An evaluation of synthetic aperture radar noise reduction techniques for the smoothing of electronic speckle pattern interferometric fringes *Journal of Modern Optics* **42** 1795–1804

[204] Kaufmann G H , Davila A and Kerr D 1996 Speckle noise reduction in TV holography *Proc. SPIE* **2730** 96–100

[205] Frost V S , Stiles J A , Shanmugan K S and Holtzman J C 1982 A model for radar images and its application to adaptative digital filtering of multiplicative noise *Transations of Pattern Analysis and Machine Intelligence* **4** 157–165

[206] Lee J -S 1986 Speckle suppression and analysis for synthetic aperture radar images *Optical Engineering* **25** 636–643

[207] Crennell K M and Bowler I W 1986 The smoothing of electronic speckle pattern interferometric images *Optics and Lasers in Engineering* **7** 163–173

[208] Crimmins T R 1986 Geometric filter for reducing speckle *Optical Engineering* **25** 651–654

[209] Wong Y F 1993 A non-linear scale-space filter by physical computation *Proc. IEEE Workshop on Neural Networks for Signal Processing* eds Kamm C A *et al* 241–250

[210] Kujawińska M 1993 The architecture of a multipurpose fringe pattern analysis system *Optics and Lasers in Engineering* **19** 261–268

[211] Robinson D W 1993 Phase unwrapping methods *Interferogram analysis. Digital fringe pattern measurement techniques* eds Robinson D W and Reid G T (Bristol:Institute of Physics Publishing) 194–229

[212] Judge T R and Bryanston-Cross P J 1994 A review of phase unwrapping techniques in fringe analysis *Optics and Lasers in Engineering* **21** 199–239

[213] Takeda M 1996 Recent progress in phase unwrapping techniques *Proc. SPIE* **2782** 334–343

[214] Gu J and Chen F 1995 Fast Fourier transform, iteration, and least-squares-fit demodulation image processing for analysis of single-carrier fringe pattern *J. Opt. Soc. Am. A* **12** 2159–2164

[215] Moore A J , Tyrer J R and Mendoza-Santoyo F 1994 Phase extraction from electronic speckle pattern interferometry addition fringes *Applied Optics* **33** 7312–7320

[216] Owner-Petersen M 1991 Digital speckle pattern shearing interferometry: limitations and prospects *Applied Optics* **30** 2730–2738

[217] Pryputniewicz R J 1992 Electro-optic holography *SPIE Critical Reviews of Optical Science and Technology* **CR46** ed Trolinger J D 148–174

[218] Slettemoen G Å and Wyant J C 1986 Maximal fraction of acceptable measurements in phase-shifting speckle interferometry: a theoretical study *J. Opt. Soc. Am. A* **3** 210–214

[219] Maack T and Kowarschik R 1996 Camera influence on the phase-measurement accuracy of a phase-shifting speckle interferometer *Applied Optics* **35** 3514–3524

[220] Hong C K , Ryu H S and Lim H C 1995 Least-squares fitting of the phase map obtained in phase-shifting electronic speckle pattern interferometry *Optics Letters* **20** 931–933

[221] Robinson D W and Williams D C 1986 Digital phase stepping speckle interferometry *Optics Communications* **57** 26–30

[222] Creath K 1985 Phase-shifting speckle interferometry *Applied Optics* **24** 3053–3058

[223] Bhat G K 1995 Digital techniques for strain measurement using electro-optic holography *Journal of Modern Optics* **42** 1909–1919

[224] Vikhagen E 1990 Nondestructive testing by use of TV holography and deformation phase gradient calculation *Applied Optics* **29** 137–144

[225] Kreis T M 1987 Quantitative evaluation of interference patterns *Proc. SPIE* **863** 68–77

[226] Reid G T 1993 Automatic analysis of interference fringes *Optical methods in engineering metrology* ed Williams D C (London:Chapman & Hall) 385–413

[227] Robinson D W and Reid G T eds 1993 *Interferogram analysis. Digital fringe pattern measurement techniques* (Bristol:Institute of Physics Publishing)

[228] Kujawińska M and Wójciak J 1991 Spatial phase-shifting techniques of fringe pattern analysis in photomechanics *Proc. SPIE* **1554B** 503–513

[229] Creath K 1988 Phase-measurement interferometry techniques *Progress in optics* **XXVI** ed Wolf E (Amsterdam:North Holland) 350–393

[230] Creath K 1993 Temporal phase measurement methods *Interferogram analysis. Digital fringe pattern measurement techniques* eds Robinson D W and Reid G T (Bristol:Institute of Physics Publishing) 94–140

[231] Dorrío B V and Fernández J L 1999 Phase-evaluation methods in whole-field optical measurement techniques. *MEASUREMENT SCIENCE AND TECHNOLOGY* **10** R33-R55

[232] Greivenkamp J E and Bruning J H 1992 Phase shifting interferometry *Optical shop testing* ed Malacara D 501–598

[233] Morimoto Y and Fujisawa M 1994 Fringe pattern analysis by a phase-shifting method using Fourier transform *Optical Engineering* **33** 3709–3714

[234] Kujawińska M 1993 Spatial phase measurement methods *Interferogram analysis. Digital fringe pattern measurement techniques* eds Robinson D W and Reid G T (Bristol:Institute of Physics Publishing) 141–193

[235] Womack K H 1984 Interferometric phase measurement using spatial synchronous detection *Optical Engineering* **23** 391–395

[236] Takeda M , Ina H and Kobayashi S 1982 Fourier-transform method of fringe-pattern analysis for computer-based topography and interferometry *J. Opt. Soc. Am.* **72** 156–160

[237] Schwider J 1988 Advanced evaluation techniques in interferometry *Progress in optics* **XXVI** ed Wolf E (Amsterdam:North Holland) 272–359

[238] Joenathan C , Franze B , Haible P and Tiziani H J 1998 Speckle interferometry with temporal phase evaluation for measuring large-object deformation *Applied Optics* **37** 2608–2614

[239] Joenathan C, Franze B, Haible P and Tiziani H J 1998 Large in-plane displacement measurement in dual-beam speckle interferometry using temporal phase measurement *Journal of Modern Optics* **45** 1975-1984

[240] Joenathan C, Franze B, Haible P and Tiziani H J 1998 Novel temporal Fourier transform speckle pattern shearing interferometer *Optical Engineering* **37** 1790-1795

[241] Joenathan C, Franze B, Haible P and Tiziani H J 1998 Shape measurement by use of temporal Fourier transformation in dual-beam illumination speckle interferometry *Applied Optics* **37** 3385-3390

[242] Kujawińska M , Spik A and Robinson D W 1989 Analysis of ESPI interferograms by phase-stepping techniques *Proceedings of the Fourth International Conference on Fringe Analysis (FASIG'89)* (Loughborough University, UK)

[243] Buckberry C H and Davies J C 1990 The application of TV holography to engineering problems in the automotive industry *Proc. SEM Conference on Hologram Interferometry and Speckle Metrology* eds Stetson K A and Pryputniewicz R J (Baltimore) 268–278

[244] Pryputniewicz R J and Stetson K A 1989 Measurement of vibration patterns using electro-optic holography *Proc. SPIE* **1162** 456–467

[245] Pedrini G, Zou Y-L and Tiziani H J 1996 Quantitative evaluation of digital shearing interferogram using the spatial carrier method *Pure Appl. Opt.* **5** 313-321

[246] Schedin S and Gren P 1997 Phase evaluation and speckle averaging in pulsed television holography *Applied Optics* **36** 3941–3947

[247] Petzing J N and Tyrer J R 1996 The effect of metallographic structure on clamped plate vibration characteristics *Experimental Mechanics* **36** 127–134

[248] Farrant D I , Kaufmann G H , Petzing J N , Tyrer J R , Oreb B F and Kerr D 1997 Transient deformation measurement using dual-pulse addition ESPI *Proc. SPIE* **3173A** 132-140

[249] Paoletti D and Schirripa Spagnolo G 1994 Fast Fourier transformed electronic speckle contouring for diffuse surfaces profilometry *Optics and Lasers in Engineering* **20** 87–96

[250] Davila A, Kauffman G H and Pérez-López C 1998 Transient deformation analysis by a carrier method of pulsed electronic speckle-shearing pattern interferometry *Applied Optics* **37** 4116-4122

[251] Fernández A, Doval A F, Dávila A, Blanco-García J, Pérez-López C and Fernández J L 1998 Double-pulsed carrier speckle-shearing pattern interferometry for transient deformation analysis *Proc. SPIE* **3478** 352-358

[252] Fernández A, Doval A F, Bugarín J, Dorrío B V, López C, Alén J M, Blanco-García J, Pérez-Amor M and Fernández J L 1997 Transient bending waves analysis by Fourier evaluation of single pulsed TV-holography fringe patterns *Proc. SPIE* **3098** 575-581

[253] Preater R W T and Swain R 1994 Fourier transform fringe analysis of electronic speckle pattern interferometry fringes from high-speed rotating components *Optical Engineering* **33** 1271–1279

[254] Kujawińska M , Spik A and Robinson D W 1989 Quantitative analysis of transient events by ESPI *Proc. SPIE* **1121** 416–422

[255] Pedrini G, Zou Y-L and Tiziani H J 1997 Simultaneous quantitative evaluation of in-plane and out-of-plane deformations by use of a multidirectional spatial carrier *Applied Optics* **36** 786-792

[256] Kreis T M, Adams M and Jüptner W P O 1997 Methods of digital holography: a comparison *Proc. SPIE* **3098** 224-233

[257] Kreis T M and Jüptner W P O 1997 Principles of digital holography *Fringe'97. Proceedings of the 3rd International Workshop on Automatic Processing of Fringe Patterns* eds. Jüptner W and Osten W (Berlin:Akademie Verlag) 353-363

[258] Pedrini G, Tiziani H J and Zou Y 1996 Speckle size of digitally reconstructed wavefronts of diffusely scattering objects *Journal of Modern Optics* **43** 395-407

[259] Yamaguchi I and Zhang T 1997 Phase-shifting digital holography *Optics Letters* **22** 1268-1270